

# **Advanced Nanoelectromechanical Systems for Next Generation Energy Harvesting**

by

Alam Mahmud

A thesis

presented to the University of Waterloo

in fulfillment of the

thesis requirement for the degree of

Master of Applied Science

in

Electrical and Computer Engineering - Nanotechnology

Waterloo, Ontario, Canada, 2018

© Alam Mahmud 2018

## **AUTHOR'S DECLARATION**

I hereby declare that I am the sole author of this thesis. This is a true copy of the thesis, including any required final revisions, as accepted by my examiners.

I understand that my thesis may be made electronically available to the public.

Alam Mahmud

## Abstract

The ever-increasing desire to produce portable, mobile and self-powered wireless micro-/nano systems (MNSs) with extended lifetimes has led to the significant advancement in the area of mechanical energy harvesting over the last few years and it has been possible not only because nanotechnology evolved as a powerful tool for the manipulation of matter on an atomic, molecular, and supramolecular scale, but also different micro-/nano fabrication techniques have enabled researchers and scientists to create, visualize, analyse and manipulate nano-structures, as well as to probe their nano-chemistry, nano-mechanics and other properties within the systems.

The dissertation first discusses briefly about energy harvesting technologies for self-powered MNSs, for example a wireless aircraft structural health monitoring (SHM) system, with a particular focus on piezoelectric nanogenerators (PENG) and triboelectric nanogenerators (TENG) as they are the most promising approaches for converting ambient tiny mechanical energy into electrical energy efficiently and effectively and then it analyzes the theoretical and experimental methodologies for efficient energy harvesting using PENG, TENG and hybrid devices. The piezoelectric property intertwined with the semiconducting behaviour of different ZnO nanostructures has made them ideal candidate for piezoelectric energy harvesting, also intensive and state-of-the-art research has been going on to enhance the performance of the PENG devices based on 1D and 2D ZnO nanostructures. In this work, a high performance and consolidated PENG device based on the integration of ZnO nanowires and nanoplates on the same substrate has been demonstrated, that produces an output electrical power of  $8.4 \mu\text{W}/\text{cm}^2$  at the matched load of  $10\text{M}\Omega$  that manifests their ability for powering up different MNSs.

Since hybrid nanogenerators (HNG) integrate different types of harvesters in a single unit, where several energy sources can be leveraged either simultaneously or individually, in the next part of this work, a HNG device integrating PENG and TENG components has been designed, fabricated and characterized where PENG and TENG parts mutually enhance the performance of each other resulting an instantaneous peak power density of  $1.864\text{mW}/\text{cm}^2$  and subsequently the device has been used to charge several commercial capacitors to corroborate their potential for aircraft SHM applications. Moreover, the hybrid device exhibits strong potential for wearable electronics as it can harvest energy from human walking and normal hand movements.

However, successful implementation of self-powered electronics, such as a wireless aircraft SHM depends not only on the performance of individual parts but also on components integration within the system, where each device/system node within the network consists of a low-power microcontroller unit, high-performance data-processing/storage units, a wireless signal transceiver, ultrasensitive sensors based on a micro-/nano electro-mechanical system, and most importantly the embedded powering units.

This dissertation aims to deepen the understanding of the different energy harvesting methods utilizing the knowledge of nanoscale phenomena and nanofabrication tools along with the associated prospects and challenges and thus, this research in the field of energy harvesting using advanced nano electro-mechanical systems could have a substantial impact on many areas, ranging from the fundamental study of new nanomaterial properties and different effects in nanostructures to diverse applications.

## Acknowledgements

I am predominantly grateful to my advisor, Professor Dayan Ban, who has been a mentor as well as a guardian to me for last two years. His vision and belief in me has been invaluable to my success. I honestly can't thank you enough for all the opportunities you've granted me, Professor Ban.

I would like to thank Dr. Sharif Mohammad Mominuzzaman and Dr. Md. Kawsar Alam for recommending me to enroll to the MASc (Nano) program at University of Waterloo. Without them, I would not have had this opportunity.

I would like to express my deepest appreciation for my committee and the readers of this thesis, Dr. Bo Cui and Dr. Guo-Xing Miao.

For the knowledge and understanding I gained by taking their courses, I would like to deeply thank Dr. Bo Cui, for his meaningful explanation on nanofabrication, which has inevitably helped me accomplish my project, Dr. Guo-Xing Miao and Dr. Bahareh Sadeghimakki, for their passionate courses on Physics and Modeling of Solid State Devices, Solid State Physics and Chemistry and, Microscopy, Dr. Zbig Wasilewski, for giving me deep insight in crystal formation mechanisms, Dr. John T.W. Yeow, for showing me the new horizon of Advanced Nanoelectromechanical Systems and again Dr Dayan Ban, for intensifying my knowledge in quantum mechanics and optoelectronic devices.

My deepest gratitude goes to the staffs of Electrical and Computer Engineering Department of University of Waterloo as well as Waterloo Institute for Nanotechnology, with special mention for Richard barber from the Giga-to-Nanoelectronics (G2N) lab and Dr. Eihab-Abdel Rahman and Dr. Taylan Das for being so kind to let me use their measurement systems and helping me with the device testing.

I wish to thank Dr. Chettyalayam (Selva) Selvakumar and Dr. Roohollah S. Tarighat, for offering me TA positions that gave me the opportunity to get lifelong experiences. I also thank all the students I get a chance to teach. It has been my pleasure to be your teacher assistant, you made this experience very enjoyable and interesting.

Thanks to all the wonderful colleagues from our group and from Dr. Eihab-Abdel Rahman's group as well as all the co-workers whom I've met along the way for all the numerous intellectual discussions and for many special memories made during my masters study. Special thanks to Dr. Czang-Ho Lee, Dr. Bright Iheanacho, Pranav Gavirneni, Muhammad Shadman Mahtab for their kind support and encouragement.

Last and most importantly, I am indebted to my loving family and my close friends for being the pillars of my success, for being there to catch me and put me on my feet whenever I fall like a statue.

*Dedicated with all my heart to my best family.*

# Table of Contents

AUTHOR'S DECLARATION .....	ii
Abstract .....	iii
Acknowledgements .....	v
Dedication.....	vi
List of Figures .....	x
List of Tables.....	xv
List of Abbreviations.....	xvi
Quote.....	xvii
<b>Chapter 1 Problem Overview and Energy Harvesting.....</b>	<b>1</b>
1.1 Self-powered Systems.....	1
1.2 Structural Health Monitoring System.....	3
1.3 Energy Harvesting Technology.....	5
1.3.1 Piezoelectric Nanogenerators.....	6
1.3.2 Triboelectric Nanogenerators.....	10
1.3.3 Hybrid Nanogenerators.....	12
1.4 Theoretical Background.....	14
1.5 Research Objectives.....	18
1.6 Thesis Overview.....	19

<b>Chapter 2</b>	<b>Experimental Methodologies.....</b>	<b>21</b>
2.1	Materials for Piezoelectric Nanogenerator.....	22
2.1.1	Synthesis Techniques for ZnO nanostructures.....	23
2.1.2	Hydrothermal Growth of ZnO Nanostructures.....	27
2.1.2.1	Effect of Growth Temperature.....	29
2.1.2.2	Effect of ZnO Seed Layer.....	30
2.1.2.3	Effect of substrate in hydrothermal method.....	31
2.2	Materials Selection for Triboelectric Nanogenerator.....	32
2.2.1	PTFE as Triboelectric Material.....	34
2.2.2	Nanostructured Materials for Improved Device Performance....	36
2.3	Design and Working Mechanism of Hybrid Nanogenerator.....	37
2.4	Device characterization set up.....	40
<b>Chapter 3</b>	<b>Controlled growth of 1D/2D hybrid zinc oxide nanostructures for piezoelectric energy harvesting.....</b>	<b>42</b>
3.1	Introduction.....	43
3.2	Material growth and device fabrication.....	45
3.2.1	Hydrothermal growth of ZnO nanostructures.....	46
3.2.2	Characterization of the nanostructures.....	47
3.3	Piezoelectric characterization.....	49
3.3.1	Measurement set up.....	49



3.3.2	Results and discussion.....	50
3.4	Conclusion.....	58
<b>Chapter 4</b>	<b>Piezo-tribo hybrid energy harvester based on inorganic-organic nanostructured materials.....</b>	<b>60</b>
4.1	Introduction.....	60
4.2	Device structure and working principle.....	62
4.3	Experimental Section.....	66
4.3.1	Materials characterization and device fabrication.....	66
4.3.2	Results and discussion.....	69
4.4	Conclusion.....	77
<b>Chapter 5</b>	<b>Conclusions, Contributions and Recommendations.....</b>	<b>79</b>
5.1	Summary and Contributions.....	79
5.2	Recommendations and Future Work.....	81
	<b>Letters of Copyright Permission.....</b>	<b>82</b>
	<b>References.....</b>	<b>92</b>

## List of Figures

<b>Figure 1.1</b>	Future perspective of electronics beyond Moore’s law. The vertical axis reflects miniaturization and increasing device density, CPU speed, and memory capacity. The horizontal axis reflects the diversity and functionality of personal and portable electronic devices. ....	2
<b>Figure 1.2</b>	Illustration of aircraft SHM system.....	4
<b>Figure 1.3</b>	Block diagram of a wireless SHM system.....	5
<b>Figure 1.4</b>	Working principle of piezoelectric VING configuration under vertical mechanical strain.....	6
<b>Figure 1.5</b>	The four fundamental modes of triboelectric nanogenerators: (a) vertical contact separation mode; (b) in-plane contact-sliding mode; (c) single-electrode mode; and (d) freestanding triboelectric-layer mode.....	10
<b>Figure 1.6</b>	Theoretical analysis approach for piezo-tribo hybrid nanogenerator (a) Motion characteristics of external load (b) PENG-TENG hybrid device. ....	15
<b>Figure 2.1</b>	(a) SEM image of aligned ZnO nanowires grown on sapphire substrate using a thin layer of gold as catalyst. (b) SEM images of gold catalyst patterns using PS sphere monolayer as mask. (c) SEM image of aligned ZnO nanowires grown with a honeycomb pattern.....	24
<b>Figure 2.2</b>	SEM images of ZnO nanorods formed on sapphire (0001) substrates. (a) Images observed from a cleaved surface. (b) Images taken with a tilt angle. (c) Image of the top of a single ZnO nanorods.....	25
<b>Figure 2.3</b>	Hydrothermal set up for the growth of ZnO nanostructures.....	28

**Figure 2.4** Effect of temperature in hydrothermal method. (a). Undesired nano-islands formation at  $< 75^{\circ}\text{C}$ , (b) nanowires at  $88^{\circ}\text{C}$ , (c) nanorods at  $90^{\circ}\text{C}$ , and (d) nanotubes grown at  $97^{\circ}\text{C}$ .....29

**Figure 2.5** Multi-chamber PECVD Cluster System. ....31

**Figure 2.6** Scanning electron microscope images of the as grown ZnO nanostructures on (a) Glass substrate with 100nm AZO seed layer. (b) 100nm Cr deposited on glass substrate with 100nm AZO seed layer. (c) PET substrate with 200nm AZO seed layer. (d) Shim substrate with 400nm AZO seed layer. ....32

**Figure 2.7** Example of a triboelectric series that shows an ordering of materials based on their empirically derived direction of charge transfer. A material closer to the top of the list contacted with a material closer to the bottom of the list will charge positively (while the other material charges negatively) .....33

**Figure 2.8** Structure and photographs of a flexible multilayered TENG. (a) Schematic and (b) an enlarged view of the zigzag-shaped structure of the TENG. (c) SEM image of nano pores on aluminum foils. Photograph of a fabricated TENG (d) Normal state (e) Bent by human finger (f) Photograph of the inner structure of shoe insole, showing a TENG installed. The scale bar is 2cm (g) Schematics from two different angles that reveal the device structure. (h) SEM image of nano-pores created at the surface of the aluminum foils. The scale bar is 200nm.....35

**Figure 2.9** (a) Schematic view and photograph of the hybrid NG. (b) SEM images of the nanostructured aluminum electrode. (c) SEM images of the micro/nano dual-scale PDMS.....36

**Figure 2.10** Working mechanism of the piezo/tribo hybrid generator in a press-and-release cycle. (a) Initial state without a mechanical force. (b) Piezoelectric potential when the external force starts to be applied. (c) Piezoelectric and triboelectric charge

distribution at full-contact state. (d) Negative piezoelectric and triboelectric generation at separating state. (e) Maximized negative piezoelectric potential at Full separation state.....38

**Figure 2.11** Block diagram of the setup for measuring the input mechanical vibration and output electrical signals of the PENG/TENG/Hybrid devices. This system includes a closed-loop controller, a linear shaker, a power amplifier and an accelerometer on the input side and Stanford low-noise voltage/current preamplifiers along with oscilloscope and force sensors on the output side. ....40

**Figure 3.1** (a) 3D schematic of the PENG. (b) Step-by-step fabrication process of the PENG. ....45

**Figure 3.2** (a) – (b) 450 tilted view SEM images of the hydrothermally grown ZnO nanostructure showing the average diameter of the 1D ZnO nanowires is ~70nm and the thickness of 2D ZnO nanosheets is approximately 50 nm. (c) SEM image of the cross-section of the ZnO nanostructures showing an average height of 1.3 μm.....48

**Figure 3.3** (a) Packaged PENG prototype device ready for testing. (b) General setup of the piezoelectric characterization system. The system includes a closed loop controller, a linear shaker and a power amplifier unit to provide sinusoidal waves simulating a vibration source with a known amplitude and frequency. ....49

**Figure 3.4** (a) Measured open-circuit voltage (average peak value ~4.2 V) and (b) short-circuit current (average peak value ~8.2 μA) for the PENG. The peak-to-peak displacement was kept constant at 5 mm.....50

**Figure 3.5** Structure and working mechanism of 1D and 2D ZnO nanostructure based PENGs. (a) ZnO nanowire based PENG with no external applied force. (b) Electrons flow from the top electrode to the bottom electrode through the external circuit by the negative piezoelectric potential generated at the top side of the ZnO nanowires under external strain. (c) Electrons flow back via the external circuit till it

goes back to its initial state when the force is released. (d) As fabricated ZnO nanosheets based PENG in the absence of any external force. (e) Piezoelectric potential causes electrons' flow from the top electrode to the bottom electrode side through the external circuit under direct compression in the vertical direction. (f) As the compressive strain is released, the piezopotential disappears and device goes back to its initial state. (g) SEM image of 1D ZnO NWs grown on PET substrate using the same hydrothermal process as the current PENG device. (h) Open circuit voltages for the PENG devices on PET (blue) and shim (red) substrates. ....52

**Figure 3.6** Output performance of the PENG. (a) Open circuit voltages and (b) Short circuit currents at different frequencies. (c) Open circuit voltages and (d) Short circuit currents at different accelerations. ....56

**Figure 3.7** The load resistance dependence of instantaneous electrical power from the fabricated PENG. As the load increases from 10kΩ power increases, then reaches a maximum value of 8.4 μW/cm<sup>2</sup> at the matched load of 10MΩ and drops off with further increase in load. ....57

**Figure 4.1** (a) 3D schematic of the curved shaped hybrid device. (b) Average peak-to-peak output open circuit voltage from the two components of the device at different frequencies. (c) Output open circuit voltage from the piezo and triboelectric components in a single press-and-release cycle. [To visually compare the results from the PENG and TENG parts, output from the PENG has been multiplied by 8 and 10 in (b) and (c) respectively] .....64

**Figure 4.2** Illustration of the working mechanism of the device in a single press-and-release cycle of applied mechanical vibration. ....65

**Figure 4.3** The fabrication process of the hybrid nanogenerator. (a) – (g) Step-by-step progress towards the piezoelectric part of the device. (h) – (k) Fabrication steps

for the triboelectric part of the device. (l) Integration of piezo and tribo components together to make the hybrid structure. ....66

**Figure 4.4** Materials characterization (a) AFM image of shim substrate. Top view SEM images of (b) the nanostructured shim surface (c) as grown ZnO NWs along with nano plate structures (d) PTFE nanostructures. ....67

**Figure 4.5** Output open circuit voltage of (a) piezoelectric, (b) triboelectric and (c) hybrid nanogenerator without using rectifiers. (d) Concurrent measurement method for piezo and tribo electric outputs. (e) The piezoelectric and triboelectric outputs are combined in parallel for the hybrid output measurement. Measured piezoelectric, triboelectric and hybrid output open-circuit voltages (e) and short-circuit currents (f) using the rectifier circuits. ....70

**Figure 4.6** Mutual output enhancement of PENG and TENG (a) Voc of PENG when acting alone, (b) Voc of PENG enhanced by the electrostatic induced charge on the shim substrate, (c) Voc of TENG when acting alone, (d) Voc of TENG enhanced by the piezoelectric induced charge on the common electrode. ....72

**Figure 4.7** The measured output voltage signals of the PENG device in (a) forward connection, and (b) reverse connection of the measurement instrument during testing.....73

**Figure 4.8** Electrical characterization of the hybrid device (a) output voltages and currents for different loads varying from 20kΩ to 105MΩ, (b) output power as a function of load resistance (c) Charging characteristic of the device with a 4.7μF capacitor. (d) Fast charging behavior of the device with different capacitors (e) –(f) Output voltage signal and charging behavior of the device with normal human movements (g) Collected output signal by the harvester from human walking. ....74

**Figure 4.9** (a) Energy collection using commercial piezoelectric energy harvesting unit with 6.8μF and 47μF capacitors in the input and output side respectively. (b)

Circuit diagram for energy collection from the hybrid device using Linear Technology's LTC3588-1LTC. (Input side capacitor =  $6.8\mu\text{F}$  and output side capacitor  $47\mu\text{F}$ ). .....75

**Figure 4.10** Measured open-circuit voltage of the (a) – (d) PENG, and (e) - (h) TENG device tested over three consecutive weeks. The response remains unchanged, which demonstrates the stability and reliability of the device. The excitation frequency and the acceleration amplitude were 25Hz and 1G respectively in all tests. ....76

## List of Tables

<b>Table 1.1</b>	Comparison of some of the reported piezoelectric nanogenerators using different materials.....	9
<b>Table 1.2</b>	Key points of some of the current hybrid nanogenerators.....	13



## List of Abbreviations

AZO	aluminum-doped ZnO
AFM	atomic force microscopy
SEM	scanning electron microscope
HMTA	hexamethylenetetramine
MEMS/NEMS	micro/nano-electromechanical system
NG	nanogenerator
PENG	piezoelectric nanogenerator
NW	nanowire
PDMS	polydimethylsiloxane
PTFE	polytetrafluoroethylene
PEN	polyethylene naphthalate
TENG	Triboelectric nanogenerator
PMMA	polymethyl methacrylate
PVDF	polyvinylidene difluoride
SHM	structural health monitoring
MNS	micro-/nano system
XRD	X-ray diffraction
NS	nanostucture
HNG	Hybrid nanogenerator

***“Knowing is not enough; we must apply. Willing is not enough; we must do.***

***In the realm of ideas everything depends on enthusiasm... in the real world all rests on perseverance.”***

***—Johann Wolfgang von Goethe***

# Chapter 1

## Problem Overview and Energy Harvesting

This research is mainly focused on energy harvesting using two different methods – piezoelectric and triboelectric nanogenerators by utilizing the recent understandings of nanotechnology and taking advantage of different micro-/nano fabrication tools. This chapter starts with the basic concept of self-powered electronics and nanotechnology enabled energy harvesting for powering up mobile micro-/nano systems.

Part of this chapter has been submitted as a journal publication:

A. A. Khan, A. Mahmud, D. Ban, Evolution from Single to Hybrid Nanogenerator: A Contemporary Review on Multimode Energy Harvesting for Self-Powered Electronics, *IEEE Transaction on Nanotechnology*, under review.

### 1.1 Self-powered Systems

Self-powered systems are defined as those that operate without an external electricity source and instead harness the required energy from the ambient environment of the system. The speedy growth of personal and mobile electronics for various applications, for example entertainment, communication, health care, home-office activities, environmental monitoring etc. has been possible due to fast development of the micro-/nano systems (MNSs) [1]. Besides, due to the traditional trajectory of shrinking device dimensions as per well-established Moore's law [2], extensive efforts and state-of-the art research have been focused on integrating individual MNSs with diversified functionalities into multi-functional MNSs to build up large-scale networks for multifarious applications (Figure 1.1). Although the power consumption

of these MNSs is low individually, the number of such functional MNSs deployed can be huge and those systems rely on rechargeable batteries to power up the electronic devices.

On the other hand, the rapid technology growth is leading the world towards automation where Artificial Intelligence (AI), Big Data, Internet of Things (IoT) etc. are going to be the dominating technologies in future that require trillions of sensors. Using external power sources to power-up these tremendous amount of sensors is not feasible and reliable and to address this problem self-powered sensor networks with good sensing capabilities can be utilized [3].

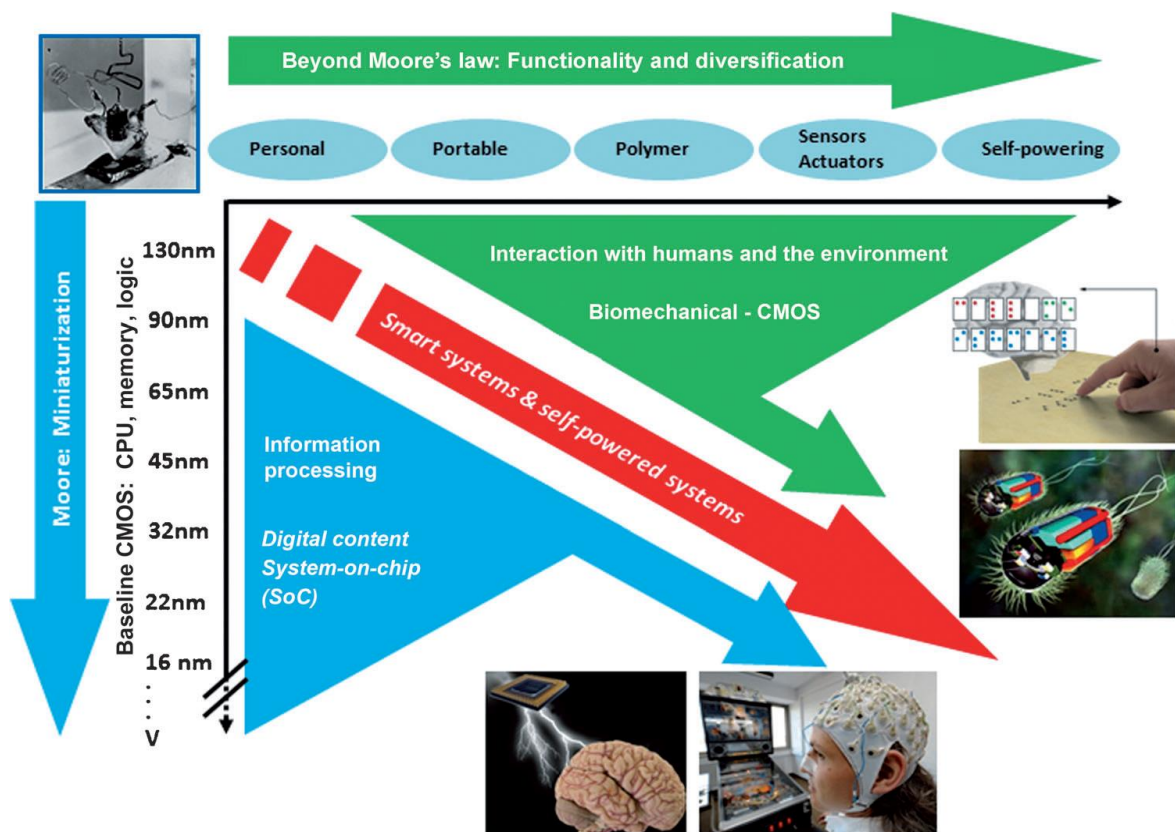


Figure 1.1 Future perspective of electronics beyond Moore's law. The vertical axis reflects miniaturization and increasing device density, CPU speed, and memory capacity. The horizontal axis reflects the diversity and functionality of personal and portable electronic devices [Reproduced from Ref. 1 with permission from John Wiley and Sons].

Energy harvesting technology has strong potential to not only meet growing global energy demand but also support a wide range of self-powered electronics applications [4]. Solar cells [5], electrochemical cells [6], piezoelectric/triboelectric/pyroelectric nanogenerators [7-9] and magneto-electric energy harvesters [10] are enabling technologies for converting solar, chemical, mechanical, thermal and magnetic energy to electricity. Piezoelectric nanogenerators (PENG) [11] and triboelectric nanogenerators (TENG) [12] have been developed to scavenge available but mostly wasted mechanical energy from the ambient environment by utilizing the piezoelectric and triboelectric property of materials. Using vibrations, wind, rain drops, ocean waves, mechanical rotation and human body movement, these nanogenerators can potentially drive various personal electronics like smart phone, electronic watch, Bluetooth transceiver etc.

The current rapid advancement of micro-/nanotechnology along with available state-of-the-art micro-/nanofabrication techniques, it is highly desired that different innovative energy harvesting devices and their hybridization will enable multifunctional MNSs to operate wirelessly and self-sufficiently without the use of a battery and thus leading to self-powered systems [1]. Part of this research work on self-powered electronics is particularly focused on aircraft structural health monitor (SHM) system since in an aircraft operation environment, energy sources such as solar, wind, vibration, temperature differentials, electromagnetic, acoustic etc. are present and can potentially be used to harvest energy and use it to power up the small electronic components within the SHM system and hence making the system fully wireless.

## **1.2 Structural Health Monitoring System**

Aircraft structural health monitoring (SHM) system is designed to identify the “state” of the constituent materials, of the different parts, and of the full assembly of these parts constituting the aircraft structure which is based on the observation of the

system over time using periodically sampled dynamic response measurements from an array of sensors [13-14]. To perform the tasks such as sensing, signal conditioning and processing, data storage and communication, supplying power to those sensors and electronic components is indispensable no matter how. Depending on whether wire connection is used or not, SHM system can be categorized into two types – wired and wireless.

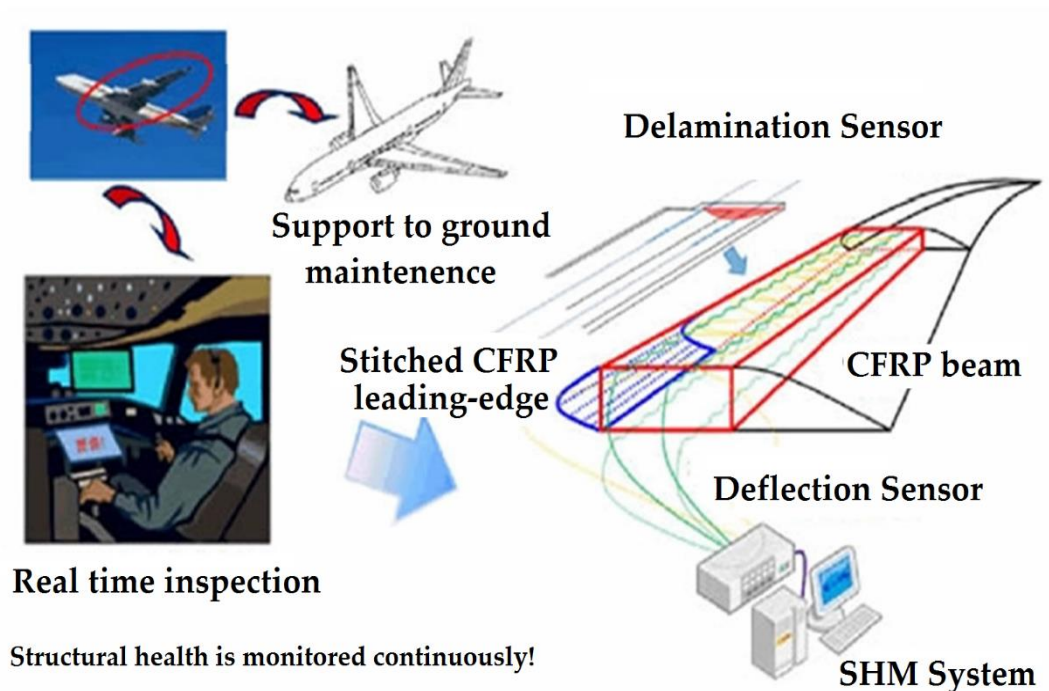


Figure 1.2 Illustration of a structural health monitoring system [Reproduced from Ref. 51(open access journal)].

Although wired SHM system design provides flexibility, versatile SHM capabilities and immune to electromagnetic interference, tremendous progress has been made in the area of wireless SHM for civil structures and aircrafts as they can provide some unprecedented advantages over the wired SHM systems, for example, reduction in the aircraft weight by eliminating physical wired connections, elimination of the installation of complex harnesses within the fuselage, easier installation and maintenance of the system, etc. A wireless SHM system includes sensing unit, data

processing unit, conditioning and transmission unit, and power supply [15]. However, supplying power to those electronic units by means of battery is the only viable option yet which requires cable connections thus weakening the justification of the wireless system.

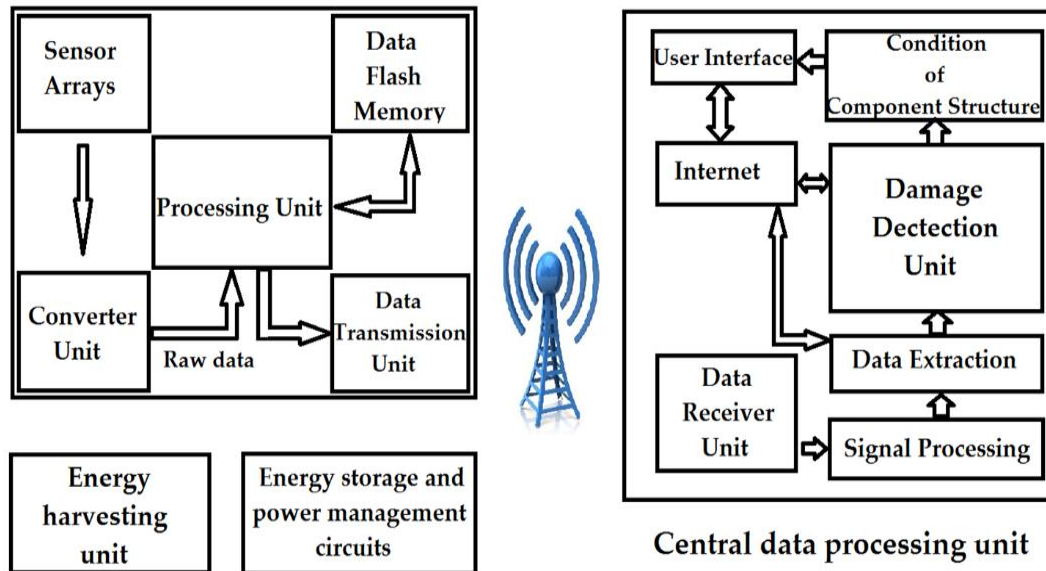


Figure 1.3 Block diagram of a wireless SHM system.

### 1.3 Energy Harvesting Technology

As energy harvesting technology has evolved dramatically in the last decade with an aim to realize self-powered organic/inorganic electronic systems, it has opened up many new areas of utilizing energy harvesting technique including aircraft SHM. In an aircraft operation environment, sources such as solar, wind, mechanical vibration, temperature gradient, etc. can potentially be used to convert them into electrical energy and properly designed and integrated energy storage units can be used to efficiently and effectively store the converted energy to power up the electronic components within the aircraft SHM system, thus making the system fully wireless. The power required for driving each electronic unit is small, but the number of such units can be massive in the order of billions to trillions. Three most common energy-harvesting techniques are mechanical vibration energy harvesters, thermoelectric

power generators, and photovoltaic (PV) cells. As the mechanical vibration energy is the most available type of energy in an operating aircraft environment, mechanical energy-harvesters commonly known as nanogenerators [7-8] are the most suitable candidate in the aforementioned case.

### 1.3.1 Piezoelectric Nanogenerators

A piezoelectric nanogenerator is an energy harvesting device that converts external tiny kinetic energy into electrical energy using piezoelectric materials. Although there are huge number of piezoelectric materials, the use of nanostructured piezoelectric materials, however, is a relatively recent development, and the understanding of the nanoscale size effects on piezoelectricity is still being formulated [16-17]. Despite that, using nanotechnology in the realm of piezoelectric energy harvesting has demonstrated tremendous improvements and possibilities towards practical applications [11].

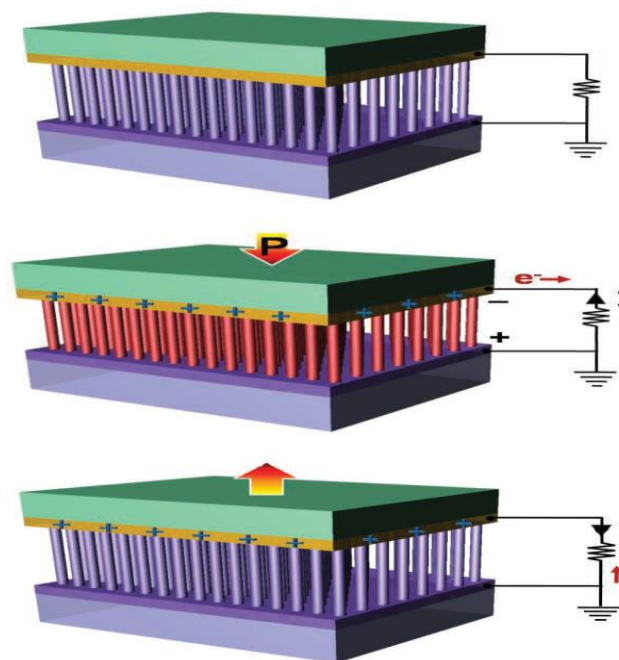


Figure 1.4 Working principle of piezoelectric VING configuration under vertical mechanical strain [Reproduced from Ref. 22 with permission from John Wiley and Sons].



First piezoelectric nanogenerator showed the successful conversion of nanoscale mechanical energy into electrical energy by means of piezoelectric zinc oxide nanowire (NW) arrays. Since then although some other piezoelectric materials, e.g. gallium nitride (GaN), indium nitride (InN), lead zirconate titanate (PZT), barium titanate (BaTiO<sub>3</sub>), etc. have also been studied and investigated to harness the mechanical energy [18], zinc oxide (ZnO) still stays in the heart of piezoelectric energy harvesting mostly because nanostructures of ZnO can be formed relatively easily and less expensively using low temperature methods [19]. Growth of ZnO nano structures has been one of the most active fields in nanotechnology because ZnO exhibits interesting properties such as semiconducting and piezoelectric, a typical wide band gap (3.37 eV), a large exciton binding energy (60 meV), near-UV emission, transparent conductivity, etc. [20]. ZnO could form three types of crystal structures: wurtzite, zinc blende, or rock salt; of which wurtzite structure is the natural form. Wurtzite structured ZnO is composed of two alternating layers of atoms respectively corresponding to cation Zn<sup>2+</sup> and anion O<sup>2-</sup>, that forms a tetrahedral configuration and results in non-centro symmetry inevitably. Among the semiconductors that have tetrahedral molecular geometry, ZnO has the highest piezoelectric tensor or at least one comparable to that of GaN and AlN that makes it a technologically important material for many applications, which require a large electromechanical coupling [21]. Typically, in a PENG, a piezoelectric material is covered by top and bottom electrodes on its two surfaces and a Schottky contact is formed at either surface. Although several geometrical configurations have been proposed and demonstrated, e.g. Lateral nanowire integrated nanogenerator (LING), Nanocomposite electrical generators (NEG), fabric-like geometrical configuration, etc., Vertical nanowire integrated nanogenerator (VING) has been studied extensively.

In VING configuration, when a piezoelectric structure is subjected to the external force, the deformation occurs throughout the structure. The piezoelectric effect creates

the electrical field inside the nanostructure; and due to the relative displacement of cations with respect to anions in its crystalline structure, the stretched part with the positive strain exhibits the positive electrical potential, whereas the compressed part with the negative strain displays the negative electrical potential and thus creates a potential difference between the electrodes. Because of the potential difference between top and bottom electrodes and the formation of a schottky junction, electrons are driven through an external load producing a current pulse and this continues until the material system reaches an equilibrium which eventually stops the flow of electrons. When the force is released, the piezopotential fades away and the electrons flow back through the external load to establish an equilibrium and a negative current pulse is observed and after the equilibrium is achieved, the device gets back to its initial state.

**Table 1.1** Comparison of some of the reported piezoelectric nanogenerators using different materials.

Material	Type	Synthesis	Geometry	Output voltage	Output power	Ref.
ZnO(n-type)	Wurtzite	CVD, hydrothermal process	D:~100 nm, L:200~500 nm	~9 mV	~0.5 pW	[16]
ZnO(p-type)	Wurtzite	CVD	D: ~50 nm, L: ~600 nm	50~90mV	5~16.2 pW	[23]
ZnO-ZnS	Wurtzite	Thermal evaporation and etching	Not stated	~6 mV	~0.1 pW	[24]
GaN	Wurtzite	CVD	D: 25~70 nm, L: 10~20 $\mu\text{m}$	~20 mV	~0.8 pW	[25]
CdS	Wurtzite	PVD, Hydrothermal Process	D: ~100 nm, L: 1 $\mu\text{m}$	~3 mV	Not stated	[26]
BaTiO <sub>3</sub>	Pervoskite	High temperature chemical reaction	D: ~280 nm, L: ~15 $\mu\text{m}$	~25 mV	~0.3 aJ	[27]
PVDF	Polymer	Electro spinning	D: 0.5~6.5 $\mu\text{m}$ , L: 0.1~0.6 mm	5~30 mV	2.5~90 pW	[28]
PZT	Nanofibers	Electro spinning	D: 60 nm, L: 500 $\mu\text{m}$	1.6V	0.03 $\mu\text{W}$	[29]
ZnO	2D Nanosheets	Aqueous solution	W: 80 nm, H: 3 $\mu\text{m}$	0.44V	2.86 $\mu\text{W}/\text{cm}^2$	[30]

### 1.3.2 Triboelectric Nanogenerators

The triboelectric nanogenerator (TENG) that converts ambient mechanical energy into electricity by a conjunction of triboelectric effect and electrostatic induction, was first reported by Z.L. Wang *et al* as a new power generation technology in 2012 [8] and since then TENGs have evolved dramatically mainly because of its great potential for scavenging mechanical energy from surrounding environment and sustainably driving portable devices [31]. TENG is based on the triboelectric effect that has been known for thousands of years and it happens when two different materials come into contact through friction and charge transfer occurs where one material tends to gain electrons and other tends to give electrons away to equalize their electrochemical potential, thus producing triboelectric charges on the surfaces.

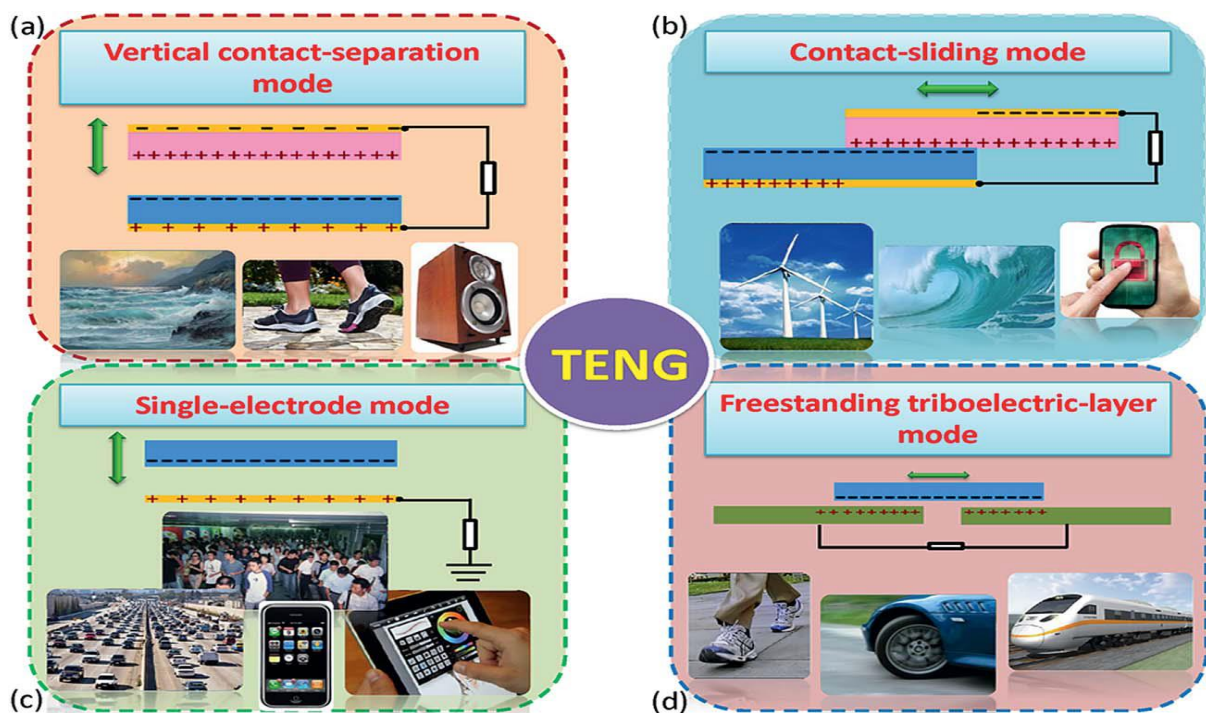


Figure 1.5 The four fundamental modes of triboelectric nanogenerators: (a) vertical contact separation mode; (b) in-plane contact-sliding mode; (c) single-electrode mode; and (d) freestanding triboelectric-layer mode [Adapted from Ref. 34 with permission from Royal Society of Chemistry].

The cycled separation and re-contact of the inner surfaces of the two dissimilar triboelectric layers induces a periodic potential difference between the electrodes connected to the two materials and this periodic potential difference drives the electrons back and forth in order to balance the electric potential drop created and hence producing alternating current (AC) signals.

Figure 1.4 shows four different working modes of TENGs. In vertical contact separation mode, two dissimilar triboelectric films face with each other, make physical contact between them and then separate due to external mechanical vibration as shown in Figure 1.4 (a) and because of this periodic contact and separation, two current signals in opposite directions are found. In lateral sliding mode, a relative sliding in parallel to the surface creates triboelectric charges on the two surfaces resulting lateral polarization as shown in Figure 1.4(b), which drives the electrons between the top and bottom electrodes to balance the field created by the triboelectric charges. A single electrode based TENG is a more feasible design for some applications, for example in the case when the object that is part of the TENG cannot be electrically connected to the load. In this operation mode, the bottom part of the TENG is grounded as shown in Figure 1.4(c). The freestanding triboelectric-layer TENG is based on the triboelectric effect between a freestanding dielectric layer and two metal films as shown in Figure 1.4(d) that serve not only as the counter triboelectric material, but also as two electrodes. When the two surfaces are in contact, the triboelectric effect will render the dielectric surface with negative charges, and other metal electrodes with positive charges and the movement of the dielectric layer drive the electrons back and forth between two electrodes and results current signals passing through external load.

Among various energy harvesting technologies, TENG has many advantages over others, such as high electrical output power, low cost, easy fabrication processes, high conversion efficiency etc. To optimize performance of TENGs, various methods have

been adapted including using different triboelectric materials, creating of micro-/nano structures on the materials' surfaces, developing novel device structures, designing multi-layered devices, incorporating electric double layer effect etc. [33]. TENGs can be used not only as micro-scale power sources and self-powered sensors but also as macro-scale power sources through proper materials selection, innovative device structure design and modifications. Although TENGs have experienced a rapid development both in fundamental understanding and technological improvements, there are several areas for further improvement [34], for example understanding the fundamental mechanism of contact-electrification and quantifying the surface charge density, exploring new materials, developing proper power management and energy storage units etc.

### **1.3.3 Hybrid Nanogenerators**

Hybrid nanogenerators integrate different types of harvesters in a single unit, where several energy sources can be leveraged either simultaneously or individually, making it possible to use whatever energy is available at any time. This approach provides a continuous supply of power through renewable and green energy resources, and helps maximize energy utilization to achieve a stable electrical output. With the integration of different kinds of energy harvesting techniques in the same platform, for example, pyroelectric nanogenerator, PENG, TENG, electromagnetic generator, solar cell, and/or electrochemical cells, hybrid energy cells have opened up a novel branch of nanotechnology research soon after their first demonstration in 2009 [35], that could lead to a highly effective method of ambient energy harvesting, particularly for self-powered electronic systems and the IoT.

**Table 1.2** Key points of some of the current hybrid nanogenerators.

Hybrid Type	Active Material	Harvested Energy	Output Performance of Hybrid NG	Applications	Ref.
Piezo and solar	ZnO NWs	Solar and mechanical	0.433 V, 252 $\mu\text{A}/\text{cm}^2$ , 34.5 $\mu\text{W}/\text{cm}^2$	Self-powered electronics	[36]
Piezo and solar	ZnO NWs and silicon	Solar and strain	3 V and 280 $\mu\text{A}$	To drive wireless strain gauge sensor	[37]
Piezo and bio-fuel cell	ZnO, Au and CNT	Mechanical and biochemical	3.1 V, 300 nA	Biological sciences, Environmental monitoring	[38]
Piezo and Tribo	PVDF (Piezo) and PTFE and Au (Tribo)	Mechanical	370 V, 12 $\mu\text{A}/\text{cm}^2$ , 4.44 $\text{mW}/\text{cm}^2$	Drive 600 LEDs with 0.2 N force	[39]
Piezo and Tribo	ZnO NRs (Piezo) and PDMS and Cu (Tribo)	Mechanical	10.2 $\text{mW}/\text{m}^2$ (PENG), 42.6 $\text{mW}/\text{m}^2$ (TENG), Combined charged 1.2 V battery in 400 s	Self-powered pressure sensor	[40]
Tribo, Solar, Chemical	PTFE and Al (Tribo), Silicon (Solar), NaCl solution	Wind, Solar, Chemical	60 V, 500 $\mu\text{A}$	Self-powered wind and temperature sensor	[41]
Tribo and solar	PDMS and ITO (Tribo), Silicon (SC)	Mechanical, Solar	12 V, 17.4 mA	Electrodeposition, Pollutant degradation, Self-powered electronics	[42]
Tribo and Solar	FEP and Cu	Wind, Solar and Mechanical	12 mA	To power temperature and humidity sensor	[43]
Tribo and Thermal	PTFE, Al	Mechanical, Thermal	14.98 $\text{mW}/\text{cm}^2$	Increase efficiency of rotation based device	[44]
EM and Tribo	PVB/PDMS, Cu	Biomechanical	100 $\mu\text{F}$ capacitor charged by 39 s	To run commercial watch	[45]
EM and Tribo	PTFE and Al (Tribo), Magnet and coils	Wind energy	17.5 $\text{mW}$ , 55.7 $\text{W}/\text{m}^3$	Real time monitoring of traffic volume	[46]

## 1.4 Theoretical Background

The physics behind nanogenerator technologies can be explained using Maxwell's electromagnetic equations. The piezoelectric nanogenerator was first proposed in 2006 based on the piezoelectric effect [16], while the triboelectric nanogenerator was later proposed in 2012 based on the triboelectric effect [8]. When two dissimilar materials are brought into contact, electrostatic charges are created on the surface of the two materials owing to their different electron affinities. When the two materials are subsequently separated, a voltage is developed that forces the electrons to flow between the two electrodes, generating an alternating current for a triboelectric nanogenerator (TENG). However, when a mechanical stress is applied on a piezoelectric material, it becomes polarized, creating a piezo-potential.

To fully understanding the difference between the physics underlying electromagnetic generators and nanogenerators, it is necessary to understand the relationship between Maxwell's displacement current and nanogenerator's output. Ampere's circuital law with Maxwell's addition is given by:

$$\nabla \times H = J + \frac{\partial D}{\partial t} \quad (1)$$

Where H is magnetic field and D is displacement field.

$$D = \epsilon_0 E + P \quad (2)$$

Here P is the polarization field and E is the electric field. So, the Maxwell's displacement current can thus be defined as:

$$J_D = \frac{\partial D}{\partial t} = \epsilon_0 \frac{\partial E}{\partial t} + \frac{\partial P}{\partial t} \quad (3)$$

The first part of this equation gives the birth of electromagnetic wave. The second part



relates the output of the nanogenerator. If the density of charges on the surface of the piezoelectric nanogenerator is  $\sigma_p$ , and there is no external electric field, then the displacement field will be the polarization vector. So, the displacement current will thus be [47].

$$\frac{\partial D}{\partial t} = \frac{\partial P}{\partial t} = \frac{\partial \sigma_p}{\partial t} \quad (4)$$

Equation (4) denotes the observed output current for the piezoelectric nanogenerator (PENG). Similarly, for the TENG, if the triboelectric charge density in dielectrics is  $\sigma_c$ , and therefore the free electron density on the electrodes is  $\sigma_1$ , then the displacement current will be [47]

$$\frac{\partial D}{\partial t} = \frac{\partial \sigma_1(z, t)}{\partial t} = \sigma_c \frac{\partial x}{\partial t} \quad (5)$$

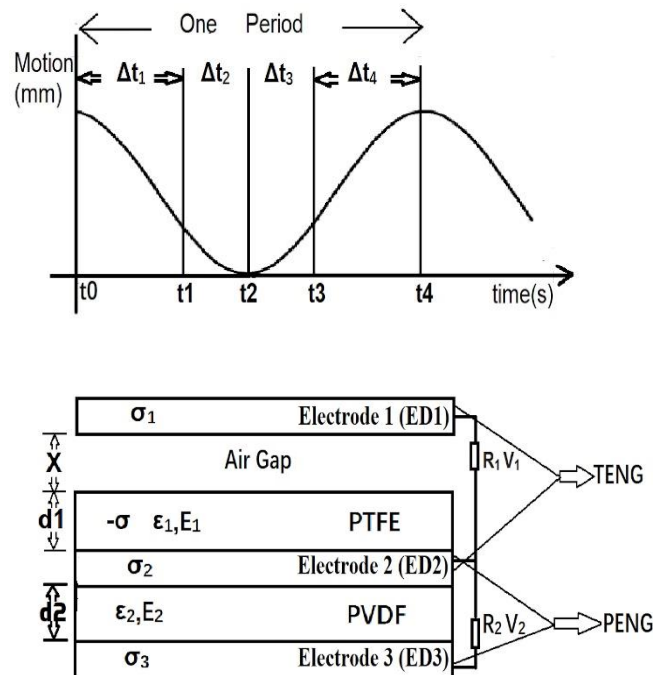


Figure 1.6 Theoretical analysis approach for piezo-tribo hybrid nanogenerator (a) Motion characteristics of external load (b) PENG-TENG hybrid device.

This is the observed current for TENG.  $\partial x/\partial t$  depicts the speed at which two tribo layers contacts with each other. This basic understanding of nanogenerator operation was vital to further modeling and analysis; however, a specific theoretical model for hybrid nanogenerators was developed only recently, in 2017. Song et al. [48] presented the first theoretical model for piezo-tribo based hybrid nanogenerators, and later extended the analytical approach based on the following three conditions: (a) PENG and TENG are separate units (b) tribo charges are uniformly distributed on the electrode (c) electric potentials are regarded as a closed loop in a circuit. Considering the above three conditions, it is possible to write from Fig. 1.6(b) that

$$V_a + V_{PT} + V_1(t) = 0 \text{ and } V_{PV} + V_2(t) = 0 \quad (6)$$

Where  $V_a$ ,  $V_{PT}$  and  $V_{PV}$  are the voltages across the air gap, the PTFE layer and the PVDF layer, respectively, and  $V_1$  and  $V_2$  are the voltages across the external resistors. The test cases for this hybrid nanogenerator can be assumed from Fig. 1.6 that, after applying the external impact from time  $t=0$ , the top electrode ED1 makes contact with PTFE at  $t=t_1$  (after  $\Delta t_1$  time from  $t=0$ ), then the whole device starts deforming and reaches its highest deformed stage at  $t=t_2$  (after  $\Delta t_2$  time from  $t=t_1$ ). So, after  $t=t_2$  time the device starts releasing and at  $t=t_3$  (after  $\Delta t_3$  time from  $t=t_2$ ) the device again reaches its same position like  $t=t_1$  and finally at  $t=t_4$  (after  $\Delta t_4$  time from  $t=t_3$ ) ED1 starts breaking contact with PTFE and reaches the initial position, thus completing one cycle of operation. In this approach,  $x_1$  and  $x_2$  will be used to express the dynamics of ED1 and ED2 (top electrode of PVDF based PENG). If the transferred charges in ED1, ED2 and ED3 are  $Q_1$ ,  $Q_2$  and  $Q_3$  respectively, then V-Q-x relationship for the top TENG unit can be expressed as [49]

$$R_1 \frac{dQ_1}{dt} + (d_{r1} + x_1(t)) \frac{Q_1}{S\epsilon_0} - \frac{\sigma}{\epsilon_0} x_1(t) = 0 \quad (7)$$

Where  $s$  is the surface area,  $d_{r1}$  is the effective thickness constant for PTFE ( $d_{r1} = \frac{d}{\epsilon_r}$ ),  $\epsilon_r$  is relative permittivity, and  $\sigma$  is the surface charge density. Assuming the initial condition

( $Q_1=Q_3=0$  and  $Q_2=\sigma s$ ) at ( $t=t_0=0$ ), equation (7) can be solved as [50]

$$Q_1(t) = S\sigma - e^{\int_0^t \frac{d_r + x_1(\tau)}{R_1 S \epsilon_0} d\tau} \left( S\sigma + \int_0^t \frac{\sigma x_1(\tau)}{R_1 \epsilon_0} e^{\int_0^\tau \frac{d_r + x_1(\gamma)}{R_1 S \epsilon_0} d\gamma} d\tau \right) \quad (8)$$

So, this is the charge transfer equation for the TENG unit, and is valid within the time limit  $\Delta t_1$  and  $\Delta t_4$  as TENG works at these time ranges.

From equation (6), the charge transfer equation for the PENG unit can be written as [49]

$$E_2 d_2(t) + R_2 \frac{dQ_2}{dt} = 0 \quad (9)$$

where the thickness  $d_2$  and electric field  $E_2$  inside this PENG's PVDF are

$$d_2(t) = d_0 - x_2(t) \quad (10)$$

and from Gauss's law [49]

$$E_2 = \frac{Q_2}{S \epsilon_{r2} \epsilon_0} \quad (11)$$

$d_0$  is the initial thickness of the PVDF film before deformation, and  $d_{r2}$  is the effective thickness constant for the PVDF film. As, it is assumed that the PENG and TENG units are working

independently, when deriving the charge transfer equation for PENG unit, the time ( $t$ ) is redefined as  $t=0$ , but actually PENG unit starts working at  $t=t_1$  when the device starts deforming. From Fig. 1.6(a), it is found that  $t=t_1 \neq 0$ , so the initial condition for this PENG unit can be obtained as  $Q_1=0$  and  $Q_2=Q_3=Q_0$ , where  $Q_0$  is the initial surface charge induced by the piezoelectric effect. From this initial condition combining equations (9), (10), (11), charge transfer equation for the PENG unit is found as [49]

$$Q_2 = Q_0 e^{-\int_0^t \frac{(d_0 - x_2(\tau))}{R_2 S \epsilon_r \epsilon_0} d\tau} \quad (12)$$

It is clear from Fig. 1.6(a) that equation (12) is valid for  $t=0$  and  $t= \Delta t_2 + \Delta t_3$ , because the PENG unit only works for that time frame. From the charge transfer equation for the PENG and TENG units, it is also possible to obtain the current and voltage expressions for this hybrid nanogenerator. This theoretical approach for hybrid nanogenerator can be used to qualitatively [49] describe the PENG and TENG based hybrid nanogenerator; however, it should be used with caution as it yields substantial errors in predicting PENG characteristics. Another important limitation is that the model assumes the output of the two units are added in series; it has not considered the synergetic effect of the hybrid nanogenerator.

## 1.5 Research Objectives

The fundamental goal of this research is to systematically investigate different aspects of PENG, TENG and HNG devices based on different nanostructured materials utilizing novel nano fabrication techniques and to optimize different materials synthesis as well as device parameters to enhance the device performance for different potential applications, such as aircraft SHM, wearable electronics, self-contained and non-invasive integrated self-powered data transmission system etc. For achieving this goal, the research conducted strives to design, fabricate and characterize a PENG

based on ZnO nanostructures and a HNG based on nanostructured organic/inorganic materials integrating piezoelectric and triboelectric effects.

The following approaches are used to achieve this goal:

- i) The direct synthesis and characterization of 1D/2D hybrid ZnO nanostructures on metal substrates using a simple low-temperature hydrothermal process.
- ii) Development and installation of a device characterization system for comprehensive analysis of the piezoelectric and triboelectric outputs of the energy harvesting devices.
- iii) Demonstration of a high performance consolidated PENG device based on the piezoelectric ZnO nanomaterials.
- iv) Integration of the PENG device with a TENG device to develop a compact HNG that can improve the energy harvesting efficiency as both the PENG and TENG components can work simultaneously and/or separately in a single press-and-release cycle.

## **1.6 Thesis Overview**

The focus of this thesis is to describe the design, fabrication and characterization techniques of PENG, TENG and hybrid devices for improved performance and propose new schemes to further enhance their performances. The introduction and background discussion in Chapter 1 explains the motivation for this research work and the approaches taken to reach the research goals therein by briefly elucidating on different energy harvesting technologies for self-powered systems along with their theoretical background. Chapter 2 describes various experimental methodologies that have been adapted in the research, such as approach for materials selection for the PENG and TENG parts, optimization of the synthesis processes to get desired

nanostructures, development of a characterization system for the harvester devices etc. A comprehensive study on a PENG device based on ZnO nanowires and nanoplates is presented in Chapter 4 and the chemistry behind the growth of 1D/2D hybrid ZnO nanostructures and their role in the device performance are explained as well. This chapter also discusses how to control the growth mechanism of different ZnO nanostructures, the critical role of different parameters during the hydrothermal growth process and justifies the performance improvement of the PENG device resulting from this hybrid material system. Demonstration of a hybrid nanogenerator that integrates piezo and tribo electric effects in a single device structure with a common electrode between them is presented in Chapter 4. The advantages of the hybrid device, for example mutual enhancement of the output voltages of the PENG and TENG parts, high electrical output power, potential application for self-powered wireless data transmission system etc. are also described. Finally, the thesis concludes with the contributions and future outlook of this research in Chapter 5.

## Chapter 2

### Experimental Methodologies

The thesis work can be divided into three major parts: materials synthesis, materials characterization and device application. The materials synthesis part includes the synthesis of ZnO nanowires and nanoplates on different substrates for the piezoelectric nanogenerator, creation of nanostructures on the PTFE and aluminium surfaces for the triboelectric nanogenerator. Two different levels of characterizations have been used in the work: Firstly, structural and morphological characterization and analysis of different nanostructured materials; Secondly, device characterization. To characterize the as grown nanostructures as well as nanostructured materials different techniques such as AFM, SEM, XRD etc. have been employed. And after the device fabrication using different target nanomaterials, the devices have been tested using a specially designed characterization system including a vibration controller unit, linear shaker, power amplifier and accelerometer.

This chapter starts by describing different techniques for ZnO nanostructure growth with a particular focus on hydrothermal method as well as the key factors in this method that play critical roles during the solution based growth, for example solution concentration, growth temperature, substrate type, seed layer type and thickness etc. Then, it proceeds by elucidating on different materials for triboelectric nanogenerator and different micro-/nano fabrication techniques to make nanostructures on top of the materials' surfaces as nanostructured tribo materials lead to improved efficient friction between two tribo materials thus improve the performance of the triboelectric nanogenerators. After that, a systematic way to design a hybrid nanogenerator structure has been presented to harvest energy more efficiently and elegantly. Finally, this chapter ends by describing the systematic way of device characterization by illustrating the set up schematic and required instruments.

## 2.1 Materials for Piezoelectric Nanogenerator

Recently different piezoelectric materials have attracted close attention as active materials in piezoelectric energy harvesters, self-powered sensors, and actuators [52-53]. To date, many piezoelectric materials, including ZnO nanowires [54-55] and nanoplates [56], III-N nanowires [57], piezoelectric ceramics, i.e. lead zirconate titanate (PZT) [58-59], barium titanate ( $\text{BaTiO}_3$ ) [60] and poly polyvinylidene difluoride (PVDF) [61], have been synthesized and exploited to fabricate piezoelectric nanogenerators (PENG) as they significantly improve the device output performance. On the other hand, various fabrication processes such as densely aligned nanowire growth, transfer techniques, electrospinning, compositing methods, nano-patterning, etc. have been extensively studied to achieve high-performance PENG devices [62-64]. Although the use of nanostructured piezo electrics is a relatively recent development, and the understanding of the nanoscale size effects on piezoelectricity is still being formulated, the application of piezoelectric nanostructures to energy harvesting has expanded rapidly in the last decade leading to a huge range of reported devices and most studies focus on zinc oxide, as its nanostructures are formed relatively easily using low temperature methods [65-66]. Until now, numerous works have demonstrated the growth of crystallographically-aligned ZnO nanowire (NW) arrays using low-temperature chemical synthesis methods on a wide range of substrates [67-69]. Besides, some reports indicate that it is possible to easily tweak the chemical synthesis method to form different nanostructures of ZnO, i.e. nanosheets (NS), nanocombs, nanorings, nanohelices/nanosprings, nanobows, nanobelts, nanocages etc. by using of different chemical compositions, or different substrate materials [70]. In the first part of this research, our aim is to grow ZnO nanowires and nanosheets on different substrates for efficiently harvesting piezoelectric energy and improve the performance of the PENG devices based on the ZnO nanostructures. It is well-established that the performance of a PENG device based on ZnO nanostructures depends not only on their piezoelectric coefficient, but also on their ability to suppress



the screening effect of mobile charge carriers [71]. As undoped ZnO NWs and NSs are typically n-type semiconductors with a high density of electrons and these mobile electrons can completely screen out the strain-induced piezoelectric potential [72], several approaches have been demonstrated to overcome this fundamental constraint, including surface oxygen plasma treatment [73], triboelectric layer insertion [74], p-n junction formation [75-76], metal-semiconductor Schottky junction formation [64] etc. G. Liu *et al* have demonstrated that growing p-n junction type ZnO nanowires instead of using intrinsic ZnO nanowires can dramatically suppress the piezoelectric charge screening effect and thus enhances the overall PENG performance up to eleven-fold if the doping concentration is properly controlled [77]. So, instead of growing pristine ZnO nanostructures, growing p-n junction type ZnO NWs and NSs as well as utilizing an easier, straight forward and cost effective method is another focus of this work.

#### 2.1.1 Synthesis Techniques for ZnO nanostructures

During the last few decades, various one-dimensional and two-dimensional nanostructures have been extensively investigated as they have demonstrated enthralling properties due to their quantum confinement effects which results from their low dimensionality. Most of the studies have primarily been focused on the synthesis and fabrication of this nanostructures cost effectively at the same time keeping superior material quality for their practical applications. Typically, two types of synthesis and fabrication techniques are generally used for creating and manipulating different kinds of nanostructures. One is the so called “bottom-up” technique using vapor phase deposition, chemical synthesis, self-assembly and location manipulations. The other is the “top-down” approach utilizing different lithography equipment and precision engineered tools like cutting, etching, grinding etc. to fabricate nanoscale objects out of bulk materials. In the bottom-up category, several approaches have been well-established, which include an extensively explored vapor phase deposition method, including chemical vapor deposition (CVD) and

physical vapor deposition (PVD), and liquid phase deposition (solution synthesis approach).

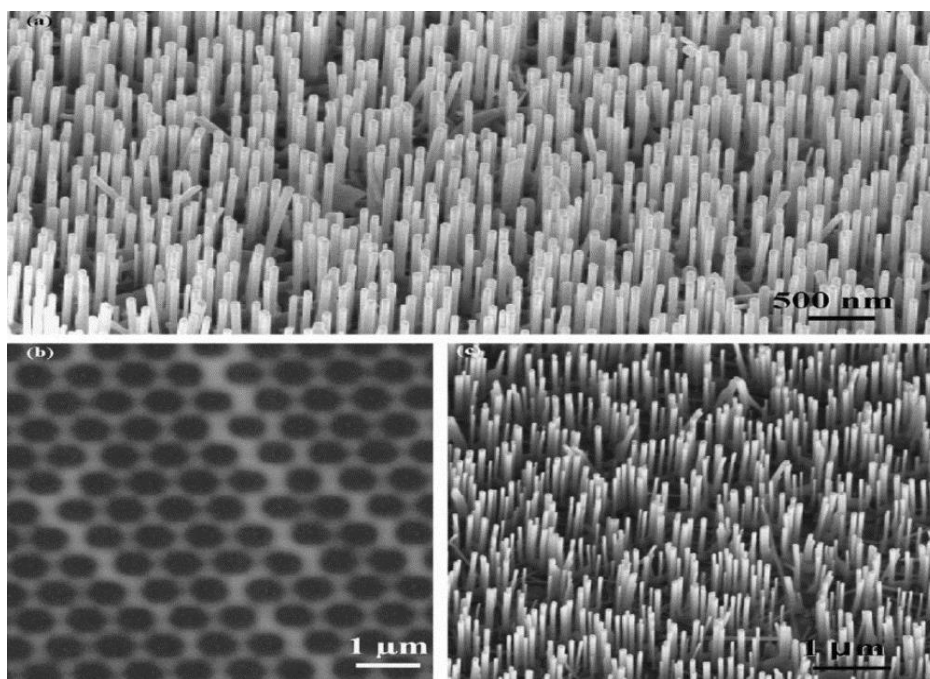


Figure 2.1 (a) SEM image of aligned ZnO nanowires grown on sapphire substrate using a thin layer of gold as catalyst. (b) SEM images of gold catalyst patterns using PS sphere monolayer as mask. (c) SEM image of aligned ZnO nanowires grown with a honeycomb pattern [Adapted from Ref. 78 with permission from The Royal Society of Chemistry].

Of all the various morphologies of ZnO nanostructures, ZnO nanowires have become increasingly popular for broad range of high-technology applications, ranging from surface acoustic wave filters, photonic crystals, light-emitting diode, photodetectors, photodiodes, optical modulator waveguides, varistors, and gas sensors, solar cells, to energy harvesting devices, due to its wide bandgap, excellent chemical and thermal stability, and its specific electrical and optoelectronic property of being a II-VI semiconductor with a large exciton binding energy. Besides, due to the simultaneous presence of semiconducting and piezoelectric properties [79], intensive and state-of-the-art research is going on in the area of synthesis and characterization of different forms of ZnO nanomaterials including nanowires, nanotubes, nanobelts, nanorods,

nanosheets etc. There are numerous techniques that have been used to synthesize vertically aligned ZnO nanowires including vapor-liquid-solid processes (VLS) [80], solution-based processes [65], electrodeposition [81], sol-gel [82], oxide or polymer-assisted growth [83] etc. VLS procedures, operating at rather high temperatures between 900-1400°C, have been a very popular and proficient means of synthesizing aligned ZnO nanowires as the vertical alignment of ZnO nanostructures can be assisted by either an electric field or through the use of lithographic patterning techniques or by proper lattice matching between ZnO and the epitaxial substrate.

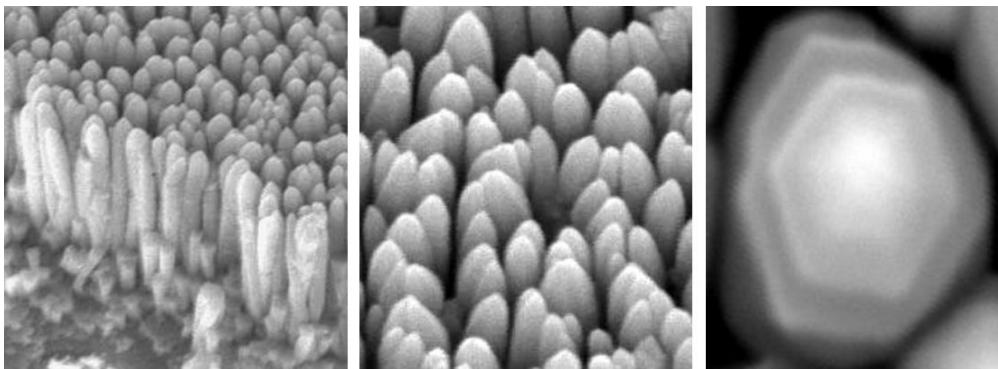


Figure 2.2 SEM images of ZnO nanorods formed on sapphire (0001) substrates. (a) Images observed from a cleaved surface. (b) Images taken with a tilt angle. (c) Image of the top of a single ZnO nanorods [Adapted from Ref. 85 with permission from IOP Publishing].

Having aligned nanowires is critical for specific applications such as light-emitting diodes, field-effect transistors, and lasers [84]. In VLS, there is a metal (e.g., Au, Fe, or Sn) that serves as a catalyst to promote the reaction between the specific nanowire component(s) and the liquid alloy drops that form for preferred site deposition. Au is most commonly used as the catalyst for VLS- based one-dimensional ZnO growth. Once the liquid is supersaturated with the reactants, nanowire growth is initiated [85]. Nanowire growth is terminated when either the reactants are completely used or when the catalyst is no longer in the liquid state due to temperature cooling below its eutectic temperature [86]. Moreover, during growth, the aligned growth of nanowires

perpendicular to the substrate can be achieved when there is a negligible lattice mismatch between the nanowire array and the substrate. The SEM images of aligned nanowires grown on AlGaN substrates via the VLS process using a gold catalyst are provided in Figure 2.1.

Another method that is very efficient in producing epitaxial growth of well-aligned ZnO nanowires is the metal-organic chemical vapor deposition (MOCVD) method. In this method, metal-organic precursors are used to aid the growth process. Some of the advantages of MOCVD over the VLS processes is that it has a catalyst-free growth mechanism, and much lower temperatures can be employed (350-500°C). Furthermore, Zhang et al. have applied MOCVD to discover a feasible means of obtaining the growth of ZnO (c-axis) normal to the substrate, which demonstrates the significance of MOCVD in large area industrial ZnO applications [87]. Typically in the MOCVD process, metal alkyls such as dimethyl zinc (DMZn) or diethyl zinc (DEZn) are used as the precursors that prompt ZnO deposition through its vapor phase chemical reactions on the substrate [86]. Typical substrates used in MOCVD include SiC, Al<sub>2</sub>O<sub>3</sub> (sapphire), GaN/Si, and GaN/sapphire. The function of the carrier gas (e.g., O<sub>2</sub>, N<sub>2</sub>, or Ar) is to transport the precursor reaction into the growth region. Moreover, it is important for the precursors that are employed to be as less reactive as possible with the carrier gases to lessen the effects of parasitic reactions in the vapor phase [86].

Figure 2.2 provides SEM images of aligned nanowires grown on sapphire (0001) substrates via MOCVD using O<sub>2</sub> gas and DEZn as reaction precursors, N<sub>2</sub> as the carrier gas, and employing substrate temperatures ranging from 400-500°C.

Although these previously mentioned processes are highly efficient and dominant in the synthesis of ZnO nanowires, solution-based processes result in sufficient nanowire structures and have proved to be more beneficial due to their simplicity and economic feasibility under less rigorous synthesis conditions. In 2003, L.E. Greene *et al.*

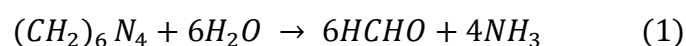
demonstrated a low-temperature wafer-scale production of ZnO nanowire arrays that enables the generation of ZnO nanostructures, at large-scale, low-cost, and moderate temperature [65].

### 2.1.2 Hydrothermal Growth of ZnO Nanostructures

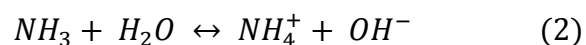
Amongst the different methods for the synthesis of ZnO nanostructures, the hydrothermal method is attractive for its simplicity and environment friendly conditions. This section summarizes the general working mechanism of the hydrothermal method as well as the salient influences of different growth parameters leading to the growth of different ZnO nanostructures using hydrothermal technique such as growth temperature, substrate type, solution concentrations, seed layer etc.

The conventional hydrothermal method for ZnO nanowires and nanorods growth requires zinc nitrate and hexamine solutions in deionized water with similar concentrations. Before the hydrothermal growth a thin ZnO seed layer is usually deposited as it not only promotes heterogeneous nucleation on an arbitrary substrate but also helps grow the nanowires in specific locations and orient the nanowires upright for subsequent nanowire growth and it has been confirmed as a requirement to grow vertically aligned ZnO nanostructures [69, 90]. ZnO nanowires are grown by submerging the seeded substrates inverted in the growth solution at around 85°C for different growth periods. The basic chemical reactions that take place in the solution mixture for the growth of nanowires can be described as follows [88]:

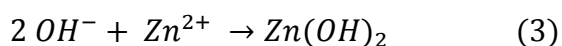
Decomposition reaction:



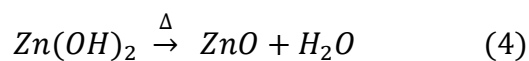
Hydroxyl supply reaction:



Supersaturation reaction:



ZnO nanowires growth reaction:



In the hydrothermal approach, due to the presence of several controlling parameters that can be easily tweaked to synthesize the desired nanostructures, a controlled growth condition is critical. In this research some key parameters such as temperature, substrate type, seed layer thickness, and sample duration in solution are few critical parameters that has been carefully controlled to assist the growth of particular type of nanostructures.

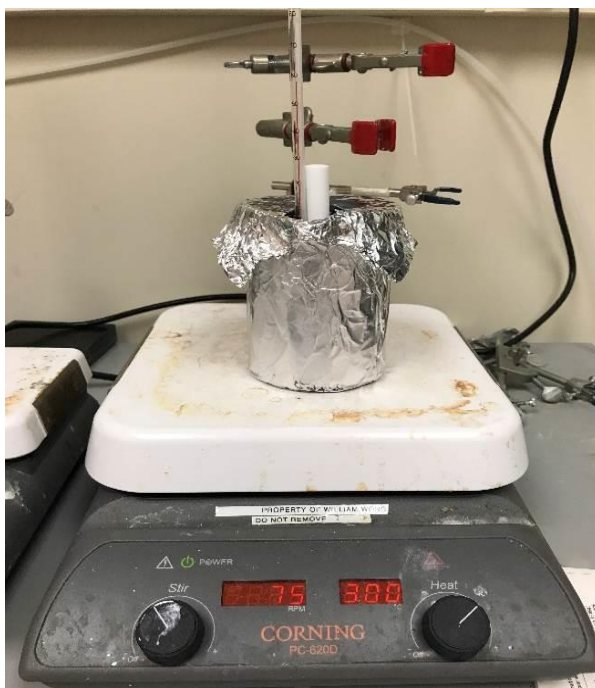


Figure 2.3 Hydrothermal set up for the growth of ZnO nanostructures.

Figure 2.3 shows the set up for the hydrothermal growth of desired ZnO nanostructures. This simple set up consists of a hotplate to precisely set the solution

temperature, a magnetic stir-bar to continually establish a uniform solution, a thermometer, Al foil covers to minimize evaporation of the solution, a Teflon sample carrier, and beakers.

As this research is aimed to grow different types of ZnO nanostructures for different purposes, their growth parameters and conditions will be discussed individually in the following chapters. However, it is worth to mention here how few critical parameters affect the growth of ZnO nanostructures and what can be the possible adjustments to control the growth of a particular type of nanostructures, i.e. nanowires, nanorods, nanosheets etc.

#### 2.1.2.1 Effect of Growth Temperature

As already discussed, synthesis of different types of ZnO nanostructures has carefully been studied because of their unique and attractive properties as well as their versatile applications. In the solution based hydrothermal growth method, solution temperature plays critical role in the formation of different types of ZnO materials.

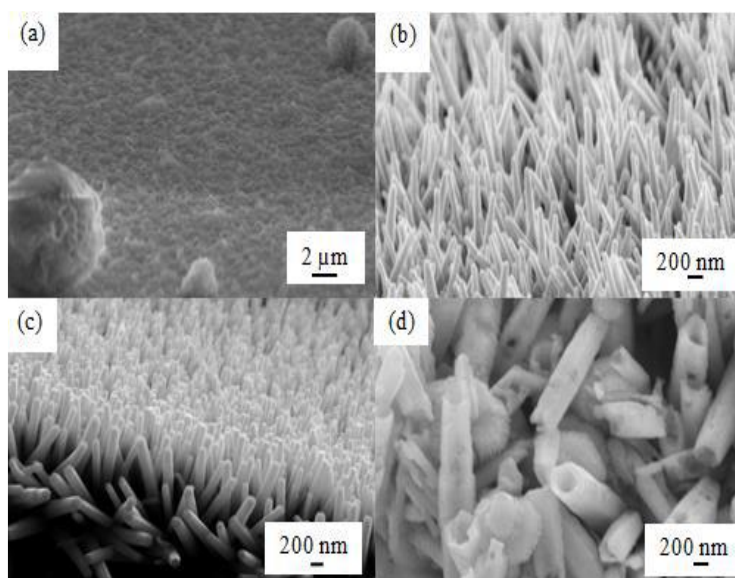


Figure 2.4 Effect of temperature in hydrothermal method. (a). Undesired nano-islands formation at  $< 75^{\circ}\text{C}$ , (b) nanowires at  $88^{\circ}\text{C}$ , (c) nanorods at  $90^{\circ}\text{C}$ , and (d) nanotubes grown at  $97^{\circ}\text{C}$ . [Adapted from Ref. 89 with permission from Minoli Pathirane]

During the growth process, the thermal decomposition of zinc nitrate hexahydrate provides the required  $Zn^{2+}$  ions while HMTA provides hydroxyl ions at a controlled rate to ensure the supply doesn't get depleted by precipitation [88]. At low temperatures, the thermal energy is not enough for species to dissociate and bond thus producing desired nanostructures and as a result there is a threshold temperature that is required for the growth of ZnO nanowires and nanoplates. Although elevated temperatures are expected to help nanostructure growth, continuing to increase the temperature beyond a certain temperature threshold lead to unexpected nanostructures such as hollow nanotubes or disordered growth of nanowires and nanoplates. Consequently, for the growth of ZnO nanowires on PET substrate as well as ZnO nanowires/nanoplates on shim substrate, the temperature has been used in the range of 85°C to 90°C.

#### 2.1.2.1 Effect of ZnO Seed Layer

In the solution based growth of ZnO nanostructures, a thin ZnO seed layer not only provides heterogeneous nucleation to facilitate the nanowire and nanoplates growth but also helps position the nanostructures in specific locations and orient them upright. After Yamabi et al. verified that ZnO nanowires can be grown only if a ZnO crystalline seed layer is used [90], researchers have been using different methods to deposit a ZnO seed layer before the subsequent hydrothermal growth such as RF-sputtering of ZnO thin-film in a vacuum chamber, production of ZnO nanoparticles from the thermal decomposition of zinc acetate dihydrate salt etc. In this research, plasma enhanced chemical vapor deposition (PECVD) has been utilized to deposit thin layer of aluminium doped zinc oxide (AZO) as the seed layer at a temperature of 250°C and process pressure of 5mT. To keep consistency among samples temperature and pressure have been kept the same, however, the process time controls the thickness of the AZO layer and the thickness of this seed layer plays a critical role in the nanostructure formation.





Figure 2.5 Multi-chamber PECVD Cluster System.

As the thickness of the seed layer increases, the nanowire length decreases and the nanowire density increases. So to get desired nanowires and nanoplates density with expected height, the seed layer thickness is critical and should be optimized. As a too thin AZO layer (few nano meters) produces longer nanostructures with lower density and too thick (few hundreds of nano meters) produces highly packed nanostructures with lower height for a given amount of growth time, AZO layers ranging between 100nm - 200 nm have been used in this research.

#### 2.1.2.3 Effect of substrate in hydrothermal method

To see the effect of different substrates on the growth of different types of ZnO nanostructures, a range of substrates have been used ranging from rigid to flexible, metal to plastic. From Figure 2.6, it is evident that substrate has a strong influence in the growth mechanism of different ZnO nanostructures as well as on their morphological properties. When shim (an aluminium alloy) has been used as the substrate, the SEM image shows the growth of ZnO nanoplates along with the nanowires as shown in Figure 2.6 (d) and for that reason some researchers avoided

using aluminium in their device as bottom electrode for optoelectronic applications even though aluminium has higher reflectivity and electrical conductivity.

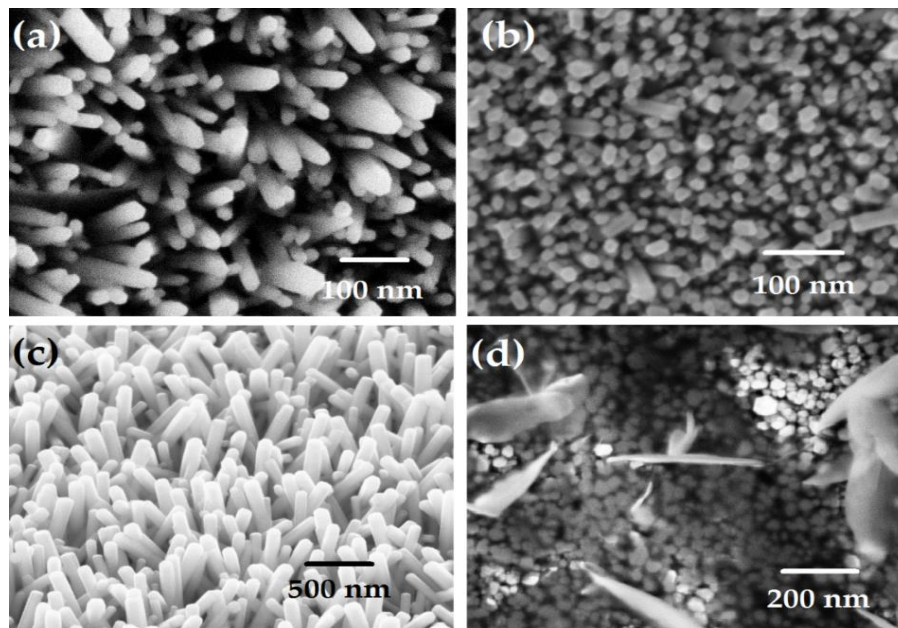


Figure 2.6 Scanning electron microscope images of the as grown ZnO nanostructures on (a) Glass substrate with 100nm AZO seed layer. (b) 100nm Cr deposited on glass substrate with 100nm AZO seed layer. (c) PET substrate with 200nm AZO seed layer. (d) Shim substrate with 400nm AZO seed layer.

The role of aluminium for the growth of ZnO nanoplates has been investigated in detail in Chapter 3.

## 2.2 Materials Selection for Triboelectric Nanogenerator

Triboelectrification is an effect that is known probably ever since the ancient time and it exists almost everywhere in our surroundings and also for almost every material that we encounter in our day to day life [91], yet it has been usually considered as a negative effect as discharges caused by triboelectricity causes many disastrous damages until recently before Z. L. Wang et al first demonstrated triboelectric nanogenerator (TENG) in 2012 [92] utilizing this triboelectrification effect between two dissimilar materials. Since then TENG has evolved drastically mainly because of

its unprecedented output performance, straight forward and low cost fabrication processes, excellent mechanical robustness and reliability, environmental-friendly etc. Besides, the most useful materials for TENG are organic, in fact TENG is the first of using organic materials for harvesting mechanical energy [93] that makes them ideal candidate for variety of applications ranging from different types of mechanical energy harvesting to self-powered sensor systems. Although there are four fundamental modes of operation of the TENG that have already been discussed in chapter 1, in general a TENG is based on the electrostatic charges created on the surfaces of two dissimilar materials when they are brought into physical contact and then separated by an external mechanical force [94].

As the electrostatic charges created on the materials' surfaces mostly determine the output performance of the device, carefully selection of triboelectric materials is of great importance. It is well-known that 'the triboelectric series' is a list of materials in order of decreasing tendency to charge positively (lose electrons), and increasing tendency to charge negatively (gain electrons) [93].

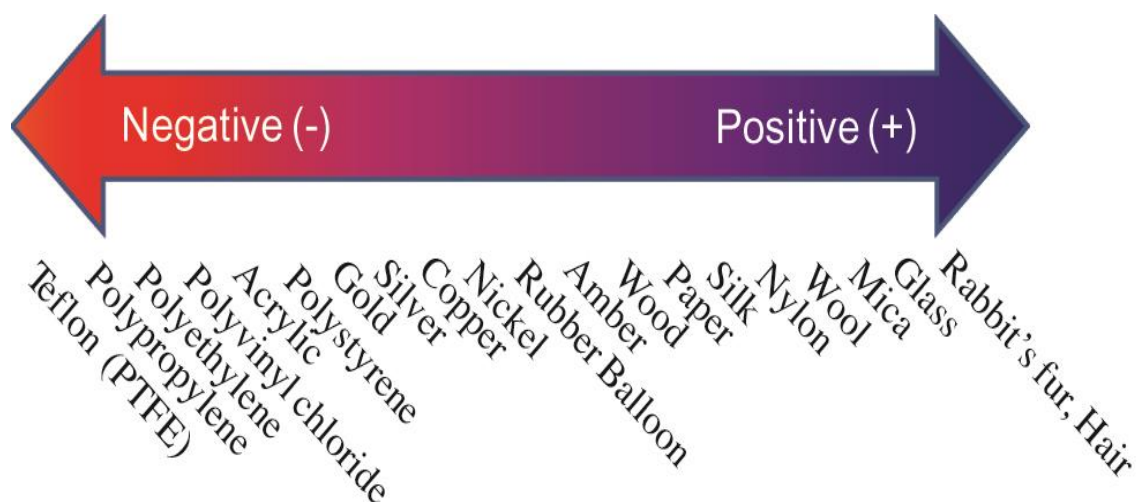


Figure 2.7 Example of a triboelectric series that shows an ordering of materials based on their empirically derived direction of charge transfer. A material closer to the top of the list contacted with a material closer to the bottom of the list will charge positively (while the other material charges negatively) [Reproduced from Ref. 96 with permission from IOP Publishing].

To design a TENG structure, two materials one from the top and another from bottom of this triboelectric series are usually selected. Once the materials are selected for a particular TENG device, there are several ways to enhance the triboelectrification effect hence to improve the device performance. For example, the morphologies of the surfaces can be fine-tuned by creating different kinds of micro- or nano-structures on the surface using different available fabrication processes that are proven to enhance the contact area and thus the triboelectrification [91]. Besides, the surface potential can be greatly enhanced by the surface functionalization by introducing various molecules, nanotubes, nanowires or nanoparticles on the materials surfaces [94]. Moreover, composite materials, such as embedding nanoparticles in polymer matrix, can be used as contact materials to improve the device performance [95] as these materials can enhance the electrostatic induction not only by changing the surface electrification, but also by changing the permittivity of the materials. Figure 2.7 shows a triboelectric series containing materials according to their tendency to gain or loose electrons in frictional and contact charging process.

### 2.2.1 PTFE as Triboelectric Material

Polytetrafluoroethylene (PTFE) is a synthetic fluoropolymer of tetrafluoroethylene that consists wholly of carbon and fluorine and is a solid compound at room temperature because of its high-molecular-weight. PTFE is the most suitable materials for TENG not only because it is one of materials on the triboelectric series having highest tendency to attract electrons but also due to its high strength, toughness and flexibility that originates from the aggregate effect of carbon-fluorine bonds [97].

Figure 2.8 shows two TENG devices based on PTFE thin films when nano porous aluminium foil has been used as another triboelectric material in the device as aluminium lies on the top side of the triboelectric series and has higher tendency to give away electrons during the electrostatic contact.

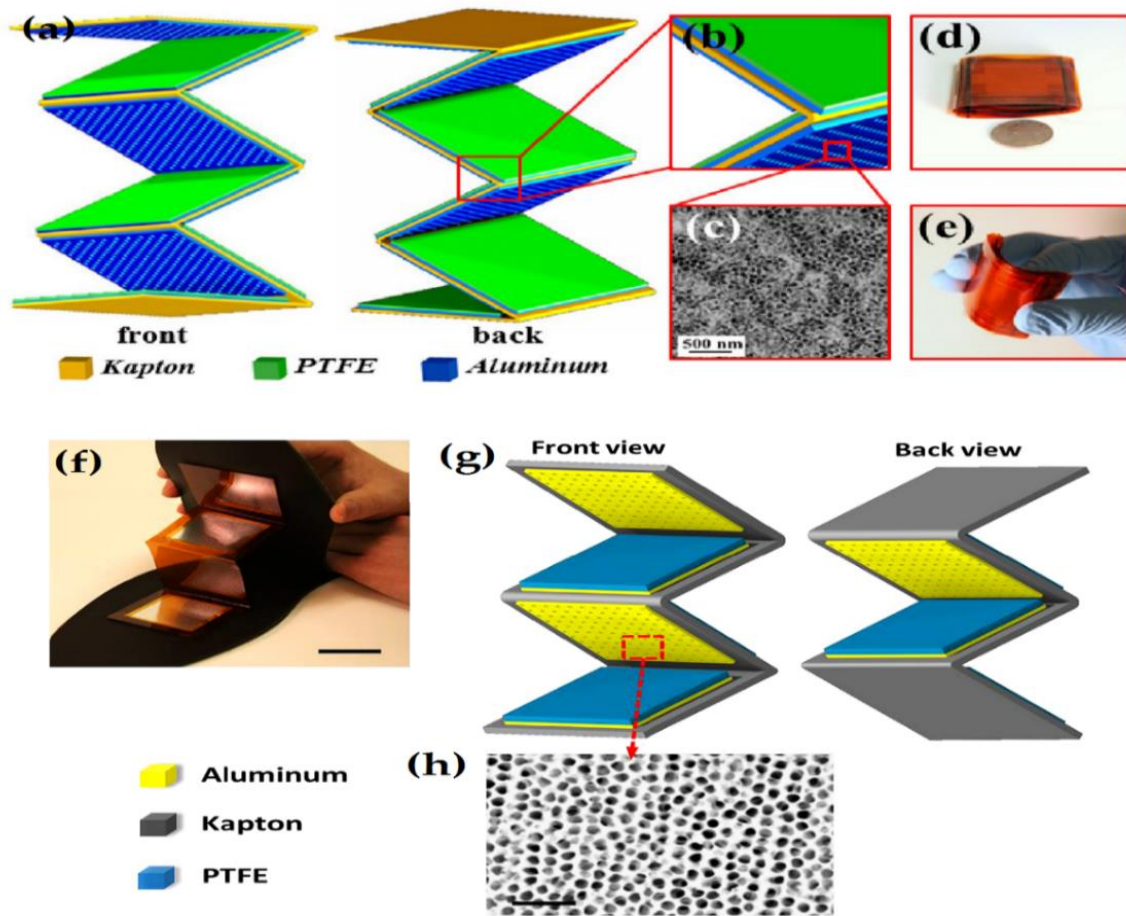


Figure 2.8 Structure and photographs of a flexible multilayered TENG. (a) Schematic and (b) an enlarged view of the zigzag-shaped structure of the TENG. (c) SEM image of nano pores on aluminum foils. Photograph of a fabricated TENG (d) Normal state (e) Bent by human finger [Reproduced from Ref. 98 with permission from American Chemical Society] (f) Photograph of the inner structure of shoe insole, showing a TENG installed. The scale bar is 2cm (g) Schematics from two different angles that reveal the device structure. (h) SEM image of nano-pores created at the surface of the aluminum foils. The scale bar is 200nm [Reproduced from Ref. 99 with permission from American Chemical Society].

The TENG device shown in Figure 2.8 (a) is a multi-layered device that produces the instantaneous short-circuit current ( $I_{sc}$ ) and the open-circuit voltage ( $V_{oc}$ ) of 0.66 mA and 215 V respectively with an instantaneous maximum power density of 9.8 mW/cm<sup>2</sup> [47] and the device shown in Figure 2.8 (f) is a flexible multi-layered TENGs enclosed

in the insole to harvest energy from foot pressure during normal walking and each TENG generates maximum open-circuit voltage of 220V and short-circuit current of 600  $\mu$ A [99]. However, none of these two devices use any surface modification of the PTFE film although it is expected to increase the effective friction between two tribo layers and to enhance the device performance. Although some other works demonstrate the use of PTFE nanowires or nanostructured polyamide (PA) polymer film as the tribo electric material layer in TENG devices [100], there is no hybrid energy harvester unit up to date that integrates a triboelectric nanogenerator with PTFE film and with nanostructures grown on both of the triboelectric layers.

### 2.2.2 Nanostructured Materials for Improved Device Performance

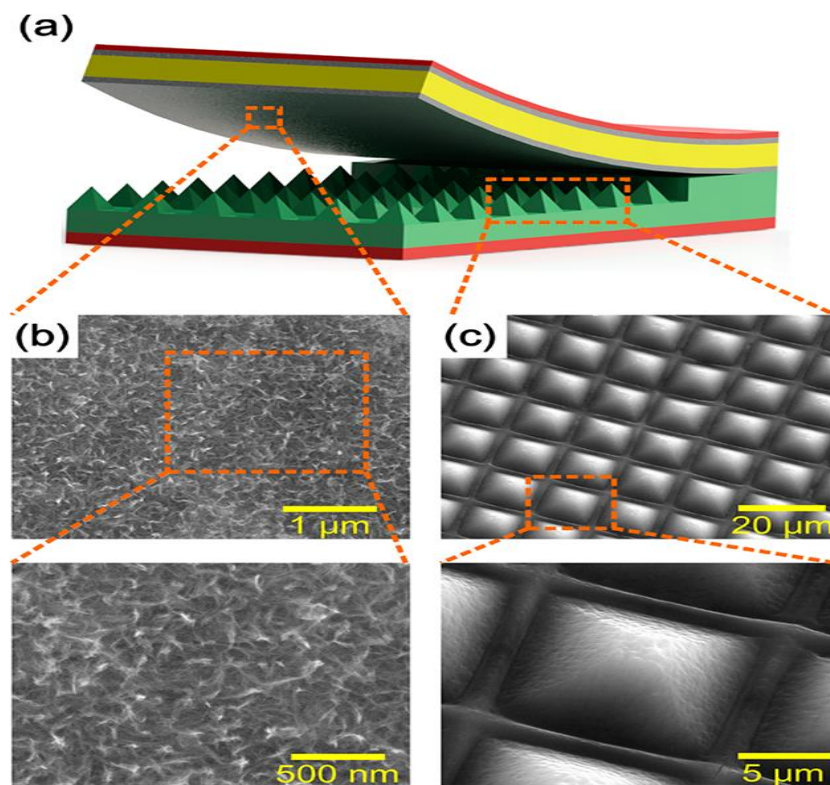


Figure 2.9 (a) Schematic view and photograph of the hybrid NG. (b) SEM images of the nanostructured aluminum electrode. (c) SEM images of the micro/nano dual-scale PDMS [Adapted from Ref. 101 with permission from American Chemical Society].

M. Han *et al* designed and fabricated an r-shaped hybrid nanogenerator as shown in Figure 2.9 (a) that uses polydimethylsiloxane (PDMS) layer and aluminum electrode as the two triboelectric layers with micro/nanostructures fabricated on both surfaces as shown in Figure 2.9 (b) – (c) with an aim of enhancing the device performance [101]. In this work, by using PVDF, nanostructured Al and micro/nano dual-scale (MNDS) PDMS, they innovatively combined the piezoelectric nanogenerator and the triboelectric nanogenerator together not only to enhance the output performance of individual components but also to improve the piezoelectric output through triboelectrification.

### **2.3 Design and Working Mechanism of Hybrid Nanogenerator**

Solar cells, electrochemical cells, piezoelectric/triboelectric/pyroelectric nanogenerators and magneto electric energy harvesters are enabling technologies for converting solar, chemical, mechanical, thermal and magnetic energy into electrical energy. Merging two or more of these harvesters to form a hybrid energy cell can help optimize operation of self-powered systems, providing multimode energy harvesting capability that can leverage several energy sources either simultaneously or individually. However, in this research since harvesting mechanical vibration energy is the main focus and both the piezoelectric nanogenerator (PENG) and the triboelectric nanogenerator (TENG) are able to produce electrical energy from vibration and dynamic motion, which makes them ideal candidates for this research work. Besides, as the output characteristic, matched resistance and the working frequency of the PENGs and the TENGs are very similar, the combination of both effects is promising to enhance the energy conversion efficiency from the ambient environment [102]. In addition, simulation analysis of the coupling between the piezoelectric and triboelectric effects has shed light upon the fact that the output performance of the piezoelectric–triboelectric hybrid nanogenerator can be enhanced with proper structure design and polarization directions. Although the coupling

between these two devices can happen in several ways, the approach in this work is to use a shared electrode between the PENG and the TENG components so that triboelectric charges through contact with other material can add up onto the PENG electrode to enhance the PENG output [101]. Moreover, through rational structure design, the device can generate electric output based on these two effects individually in a single press-and-release cycle, which can improve the efficiency of energy conversion [103].

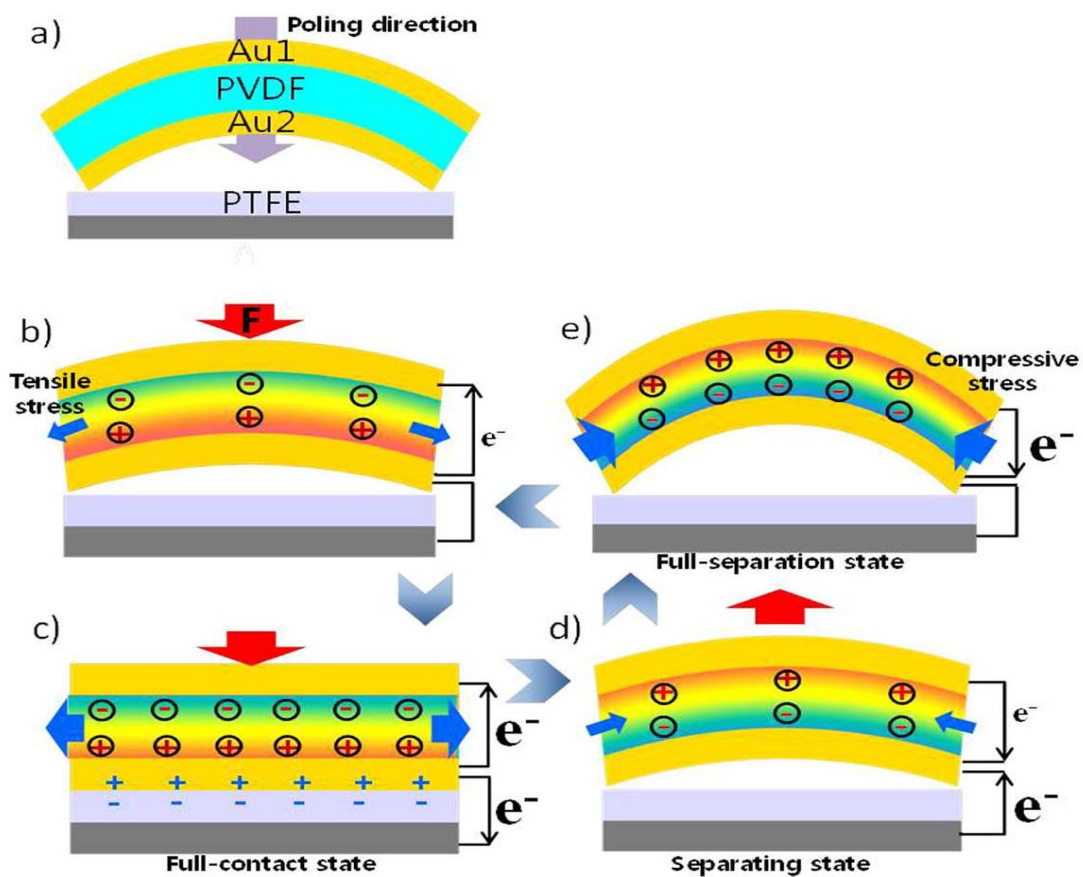


Figure 2.10 Working mechanism of the piezo/tribo hybrid generator in a press-and-release cycle. (a) Initial state without a mechanical force. (b) Piezoelectric potential when the external force starts to be applied. (c) Piezoelectric and triboelectric charge distribution at full-contact state. (d) Negative piezoelectric and triboelectric generation at separating state. (e) Maximized negative piezoelectric potential at Full separation state [Reproduced from Ref. 104 with the Creative Commons license].



The PENG and TENG devices can work individually or simultaneously in a single press-and-release cycle and piezoelectricity can enhance the triboelectric output or triboelectricity can enhance the overall output from the PENG device. Figure 2.10 (a)–(e) shows the schematic illustration of operating mechanism of a typical piezo/tribo hybrid energy harvester unit. At the initial state before the contact of the two layers, neither piezoelectric nor triboelectric potential is present, as shown in Figure 2.10 (a). When an external force starts to be applied on the top layer, in this case, the PVDF has a tensile stress and generates a piezoelectric potential between the electrodes on two sides of the PVDF film by its deformation and electrons flow from Au2 to Au1, as shown in Figure 2.10 (b). Once the top layer touches the bottom layer (full-contact state), a physical contact results the triboelectric effect between Au2 electrode and PTFE. Since the PTFE tends to gain electrons than the Au, electrons are transferred and remain there as electrostatic charges as shown in Figure 2.11 (c). At the moment of the full-contact the piezoelectric and triboelectric outputs reaches the maximum and then decreases. When the applied force is released (separating state), the PVDF film starts to bounce back as shown in Figure 2.10 (d); in such case, since the Au2 receives electrons back to be neutral charges and the PVDF have a compressive force, the hybrid generator produces both negative triboelectric and piezoelectric output voltages, and electrons flows from the Al and Au1 to the Au2. When the two layers are fully separated, there are no triboelectric potential because it becomes neutral charges (Figure 2.10 (e)). The PVDF, on the other hand, generates the maximum piezoelectric output because of the maximum strain at the moment of initial state, and piezoelectric charges are slowly decreased. Then a full cycle is achieved, and it will go back to the equilibrium state. Therefore, both piezoelectric and triboelectric output signals are simultaneously obtained within one press-and-release cycle.

With an aim to harness electrical energy from ambient tiny mechanical vibrations more efficiently and effectively, a piezo/tribo hybrid device structure has been designed in this work that combines a PENG part that is based on ZnO nanostructures



characterize the PENG and TENG devices, it is important at the same time to know the details about the mechanical vibration that is applied to the device, i.e., frequency, acceleration, impact, force etc. and to measure the exact electrical outputs for example, output open circuit voltage, short circuit current, delivered power to the external load etc.

In this work, the piezoelectric and triboelectric characterization has been carried out using a system that includes a closed-loop controller (Vibration Research Corporation, VR9500), a linear shaker (Labworks Inc., ET-126B-1), a power amplifier (Labworks Inc. PA-138 Linear Power Amplifier) and an accelerometer (Dytran Instruments Inc. 3055C) to provide sinusoidal waves simulating a vibration source with a known amplitude, frequency and acceleration. Output voltage and current signals have been measured using Stanford low-noise voltage/current preamplifiers (Model SR560/570) along with other required electrical circuit components. To minimize electromagnetic interference, the two copper wires connected to the device under test have been twisted together. All measurements has been carried out at ambient room temperature.

## Chapter 3

### **Controlled growth of 1D/2D hybrid zinc oxide nanostructures for piezoelectric energy harvesting**

Piezoelectric nanogenerators (PENG) have manifested their ability over the last decade to deliver sustainable electric power to micro-/nano systems (MNSs) or to make a wireless system network self-powered by harvesting ambient tiny mechanical energy. Most of the advanced PENGs are based on one-dimensional (1D) zinc oxide (ZnO) nanostructures (e.g. nanowires, nanorods) due to their high electro mechanical coupling behaviour. However, two-dimensional (2D) ZnO nanosheets due to their buckling behaviour and formation of a self-formed anionic nanoclay layer, contribute to generate direct current (DC) type piezoelectric output. In this chapter, we demonstrate a PENG based on the 1D/2D hybrid ZnO nanostructures on the same substrate for the first time and discuss about the performance of the device in detail.

The findings in this chapter has been filed as a patent:

A. Mahmud, A.A. Khan, P. Voss, D. Ban, "1D/2D Hybrid Piezoelectric Nanogenerator and Method for Making Same," US provisional patents, filed June. 04, 2018. (Ref. 1134-456618US)

Also, the work in this chapter has been accepted as a journal publication:

A. Mahmud, A. A. Khan, P. Voss, T. Das, E. Abdel-Rahman, D. Ban, A High Performance and Consolidated Piezoelectric Energy Harvester Based on 1D/2D Hybrid Zinc Oxide Nanostructures, *Adv. Mater. Interfaces* (Accepted)

All experiments in this chapter have been performed by A. Mahmud with the help of Dr. T. Das for the device testing unless otherwise mentioned.

### 3.1 Introduction

Aircraft structural health monitoring (SHM) system is designed to identify the “state” of the constituent materials, of the different parts, and of the full assembly of these parts constituting the aircraft structure which is based on the observation of the system over time using periodically sampled dynamic response measurements from an array of sensors [105-107]. Currently, to perform the tasks such as sensing, signal conditioning and processing, data storage and communication, supplying power to those sensors by means of battery is the only viable option. As piezoelectric energy harvesting has emerged as an attractive alternative method [108-112], they can possibly be attached to a vibrating mechanical source, such as an airframe, wing, or engine to collect the vibration energy and use that energy to power up the sensor arrays in the aircraft SHM system thus eliminating the requirement for external power source and making the system fully wireless and self-sustaining.

As nanotechnology is at the frontier of new technologies to create, visualize, analyze and manipulate nano-structures, as well as to probe their nano-chemistry, nano-mechanics and other properties within the systems, many exciting discoveries are currently being made and lots are yet to be made [113-115]. It offers not only to miniaturize the systems by replacing bulk materials with different advanced nanostructures but also to better understand the physics and chemistry at atomic levels. Due to the vast reduction in the size and power consumption of sensors and CMOS circuitry over last few decades [116], the area of ambient energy harvesting has emerged over the last decade with an aim to realize the self-powered wireless systems and networks. We are surrounded by significant amount of wasted energy: thermal, mechanical, chemical, RF, solar etc.; mechanical energy is one of the largest sources of the wasted energy in the modern civilization. As a result, conscientious and advanced research is focused to convert this mechanical energy into electricity in order to power electrical devices directly, collect for intermittent higher power devices, or store for

later use. Researchers and scientists have adapted nanotechnology as a powerful tool in this area of harvesting ambient tiny mechanical energy using different kind of one-dimensional (1D) and two-dimensional (2D) nanostructures [117-118]. Four types of 1D nanostructure configurations including nanorods, nanowires (NWs), nanotubes and nanobelts have potential applications in nano-electronics, nano optoelectronics, nanoelectromechanical systems (NEMS), piezotronics, piezo-phototronics, etc.

Due to the co-existence of piezoelectric and semiconducting properties in several 1D nanostructures (e.g. ZnO and GaN) [119], they are ideal candidate for piezoelectric energy harvesting [120-121]. After the first demonstration of PENGs based on ZnO nanowire arrays [108], state-of-the-art research is going on in designing and fabricating new device structures, applying new methods to improve the device performance, integrating PENGs with other type of nano energy harvesters etc. To date, most piezoelectric power generators are based on ZnO NWs or nanorods because 1D ZnO nanostructures with high aspect ratio exhibit better piezoelectric performance - as the piezoelectric coefficient dramatically increases with the increase of the aspect ratio. However, they suffer from long-term mechanical stability and reliability. So, some piezoelectric power generators have been demonstrated based on 2D ZnO nanosheets [123,133,155,158], with an aim to get dc type output as well as to avoid the mechanical instability and some PENGs based on 2D ZnO nanosheets have been integrated with other energy harvesting devices to make hybrid nanogenerators [122]. However, it is worth to mention that the power generation from a PENG device based on ZnO nanomaterials is dependent solely on the morphology of the ZnO nanostructures [123, 156-157]. Here, we report a PENG based on the integration of 1D and 2D ZnO nanostructures on the same substrate which is grown using a simple, low temperature and low cost hydrothermal method [124] to make the device more consolidate by combining the advantages of the aforementioned two types of PENGs intertwining two different types of nanostructures.

### 3.2 Material growth and device fabrication

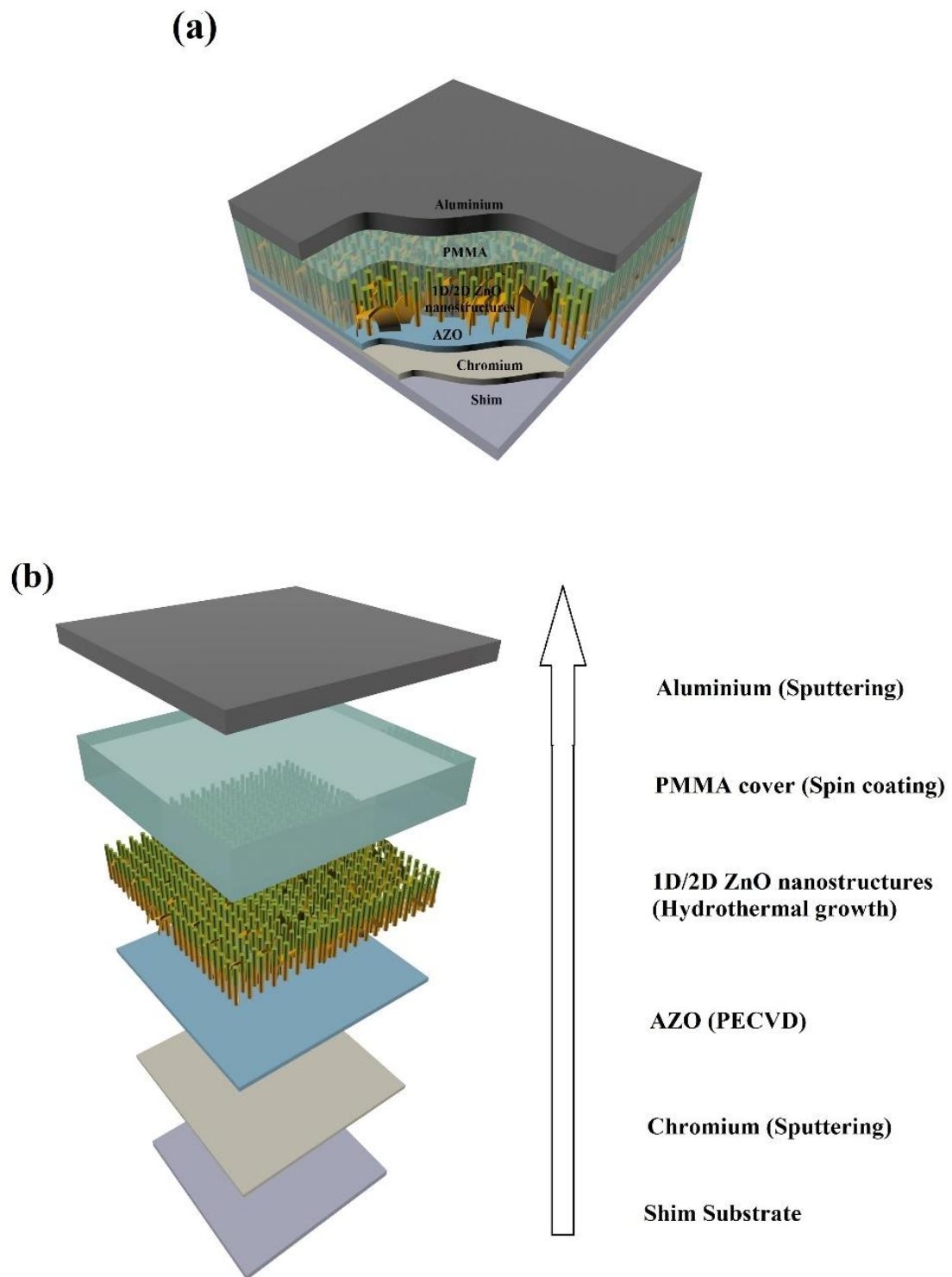


Figure 3.1 (a) 3D schematic of the PENG. (b) Step-by-step fabrication process of the PENG.

Figure 3.1(a) shows the schematic of the PENG and Figure 3.1(b) shows the illustration of the fabrication steps. The structure is fabricated on a  $1.2 \times 1.2$  cm<sup>2</sup> shim substrate. Shim substrate is an alloy with the following material compositions: aluminium (99.29%), zinc (0.04%), manganese (0.04%), silicon (0.13%), iron (0.48%), others (0.02%).

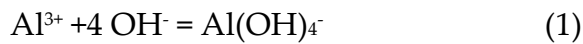
Firstly, the substrate is cleaned using acetone, isopropyl alcohol (IPA) and deionized (DI) water respectively. After that a 400 nm aluminium doped zinc oxide (AZO) layer is deposited on the substrate using plasma-enhanced chemical vapor deposition (PECVD) at 250°C and 5 mT. The AZO layer serves as the seed layer for the hydrothermal growth of subsequent ZnO nanostructures and plays a critical role in the growth process. After the hydrothermal growth of ZnO nanostructures as discussed in the following section, the sample is cleaned using standard process. Then a 2% PMMA solution in toluene is spin coated onto the sample and then cured at a temperature of 120°C for 3 hours to cover the ZnO nanostructures with 100nm PMMA layer. Finally, a 100 nm aluminium layer is deposited on top of the PMMA layer as the top electrode using magnetron sputtering. Then two copper wires are connected to the top aluminium and the shim substrate which serve as the external electrodes for the testing of the device.

### **3.2.1 Hydrothermal growth of ZnO nanostructures**

To grow the ZnO nanostructures, the substrate is attached to a precleaned glass substrate and immersed into a mixture of solutions: zinc nitrate hexahydrate (25mM), hexamethylenetetramine (HMTA) (25 mM) and aluminium nitrate nonahydrate (25mM) using a substrate holder in such a way that the AZO deposited layer faces downward in order to avoid the accumulation of any debris on the substrate during the hydrothermal process [125]. The solution is kept at a constant 88°C during the hydrothermal growth which is optimum for the growth of the desired ZnO nanostructures instead of growing nanoballs (below 75°C) and nanorods (above 95°C)



[126]. The structure height is simply controlled by the growth time. In this study, HMTA is used to synthesize the ZnO nanostructures that reacts with water to produce ammonia that provides a slow and controlled supply of OH<sup>-</sup> anions [127]. Due to the lowest surface energy of (002) facet, the wurtzite ZnO crystal grows preferentially along [001] direction and the growth velocity along <100> directions is slower than that along [001] direction that lead to the formation of 1D ZnO nanowires and nanorods [124]. However, as the substrate was shim, sheet-like morphology ZnO crystals were formed and consequently it is reasonable to assume that Al should be responsible for the 2D growth of ZnO and the suppression effect along [001] direction is also likely originated from Al. In our work, Al from shim substrate is first dissolved into the solution and produce Al(OH)<sub>4</sub><sup>-</sup> ions under alkaline conditions that originates from HMTA as Al is an amphoteric metal [129].



Al(OH)<sub>4</sub><sup>-</sup> then binds to the Zn<sup>2+</sup> terminated (001) surface and suppresses the growth along [001] direction which eventually triggers the lateral growth to form thin 2D ZnO nanoplates [129-131]. M. K. Gupta *et al* has also confirmed this phenomenon by growing 2D ZnO nanosheets with the help of vanadium doping where the doping agent vanadium pentoxide (V<sub>2</sub>O<sub>5</sub>) forms the vanadium hydroxide [V(OH)<sub>4</sub><sup>-</sup>], which can presumably bind to the positively charged Zn<sup>2+</sup> terminated (001) surface just like the Al(OH)<sub>4</sub><sup>-</sup> in this work [134].

### 3.2.2 Characterization of the nanostructures

Due to the strong influence of several process parameters in the hydrothermal approach to grow ZnO nanostructures such as temperature, seed layer type and thickness, concentration of precursor solutions, growth time etc. the process can be easily tweaked to synthesize the desired nanostructure [125-126, 128]. Figure 3.2 (a) – (b) show the 45° tilted view SEM image of as grown ZnO nanostructures at different

scales and distinctly the growth is uniform for a large area. From the magnified image in Figure 2 (b), it is clear that both 1D and 2D ZnO nanostructures are grown on the substrate. The diameter of the 1D ZnO nanowires varies between 50nm to 120nm with an average diameter of 70nm and they are closely packed on the substrate surface which is reasonable due to the thick AZO seed layer that not only facilitates to grow NWs with higher aspect ratio but also increases the NW density [132].

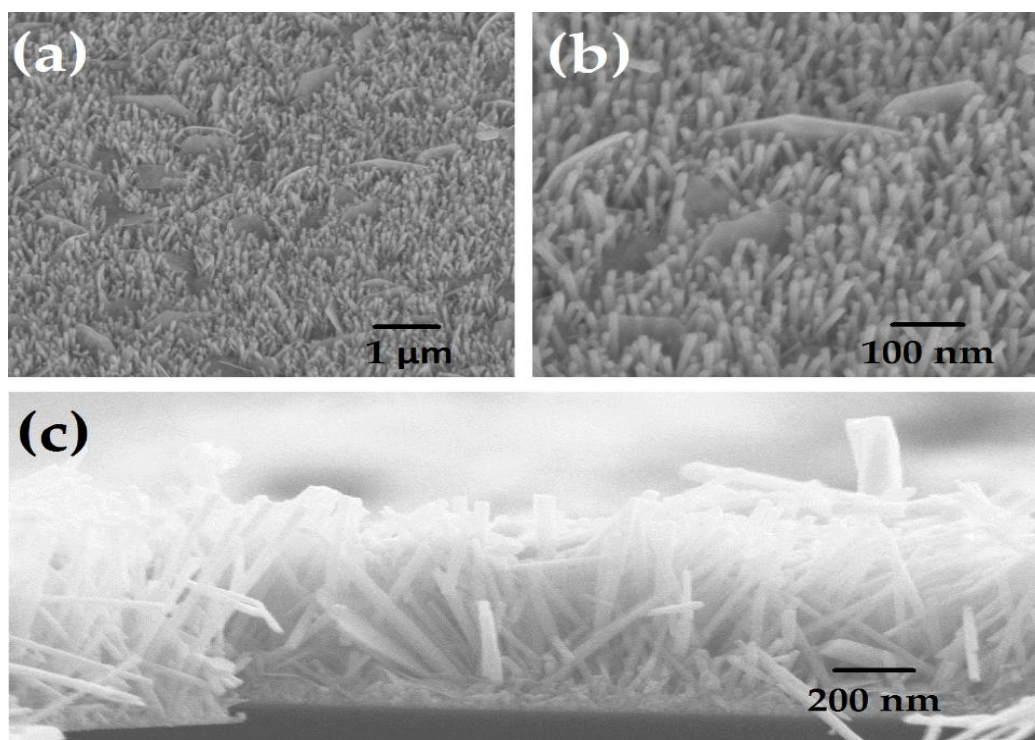


Figure 3.2 (a) – (b) 45° tilted view SEM images of the hydrothermally grown ZnO nanostructure showing the average diameter of the 1D ZnO nanowires is ~70nm and the thickness of 2D ZnO nanosheets is approximately 50 nm. (c) SEM image of the cross-section of the ZnO nanostructures showing an average height of 1.3 μm.

The SEM images are also showing that the nanoplates are buckled and having self-assembled interlaced configuration with a thickness of approximately 50 nm. Figure 3.2 (c) shows SEM image of the cross-section of the ZnO nanostructures showing an average height of 1.3 μm.

### 3.3 Piezoelectric characterization

#### 3.3.1 Measurement set up

After the packaging of the fabricated prototype up as shown in Figure 3.3 (a), it has been tested using a characterization set up as shown in Figure 3.3 (b) to get the quantitative information about piezo response of the device for a particular amount of applied vertical strain on top of the device with a particular acceleration and known frequency.

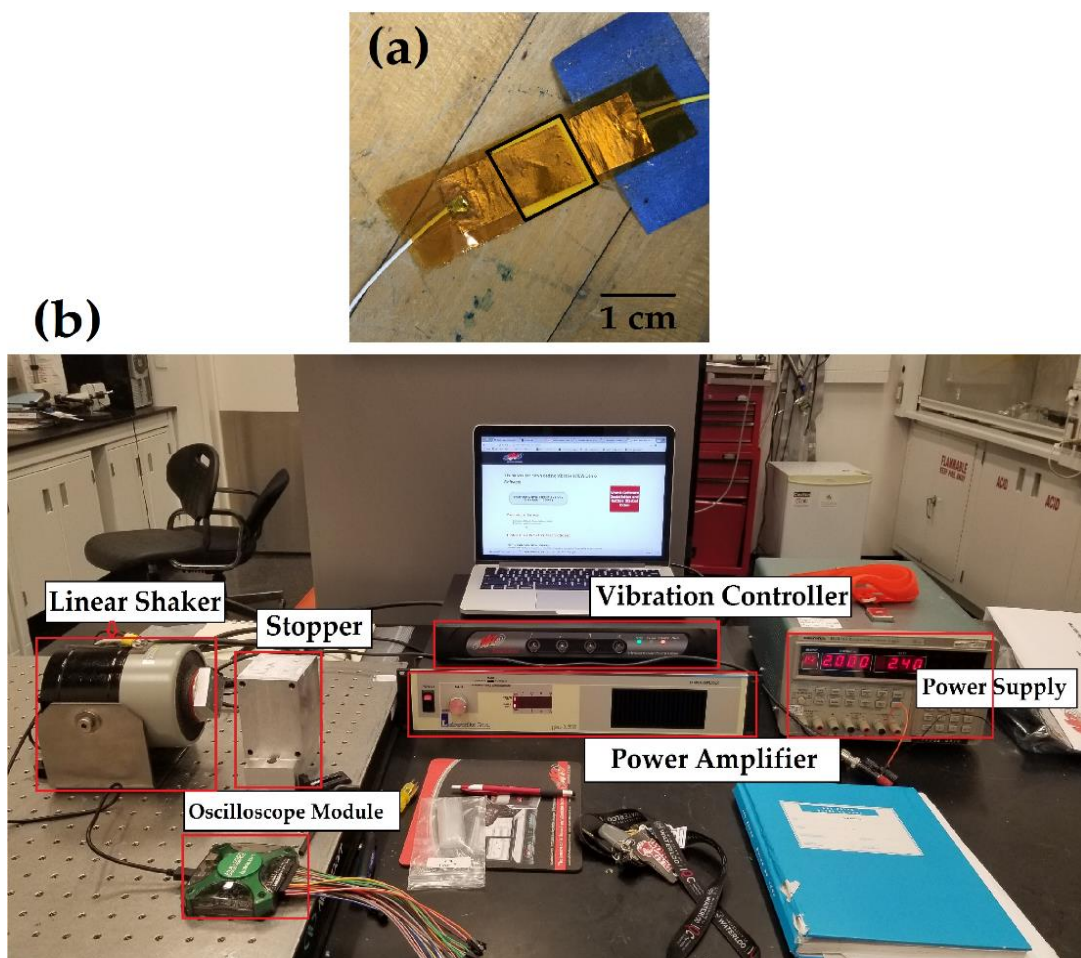


Figure 3.3 (a) Packaged PENG prototype device ready for testing. (b) General setup of the piezoelectric characterization system. The system includes a closed loop controller, a linear shaker and a power amplifier unit to provide sinusoidal waves simulating a vibration source with a known amplitude and frequency.

An electromagnetic shaker unit, Labworks Inc.'s ET-126-1, is used to deliver acceleration to a brass rod with a known mass ( $m = 0.45 \text{ kg}$ ) acting as a hammer which applies the vertical mechanical strain on top of the device mounted on a stopper. The shaker is driven using Labworks Inc.'s Pa 138 power amplifier. A controller unit, Vibration Research's VR9500 Revolution, is used to control and maintain the desired acceleration amplitude and frequency via closed loop control. Output voltage was measured and stored digitally through Tektronix TDC2004C oscilloscope. For output current signal acquisition, a low noise current preamplifier, Stanford SR570, is used with an input resistance of  $10\text{k}\Omega$ .

### 3.3.2 Results and discussion

Quantitative experimental measurements are done to get the piezoelectric response from the fabricated prototype. The energy harvesting mechanism is based on the generation of piezopotential along the NWs c-axis under compressive strain to drive charge back and forth between the shim and Al electrodes.

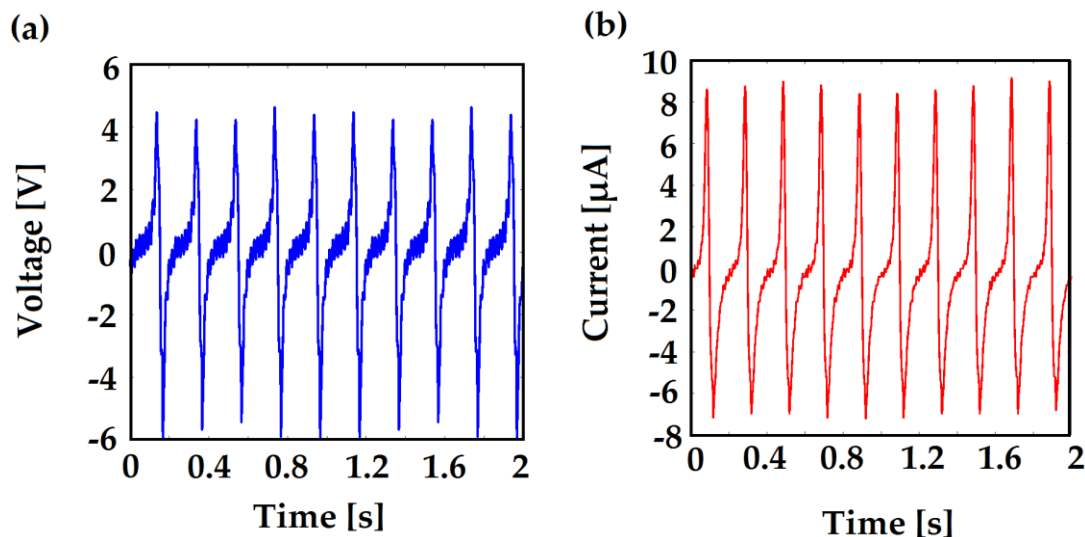


Figure 3.4 (a) Measured open-circuit voltage (average peak value  $\sim 4.2 \text{ V}$ ) and (b) short-circuit current (average peak value  $\sim 8.2 \mu\text{A}$ ) for the PENG. The peak-to-peak displacement was kept constant at 5 mm.

At the initial state before the hammer strikes the top layer of the device, no piezopotential is present. When an external force is applied on the top layer, the tensile side surface gives a positive potential; while a negative potential appears on the compressive side surface and consequently it generates a negative piezopotential ( $V^-$ ) at the p-ZnO/PMMA interface and a positive piezopotential ( $V^+$ ) at the AZO/n-ZnO interface [132]. Owing to this potential difference between the electrodes and the presence of a schottky barrier formed in the metal-insulator-semiconductor (MIS) junction with Al/PMMA/p-ZnO, electrons flow from the Al electrode to shim electrode through an external circuit creating a positive current pulse and this continues until the material system reaches an equilibrium which eventually makes the output zero. When the force is released, the piezopotential fades away and the electrons from shim electrode flow back to Al electrode to establish an equilibrium and a negative pulse is observed and after the equilibrium is achieved, the device gets back to its initial state. Figure 3.4 shows the open circuit voltage and short circuit current that is obtained from the device when tested under a sinusoidal mechanical force with a frequency of 5 Hz and the hammer peak-to-peak displacement is kept 5mm. The force applied on the device is set to be 5N for all the measurements by using a force sensor. Under the above condition, the device produces peak to peak open circuit voltage of  $\sim 10.18\text{V}$  and short circuit current of  $\sim 15.9\mu\text{A}$ . The device produces an average peak output voltage of  $\sim 4.2\text{V}$ , an average current density of  $\sim 6.08\mu\text{A}/\text{cm}^2$  (average current is  $8.75\mu\text{A}$  and device area is  $1.44\text{cm}^2$ ) and an instantaneous peak power density of  $\sim 25.536\ \mu\text{W}/\text{cm}^2$ . Another PENG device on Polyethylene terephthalate (PET) substrate with the same device structure and size is fabricated following the exact same fabrication steps and processes. Figure 3.5(g) shows the SEM image of the grown 1D ZnO NWs when PET substrate has been used and it corroborates that Al from the shim substrate mainly results the formation of 2D ZnO nanoplates. The average peak-to-peak output open circuit voltages from the PENG on PET substrate and the PENG on shim substrate are  $7.85\text{V}$  and  $10.65\text{V}$  respectively as

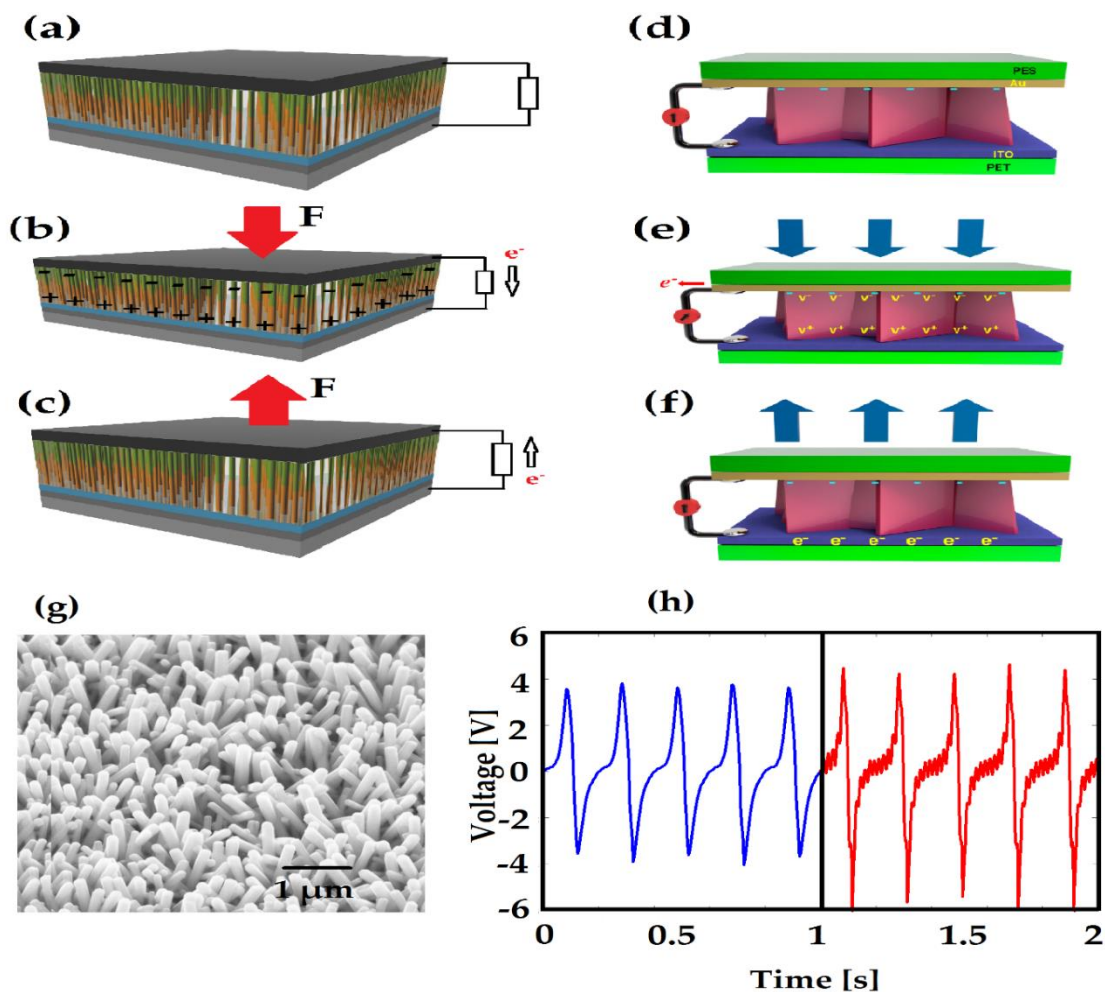


Figure 3.5 Structure and working mechanism of 1D and 2D ZnO nanostructure based PENGs. (a) ZnO nanowire based PENG with no external applied force. (b) Electrons flow from the top electrode to the bottom electrode through the external circuit by the negative piezoelectric potential generated at the top side of the ZnO nanowires under external strain. (c) Electrons flow back via the external circuit till it goes back to its initial state when the force is released. (d) As fabricated ZnO nanosheets based PENG in the absence of any external force. (e) Piezoelectric potential causes electrons' flow from the top electrode to the bottom electrode side through the external circuit under direct compression in the vertical direction. (f) As the compressive strain is released, the piezopotential disappears and device goes back to its initial state. Reproduced from Ref. 134 with from American Chemical Society. (g) SEM image of 1D ZnO NWs grown on PET substrate using the same hydrothermal process as the current PENG device. (h) Open circuit voltages for the PENG devices on PET (blue) and shim (red) substrates.

shown in Figure 3.5(h) and it clearly indicates that the higher piezopotential is generated in the later device under the same testing condition. The enhanced output of the device compared to PENGs based on 1D ZnO NWs[112,117,154] and PENGs based on 2D ZnO nanosheets[112-123, 133, 158] can be attributed to the following: Firstly, when an external mechanical force is applied, as the ZnO nanowires are compressed along their growth (c-axis) direction, piezoelectric fields are created inside the 1D ZnO nanostructures with the upper side negatively charged and the bottom surface positively charged [120] as shown in Figure 3.5 (a) – (c) and at the same time the buckling behavior of 2D ZnO nanosheets also contributes to the piezopotential which comes from the piezoelectric behavior of the nanosheets and a negative piezoelectric potential is induced in the compressive side of nanosheets (top side) and a positive piezoelectric potential on the other side (bottom side) of nanosheets as shown in Figure 3.5(d) – (f) [133-134]. Interestingly, M. K. Gupta and co-workers demonstrated a 100-fold increase in the current density in case of 2D V-doped ZnO nanosheet based PENG compared to 1D ZnO nanowire based PENG under the same applied mechanical force. So, it is intuitive to primarily attribute the enhancement of the output to the integration of 1D/2D ZnO nanostructures [134].

Besides, Sang-Woo Kim and co-workers implied that the strain-energy density of the ZnO nanosheets is about ten times higher than that of the ZnO nanowires and unlike ZnO NWs, 2D ZnO nanosheets can sustain mechanical forces above critical load [133]. And as in this work the device is based on the integration of 1D/2D ZnO nanostructures, it is also expected to be more robust in terms of load handling compared to the PENG based on only 1D ZnO nanowires. Moreover, the work by M. H. Jung *et al* has manifested that the electron diffusion coefficient ( $D_n$ ) of the ZnO nanowires is higher compared to that of the ZnO nanosheet ones, which has been credited to the effective charge screening in the ZnO nanowire [159].

Secondly, to suppress the piezoelectric ‘charge screening effect’ which is one of the most detrimental effects for PENGs, in our previous work we have used a novel two-step hydrothermal method to grow p-n junction type ZnO nanowires instead of using intrinsic ZnO nanowires and demonstrated that the overall NG performance can be enhanced by up to eleven-fold if the doping concentration is properly controlled [136]. The p-n junction prevents the piezo-induced charges to be screened out within a NW that suppresses the local charge screening effect and consequently enhances the overall device performance [135-136, 154]. In this work, the same hydrothermal growth method has been adapted to make the ZnO nanostructures p-n junction type by adding a doping reagent (LiNO<sub>3</sub>) during the second half of the hydrothermal growth of nanostructures. Thirdly, it is well established that for a PENG to work, the difference between the work function of the top metal electrode and the electron affinity of ZnO nanowire arrays must be high enough to hold the charges from leaking [148]. Although Pt, Au, graphene etc. electrodes have been mostly used to form high enough Schottky barrier between the metal electrode and the ZnO nanostructures [149-150], it has also been demonstrated that rather than a metal-semiconductor Schottky barrier, it is possible to build a ZnO nanowire based PENG device using a semiconductor p-n junction [151-152]. The key point is to make enough effective Schottky barrier height (SBH) between the top electrode and the semiconducting ZnO nanostructures so that the piezoelectric charges can’t leak to screen out the piezopotential. In 2014, Z. Zhang *et al* has demonstrated an innovative way to avoid the SBH lowering at the ZnO–metal interface by inserting an insulator (Al<sub>2</sub>O<sub>3</sub>) layer between semiconductor and metal electrode thus forming a metal-insulator-semiconductor (MIS) junction [153]. In the present work after the growth of the nanostructures, they are covered with a thin PMMA insulating polymer layer not only to form a MIS junction at the top of the device but also to provide a polymer matrix to protect the nanostructures against damage during the device operation hence making it more robust [137]. As the electron affinity of ZnO (4.3 eV) and work function of



aluminium (4.26 eV) can't make a high enough Schottky barrier to hold the charges from leaking, an insulating PMMA layer with high work function (5 eV), is inserted between them to form a MIS junction that increases the effective SBH of the MIS junction to hold the piezoelectric charges from leaking. Besides, due to its flexibility, PMMA doesn't interfere with the external mechanical strain applied to the nanostructure and it also prevents electrical shortage between the top and bottom electrodes of the device [138]. Finally, there are some other effects such as flexoelectricity [139-140], polarization gradient [141] and surface effect [140], they can contribute to the enhancement of the performance of the device. Flexoelectricity is a property of a dielectric material that causes polarization due to non-uniform strain in the material. When a dielectric material experiences mechanical stress, its electric polarization ( $P_i$ ) can be expressed as follows [142],

$$P_i = d_{ijk} \sigma_{jk} + \mu_{ijkl} \delta \varepsilon_{jk} / \delta x$$

Where,  $d_{ijk}$  corresponds to direct piezoelectric effect,  $\mu_{ijkl}$  is a fourth-rank polar tensor corresponding to flexoelectric effect,  $\sigma_{jk}$  and  $\varepsilon_{jk}$  are second-order Cartesian stress and permittivity tensor respectively. Although under the classical piezoelectric theory, the flexoelectric effect is not considered, they can play significant role for nano devices because NWs have different heights, which can result in non-uniform mechanical stress from point to point in the material. It is highly possible in the aforementioned PENG incorporating 1D/2D ZnO nanostructures as the nanostructures have different heights as it can be noticed from Figure 2.

Figure 3.6 (a) – (b) show the output open circuit voltages and short circuit currents respectively at different frequencies when the force is kept fixed at 5N and the hammer peak-to-peak displacement is 5mm. Since the impact acceleration on the device increases as the frequency increases at constant force, the output piezopotential increases and eventually enhances the output open circuit voltage and current [132].

Figure 3.6 (c) - (d) show the output open circuit voltages and short circuit currents

respectively at different acceleration levels when the force and the frequency are kept fixed at 5N and 5Hz respectively. The average peak output voltages and currents increase linearly with the applied frequency and acceleration.

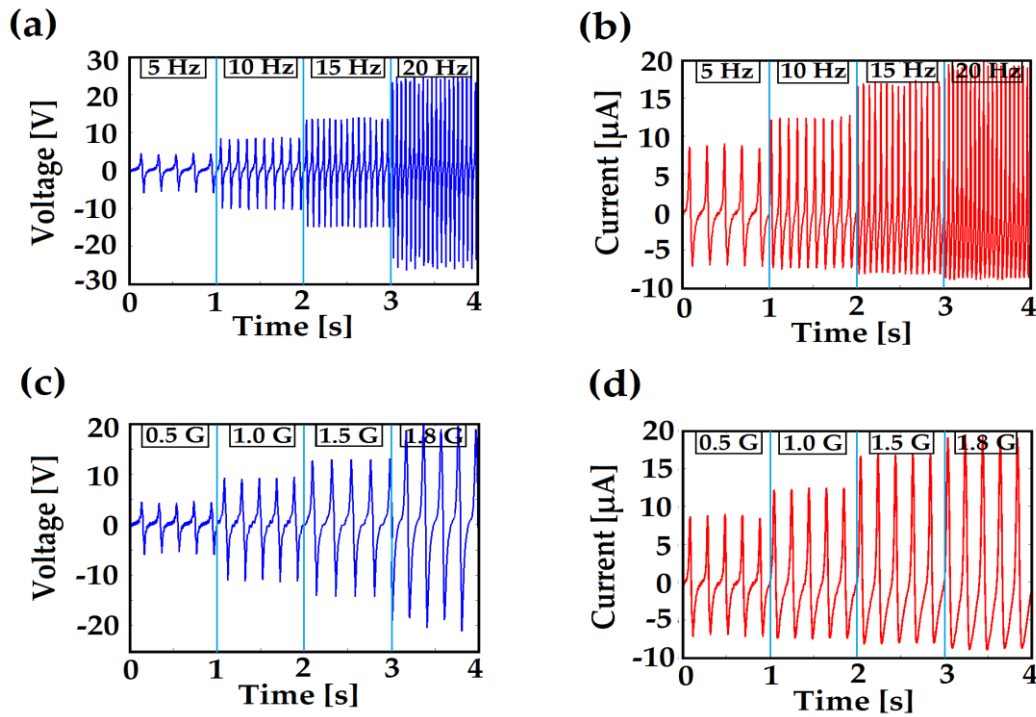


Figure 3.6 Output performance of the PENG. (a) Open circuit voltages and (b) Short circuit currents at different frequencies. (c) Open circuit voltages and (d) Short circuit currents at different accelerations.

Figure 3.6 (a) - (b) show the average open circuit voltages and short circuit currents at 5 Hz, 10 Hz, 15 Hz and 20 Hz that indicate a linear relationship of both the open circuit voltage and short circuit current with frequency.

This can be attributed to the fact that at 5 Hz the PENG is below the resonant vibration frequency, as above 5Hz the output voltage and current still increases linearly as shown by the voltage and current changing trends in Figure 3.6(a) - (b) and when a PENG operates below its resonant frequency, the output voltage and current show a

linear dependence on the acceleration level [143]. When the excitation frequency approaches to the resonance frequency, the output gets saturated and beyond the resonant frequency, the output drops quickly [143-144]. However, as the frequencies of environmental vibration sources are relatively low [145-146] this device will not reach to its resonant frequency and is capable of producing enhanced piezopotential.

In addition, when the device is excited and deflected with higher acceleration amplitudes and higher frequencies, not only the longer NWs experience larger deformation but also shorter nanowires get enough deformation to give rise to piezoelectric potential [132] This can effectively increase the output voltage and current, hence the total output power of the NGs in both the frequency and acceleration sweeps.

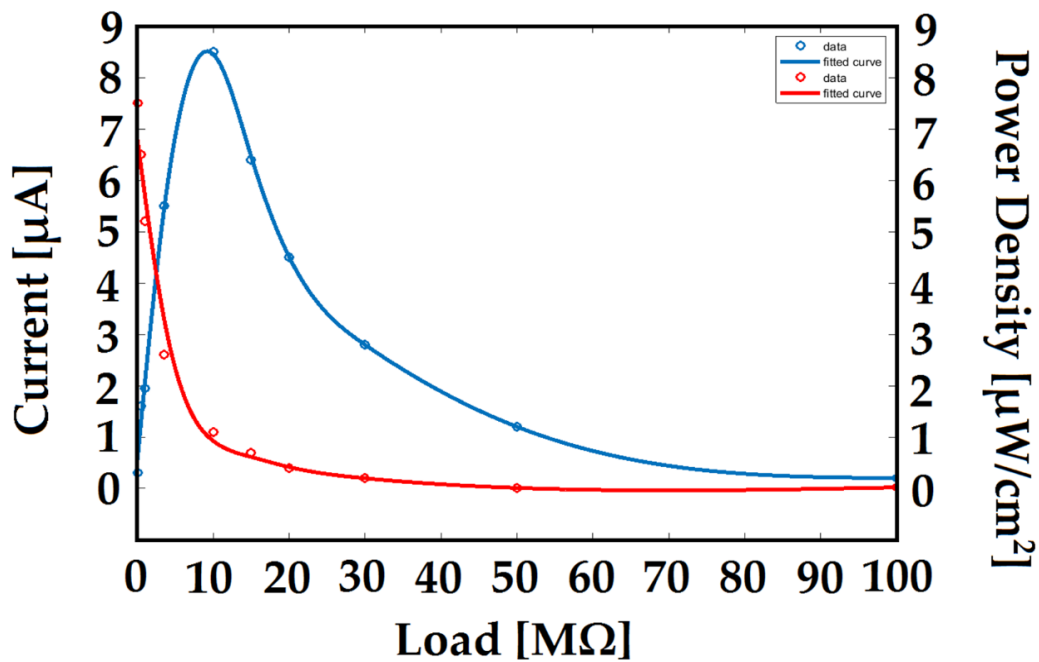


Figure 3.7 The load resistance dependence of instantaneous electrical power from the fabricated PENG. As the load increases from 10kΩ power increases, then reaches a maximum value of 8.4  $\mu\text{W}/\text{cm}^2$  at the matched load of 10MΩ and drops off with further increase in load.

Moreover, the electrical output performance of fabricated PENG to the external load is systematically investigated by connecting variable resistances from 10k $\Omega$  to 200M $\Omega$  as shown in Figure 3.7. The maximum output power density of 8.4 $\mu$ W/cm<sup>2</sup> is achieved with an external load of 10M $\Omega$ . This is because the current decreases with an increase of load resistance owing to the ohmic loss [147] as shown in Figure 3.7 and instantaneous maximum power value is achieved when the load resistance matches with the internal resistance of the device. The internal resistance for this kind of vertical nanowire array integrated nanogenerator (VING) is several M $\Omega$ s [117]. Therefore, this ZnO hybrid nanostructure based nanogenerator shows a promising output performance with a better mechanical robustness, revealing its great potential to power wearable electronic devices.

### 3.4 Conclusion

In this work, 1D/2D ZnO hybrid nanostructures are grown on the same substrate using a simple, low temperature hydrothermal method with an aim to make a PENG based on the hybrid nanostructures so that it can combine the advantages of PENGs based on ZnO NWs or nanorods (e.g. high electro-mechanical coupling) and PENGs based on 2D ZnO nanosheets (e.g. high mechanical stability). The fabricated device is tested under different mechanical stress with different applied frequencies and acceleration levels which indicates the robustness of the device. The output open circuit voltage and short circuit current is almost identical in each cycle of mechanical force under the same measurement condition and at a force of 5N and with a frequency of 5Hz the average peak-to-peak output open circuit voltage and short circuit current reach up to 10.18V and 15.9 $\mu$ A respectively which corroborates the prospective of the device to power up array of sensors in an aircraft SHM system and hence making it self-powered. The device also shows a new strategy of integrating different nanostructures on the same substrate to enhance the performance in terms of the electrical output as well as the mechanical stability both of which are critical for

practical application of the device. The incorporation of hybrid nanostructures, p-n junction type ZnO NWs and insertion of PMMA matrix lead to a miniaturized energy harvesting unit that can also be benefited from flexoelectric effect, surface effect, etc.

## Chapter 4

### **Piezo-tribo hybrid energy harvester based on inorganic-organic nanostructured materials**

Recently, different types of hybrid energy harvesting devices have been demonstrated to convert different kind of available but mostly wasted type of surrounding energies such as mechanical, chemical, thermal, solar etc. with an aim to develop self powered electronic systems. In this chapter, we have demonstrated a novel hybrid nanogenerator consisting of piezoelectric and triboelectric components that mutually enhances the performance of each other and can operate independently and/or simultaneously to convert mechanical energy into electrical energy in a single press-and-release cycle. This hybrid energy harvesting device is based on nanostructured organic/inorganic materials, i.e. ZnO nanowire and nanoplates for the piezoelectric part and nanotextured PTFE and Al for the triboelectric part.

This chapter has been submitted as a journal publication:

A. Mahmud, A. A. Khan, S. Islam, P. Voss, D. Ban, High Performance Piezo-tribo Hybrid Energy Harvester Based on Inorganic-Organic Nanostructured Materials, *Nano Energy*, under review.

All experiments in this chapter have been performed by A. Mahmud with the help A. A. Khan unless otherwise mentioned.

#### **4.1 Introduction**

Intensive and state-of-the-art research in the area of energy harvesting using nanotechnology [160, 190] is going on mainly because of two reasons: to realize the self-powered electronics [160-161, 193] as portable devices, sensors, and wireless body implantable devices consume very low electrical power [162] and to reduce global dependency on energy sources based on fossil fuels [163]. Recent advances in

piezoelectric and triboelectric power generators has corroborated the huge potential of their application to convert mechanical energy into electricity which is one of the largest sources of the wasted energy in the modern civilization [164-172]. Nevertheless, there are several physical and technological issues and challenges that need to be addressed and overcome to realize a complete self-powered electronic system based on nanogenerators [166, 170]. For example, higher and steady output power, low cost and reasonable fabrication process complexity, long-term durability and robustness are some of the critical factors that are still turning them away from practical applications and until now it is hardly possible for a single nanogenerator to meet all these criteria. Current efforts are mainly focused on enhancing the conversion efficiency and output performance of existing nanogenerators by utilizing different techniques such as prudent triboelectric materials selection<sup>[12,14]</sup>, enhancement of the effective contact area of the triboelectric materials by creative different micro/nano structures on the material surface [174-175], increasing the piezopotential by suppressing the charge screening effect [176-177], increasing the charge density via charge injection/polarization by integrating hybrid piezoelectric/triboelectric structures together [178-179] etc.

In this paper, keeping in mind the aforementioned issues and the favorable ways to enhance the performance, we demonstrate one prototype of a hybrid nanogenerator that intertwines the advantages of a piezoelectric and a triboelectric energy harvesters and due to a common electrode they enhance the performance of each other [175, 180-181] as well as the device can harvest mechanical energy from vibration based on these two effects individually in a single press-and-release cycle, which can lead to higher energy conversion efficiency [182-183]. To take advantage of the efficient friction between the two tribo layers which is known to enhance the triboelectric performance of the device [184-185], an easy and straightforward technique has been employed to make nanostructures on the PTFE surface [184] and a simple DI water treatment has been used to make the Al surface nanotextured [185].

Alongside, as the p-n junction type ZnO nanostructures have demonstrated better piezoelectric performance in compared to pristine ZnO nanowires [186-187], we have utilized the advantages of a low temperature, cost efficient and straight forward hydrothermal method to grow the p-n junction type ZnO nanostructures as reported in our previous work [186, 188]. In this hybrid device structure, since the piezoelectric part and the triboelectric part work mutually in a single press-and-release cycle, it enhances the output open circuit voltage, short circuit current and thus the output power density. Under 1g acceleration and 25Hz frequency, the piezoelectric part produces an average peak-to-peak output voltage of ~34.8V and an average peak short circuit current of ~5.2 $\mu$ A when the triboelectric part produces an average peak-to-peak output voltage of ~356V and an average peak short circuit current of ~38 $\mu$ A when they were tested separately. Using two full-wave bridge rectifiers, we combined the output of the devices together and obtained an average peak output voltage, current density, and power density of ~ 186V, 10.08  $\mu$ A/cm<sup>2</sup>, and 1.864 mW/cm<sup>2</sup>, respectively. When the triboelectric and piezoelectric components of this hybrid structure can charge a 4.7 $\mu$ F capacitor up to 3.6V and 8.3V respectively in 100s, within the same time the same capacitor gets charged up to 10.7V with the hybrid operation mode that clearly proclaims the superior performance of the hybrid device with respect to its individual parts.

## 4.2 Device structure and working principle

Figure 4.1 (a) shows the 3D schematic of the curved shaped triboelectric nanogenerator integrated on top of the flat shaped piezoelectric device. The piezoelectric part consists of the Al/ p-n junction type ZnO nanostructures (covered with PMMA)/AZO/Cr/shim substrate from bottom and the triboelectric part consists of PET/Cu/PTFE (with nanostructures on the surface)/nanoporous shim from the top of the structure. To simultaneously utilize the piezoelectric and triboelectric response, this device has a common electrode, the shim substrate, an aluminium alloy with the



following material compositions: aluminium (99.29%), zinc (0.04%), manganese (0.04%), silicon (0.13%), iron (0.48%), others (0.02%). It is worth mentioning that this device works based on vertical press and release mechanism. Figure 4.2 shows the illustration of the working mechanism of the device. At the initial state, as the nanoporous shim surface and the PTFE surface are not in contact, there is no tribo induced charge accumulation hence no triboelectric output. Also at this state as the ZnO nanostructures are not strained, there is no piezoelectric charge distribution in them, so no piezo potential in this state. When an external force is applied on top of the device, the top PTFE layer starts to move closer to the nanoporous shim surface and eventually touches each other which causes charge transfer between two layers. Since Al is much higher in the triboelectric series with respect to PTFE, electrons are transferred to Cu electrode from shim electrode which causes a current flow from Cu electrode to shim electrode through the external load. At the same time, as the ZnO nanostructures are vertically strained due to the external applied force, one side of the nanostructures gets positively charged and another side of the nanostructures gets negatively charged. And because of this negative piezopotential ( $V^-$ ) at the p-ZnO/PMMA interface and positive piezopotential ( $V^+$ ) at the AZO/n-ZnO interface, electrons flow from shim electrode to aluminium electrode resulting a current to flow in opposite direction through the external load. Soon after the device is pressed, the charges in both parts reach to equilibrium which drives the piezoelectric and triboelectric output to zero at this state. Once the compressive force is released, the two triboelectric layers start to loose contact and move away due to the elastic property of the PET layer which drives the electrons back from Cu electrode to shim electrode through external load which is opposite to the electron flow during the compressive state and causes a current to flow in opposite direction resulting an AC signal for a complete cycle. At the same time, as the strain is released, the piezopotential in the ZnO nanostructure arrays fades away and consequently the electrons around the Al electrode flow back to the shim

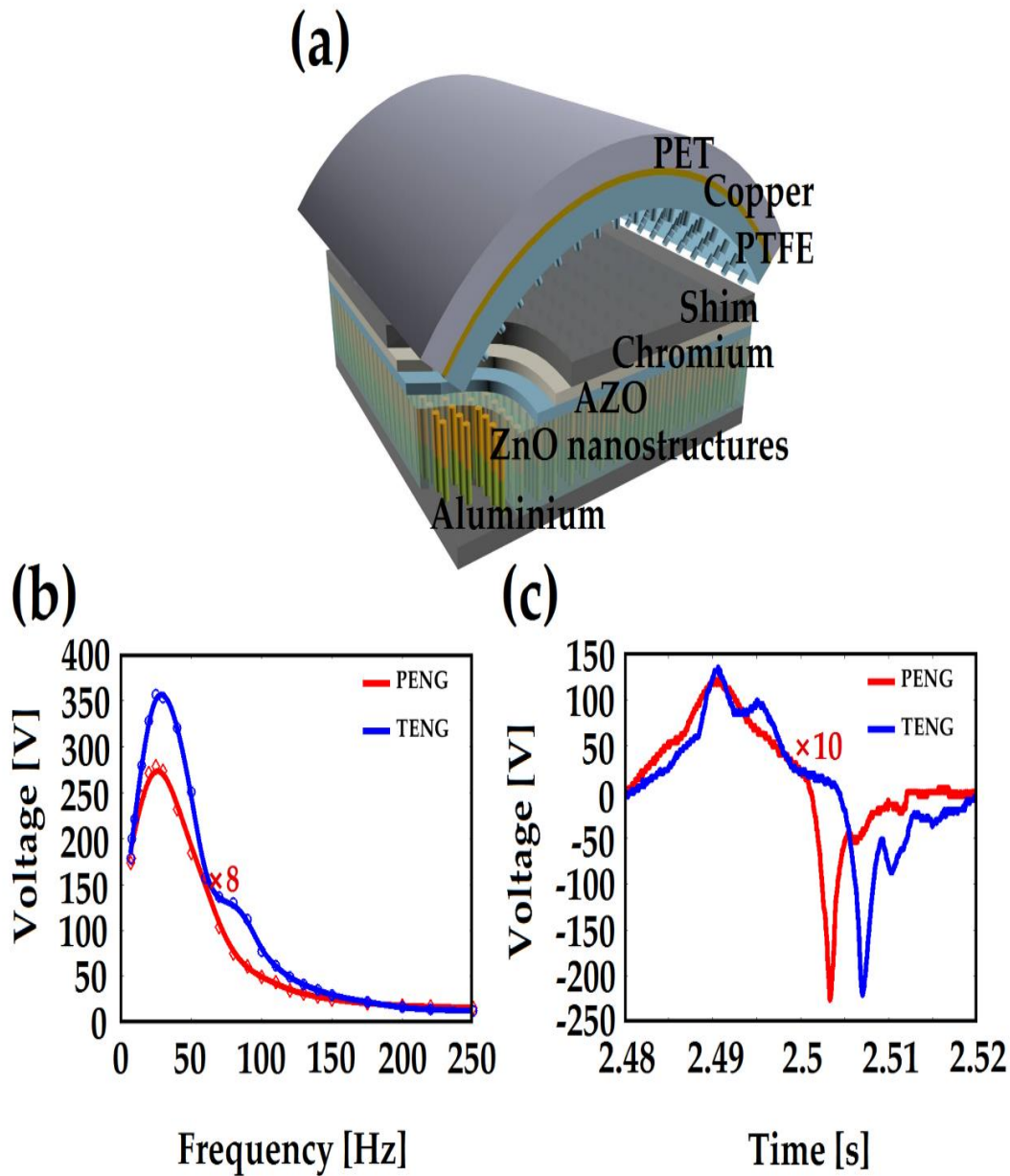


Figure 4.1 (a) 3D schematic of the curved shaped hybrid device. (b) Average peak-to-peak output open circuit voltage from the two components of the device at different frequencies. (c) Output open circuit voltage from the piezo and triboelectric components in a single press-and-release cycle. [To visually compare the results from the PENG and TENG parts, output from the PENG has been multiplied by 8 and 10 in (b) and (c) respectively]

electrode via the external load resulting a current flow in opposite direction with respect to the compressive state. Finally, both part of the hybrid NG is released and

reaches equilibrium again, thus yielding zero output. Hence, we can simultaneously get both the piezoelectric and triboelectric output signals within one press-and-release

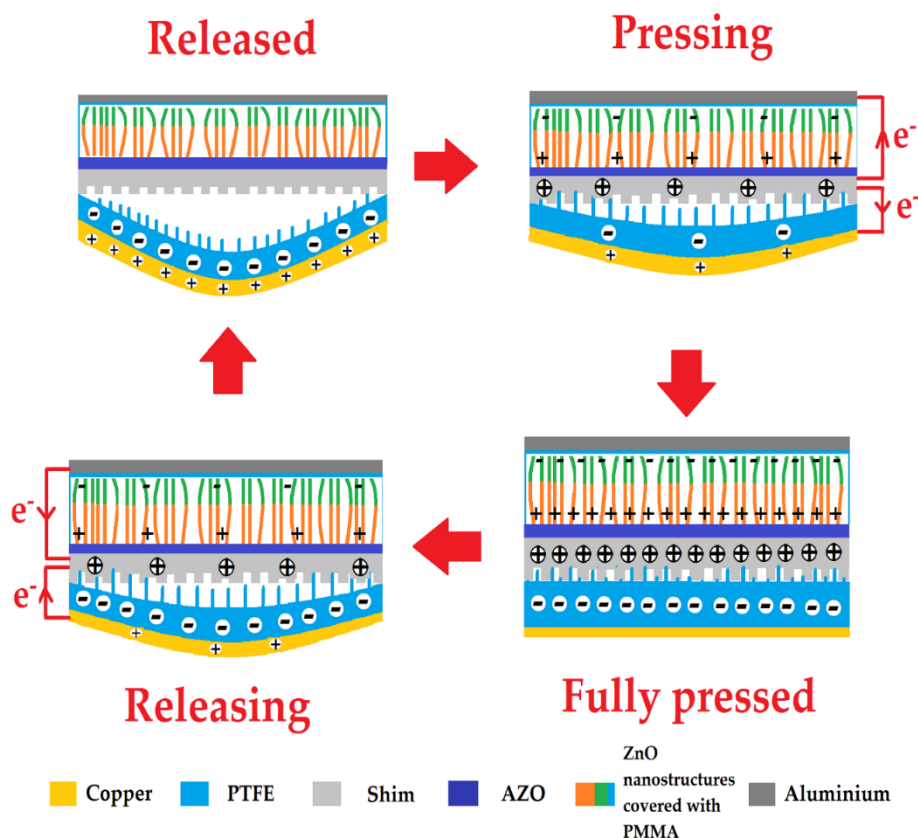


Figure 4.2 Illustration of the working mechanism of the device in a single press-and-release cycle of applied mechanical vibration.

cycle as shown in Figure 4.1 (c) and that is the main purpose of integrating the two devices together to enhance the energy conversion efficiency of the device. Before starting the device characterization, i.e. open circuit voltage, short circuit current, output power, charging capability etc., the optimized operating frequency was figured out by sweeping the frequency of the applied mechanical vibration from 1Hz to 250Hz as shown in Figure 4.1 (b) and both of the piezo and tribo electric components yield highest output voltage at 25Hz and the subsequent measurements are done at this frequency unless otherwise mentioned.

### 4.3 Experimental Section

#### 4.3.1 Materials characterization and device fabrication

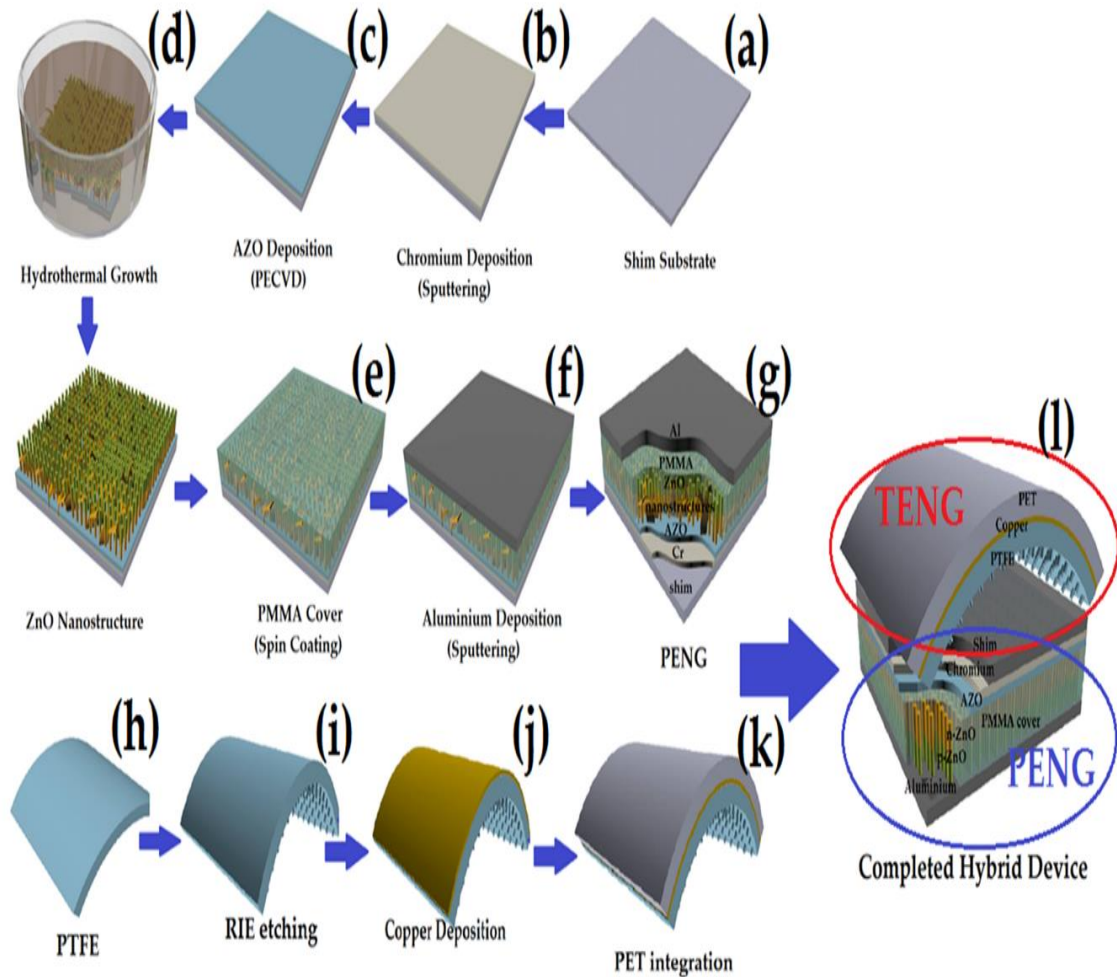


Figure 4.3 The fabrication process of the hybrid nanogenerator. (a) – (g) Step-by-step progress towards the piezoelectric part of the device. (h) – (k) Fabrication steps for the triboelectric part of the device. (l) Integration of piezo and tribo components together to make the hybrid structure.

Figure 4.3 shows the step-by-step fabrication of the hybrid nanogenerator. The fabrication of the entire device can be divided into two parts: the PENG part and TENG part. Firstly, a 2.5cm×2 cm piece of shim was cut as the substrate material. To make one of its surfaces nanoporous the substrate was immersed into DI water at a

temperature of 120°C for 30 minutes while the other surface was covered with kapton tape so that it doesn't come in contact with DI water. Then for the piezoelectric device, a 200 nm aluminium doped zinc oxide (AZO) layer was deposited on the intact side of the substrate using plasma-enhanced chemical vapour deposition (PECVD) which serves as the seed layer for the hydrothermal growth of the ZnO nanostructures. After that the hydrothermal growth was carried out in such a way that nanoporous shim surface doesn't come in contact with the solution and the AZO surface faces downward. Immediately after the growth of n type ZnO nanostructures, for the growth of p type ZnO nanostructures hence making p-n junction type ZnO nanostructures, a doping reagent was added in the second half of the hydrothermal growth [188]. In both cases the solution temperature was fixed at a constant temperature of 88°C and nanostructure length was controlled by the growth time. After the hydrothermal growth of nanostructures, sample was cleaned using standard

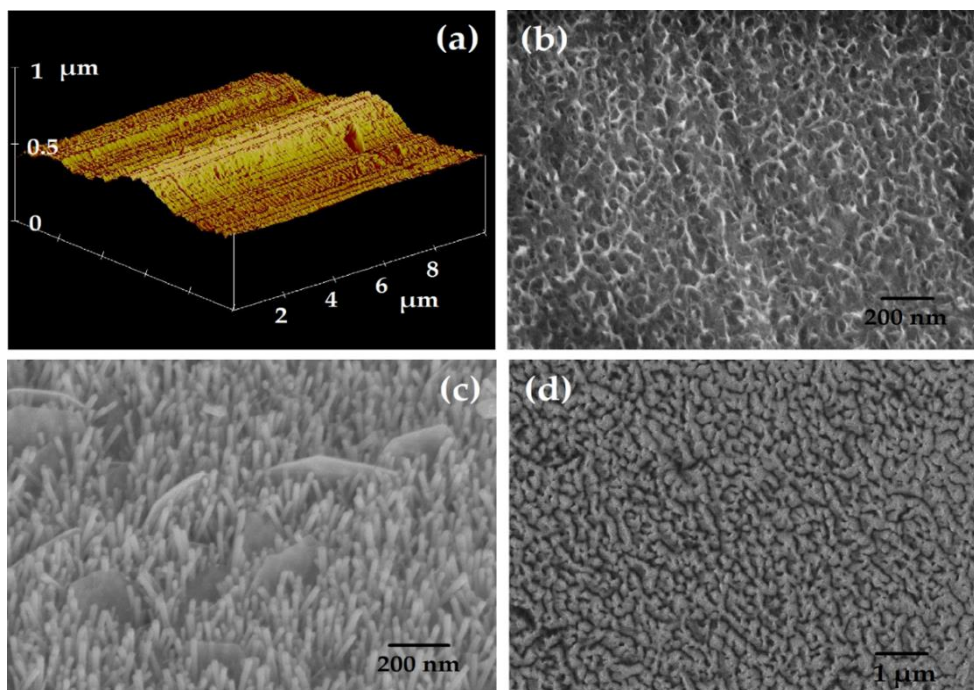


Figure 4.4 Materials characterization (a) AFM image of shim substrate. Top view SEM images of (b) the nanostructured shim surface (c) as grown ZnO NWs along with nano plate structures (d) nanostructured PTFE surface.

On the other hand to make the triboelectric part of the hybrid nanogenerator, one piece of 100µm thick PTFE of the same size as the shim substrate was cleaned using standard process and a 10nm Au layer was deposited using electron beam evaporation. Subsequently, the ICP reactive ion etching was applied to create the nanostructures on the surface [184]. After the formation for nanostructures on the surface of the PTFE, copper was deposited on the PTFE as an electrode using e-beam evaporation and then it was glued to an arc shaped PET substrate with double sided copper tape. The PET substrate was precleaned using standard process and arc shape was made using heat treatment. Later on, the two parts were assembled together to complete the hybrid device as illustrated in Figure 4.3. Finally three copper wires were connected to the three electrodes (shim, bottom Al and Cu) for the characterization of the device.

After the cleaning of shim substrate using standard cleaning process, AFM was taken to make sure the substrate surface is smooth enough not to make any issue for the subsequent materials growth particularly ZnO nanostructure growth. Figure 4.4 (a) shows the 3D topography of the substrate surface and the measured surface roughness was 45 nm which is not high to make any significant impact for the subsequent nanostructure growth. Figure 4.4 (b) shows the shim substrate surface after the DI water treatment, this nanostructured surface effectively increases the friction between the PTFE layer and the shim layer and thus enhances the tribo electric charge density.

The piezoelectric part of this device is based on 1D/2D hybrid ZnO nanostructures which was grown using the low temperature hydrothermal method. Figure 4.4 (c) shows the ZnO nanowires with an average diameter of 70 nm along with the ZnO nanoplates with an average thickness 50 nm. The growth of 2D ZnO nanoplates is mainly attributed to the use of shim substrate. Shim substrate is mostly aluminium that partly dissolves in the solutions and produces  $Al(OH)_4^-$  ions [191] and those ions

bind to the  $Zn^{2+}$  terminated (001) surface and suppresses the growth of ZNO nanowires along [001] direction [192], which eventually triggers the lateral growth to form thin 2D ZnO nanoplates. For the triboelectric part, to further enhance the triboelectric charge density, nanostructures were grown on the PTFE surface using RIE etching and thin layer of gold as a mask for the etching process. The SEM image of the top surface of the nanostructured PTFE shown in Figure 4.4 (d) manifests the uniform formation of nanostructures on the PTFE surface.

### 4.3.2 Results and discussion

After the packaging of the fabricated prototype device, it has been tested using the characterization set up as shown in Figure 2.10 to get the quantitative information about electromechanical response of the device for a particular amount of applied vertical strain on top of the device with a particular acceleration and known frequency. When the output performance is measured separately, this piezo-tribo hybrid energy harvester unit with a dimension of  $2 \times 2.5 \text{ cm}^2$  produces piezoelectric and triboelectric peak-to-peak output voltages of  $\sim 34.8\text{V}$  and  $\sim 356\text{V}$  respectively as shown in Figure 4.5 (a) - (b).

However, when the two units are combined in parallel to get the hybrid operation mode, it produces a peak-to-peak output open circuit voltage of  $\sim 106\text{V}$  as shown in Figure 4.5 (c), which can be attributed to the mismatch between the internal resistances of piezoelectric and triboelectric nanogenerator units as it is well established that when two power sources are connected in parallel, the power source with a lower internal impedance dominates the output voltage [189].

Besides, at the testing frequency, the phase difference between the voltages from two different units results voltage cancelation and thus degrades the output voltage. To eschew the foregoing issues, two bridge rectifier units have been utilized to collect the electrical signals from two different units separately (Figure 4.5 (d)) as well as from their hybrid operation mode (Figure 4.5 (e)) because full-wave bridge rectifiers do not

allow voltage degradation due to the different internal resistances and eliminate the voltage cancellation effect from the phase mismatch [180-181].

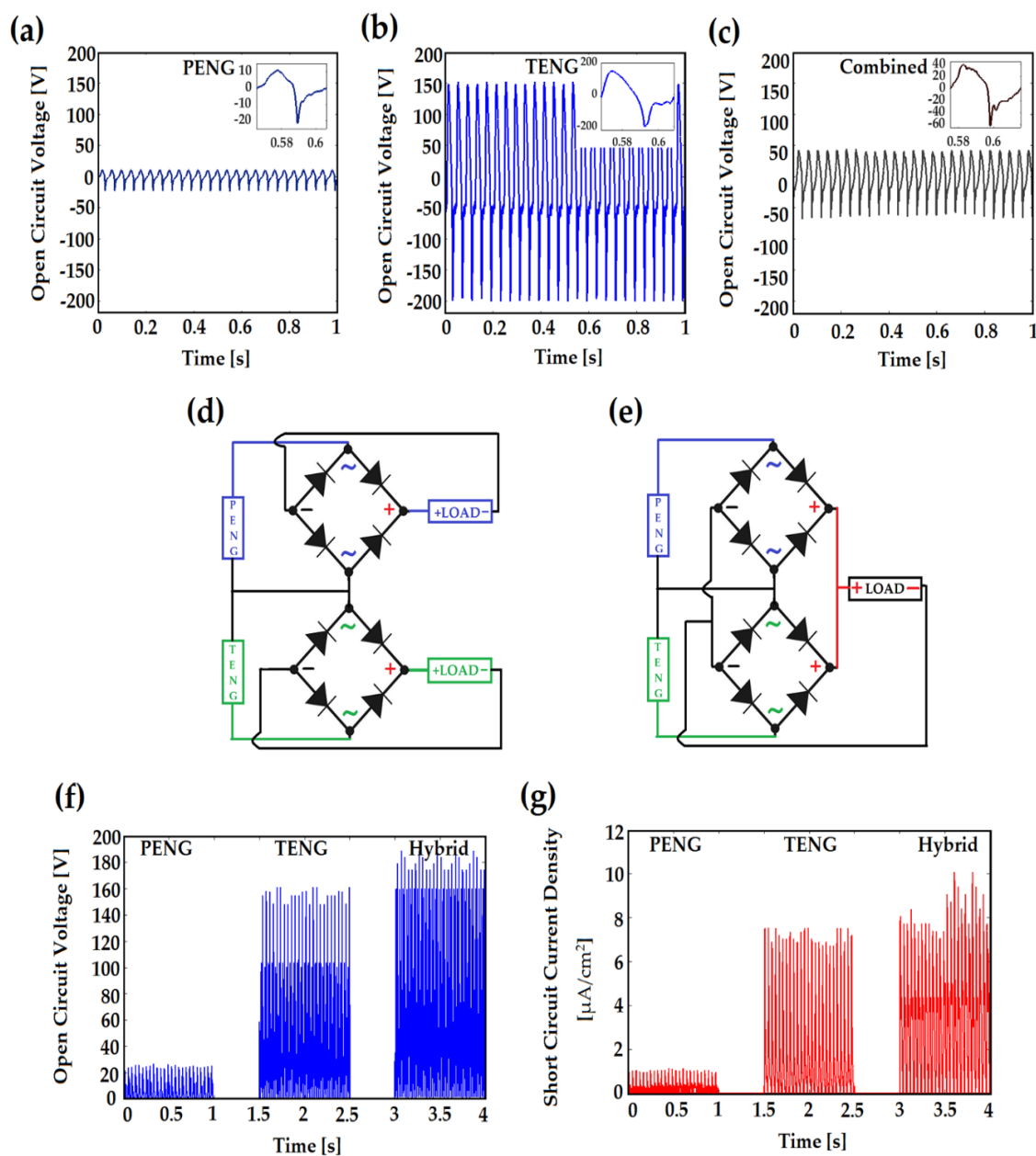


Figure 4.5 Output open circuit voltage of (a) piezoelectric, (b) triboelectric and (c) hybrid nanogenerator without using rectifiers. (d) Concurrent measurement method for piezo and tribo electric outputs. (e) The piezoelectric and triboelectric outputs are combined in parallel for the hybrid output measurement. Measured piezoelectric, triboelectric and hybrid output open-circuit voltages (e) and short-circuit currents (f) using the rectifier circuits.



Figure 4.5 (f) – (g) show the rectified piezoelectric, triboelectric, and hybrid open-circuit voltages and short-circuit currents under a periodic mechanical vibration at 25Hz frequency, 1G acceleration and 5mm peak-to-peak hammer displacement. When the two units are connected as shown in Figure 4.5 (d), the output voltages are basically the rectified voltage from two separate units and produces an average peak voltage of ~25V for PENG unit and ~160V for TENG unit but interestingly when both the piezo and triboelectric outputs are combined for hybrid operation mode as shown in Figure 4.5 (e), the measured output voltage reaches an average peak value of ~186V and this enhancement might result due to the induced charges on the common electrode caused by the triboelectric or the piezoelectric charges in addition to the original piezoelectric or triboelectric output. As shown in Figure 4.5 (g), the PENG, TENG and their hybrid operation mode produce an average short circuit current of  $\sim 1.04\mu\text{A}/\text{cm}^2$ ,  $\sim 7.02\mu\text{A}/\text{cm}^2$  and  $\sim 8.1\mu\text{A}/\text{cm}^2$  respectively. The small fluctuation in the output signals can be attributed to the small and unavoidable small fluctuation in the effective mechanical vibration impacts from the mechanical part of the testing set up. The measured short circuit current signals demonstrate that the currents from the two units are effectively added up in their hybrid operation as expected. Besides, this hybrid energy harvester unit has a maximum output open-circuit voltage and short-circuit current density of 186V and  $10.02\mu\text{A}/\text{cm}^2$  respectively, and that results an instantaneous maximum output power of  $\sim 1.864\text{ mW}/\text{cm}^2$ .

Combining PENG and TENG together in a single structure can enhance the output of each other through the interaction of the triboelectric and piezoelectric potential where the enhanced output of each component consists of two parts – (i) the original piezoelectric or triboelectric output, and (ii) the induced charges on the electrode caused by the triboelectric charges or the piezoelectric potential, which contribute to the enhancement [175, 181, 194]. The experimental measurement confirms that due to the influence of triboelectric charges, the peak to peak output voltage of PENG

increases from 34.8V to 120V. On the other hand, the induced charges on the common electrode

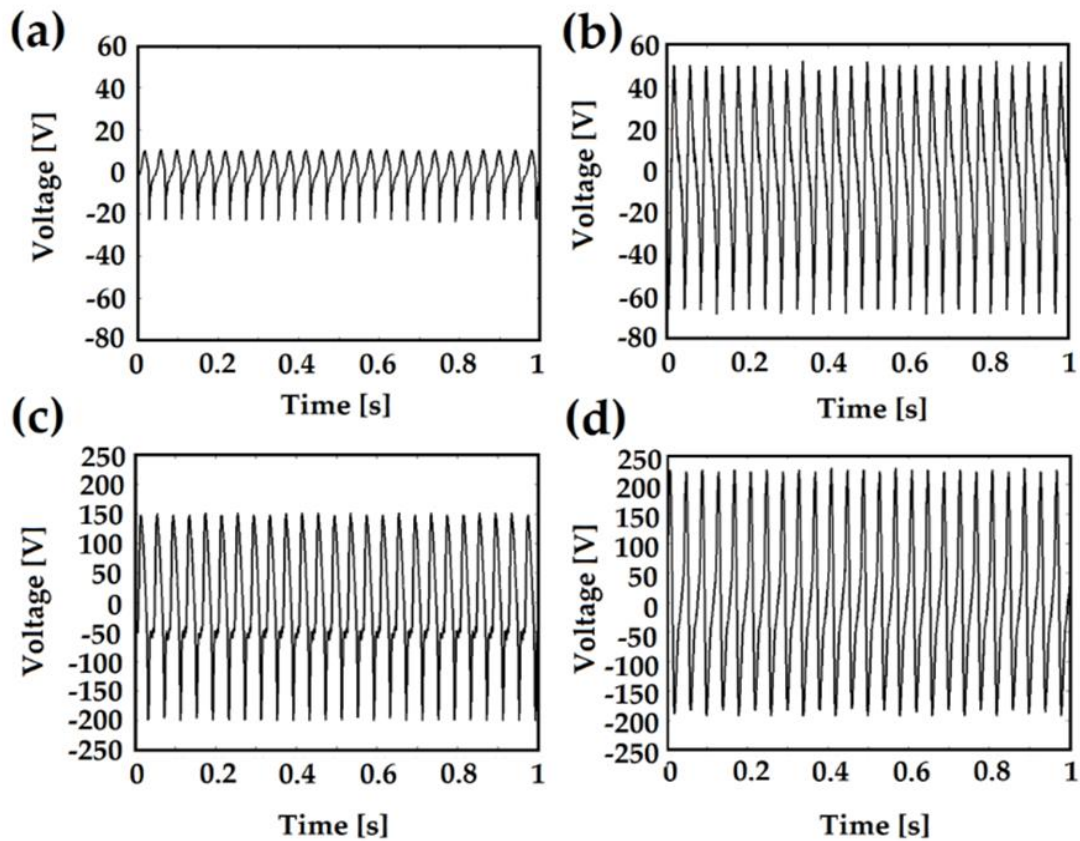
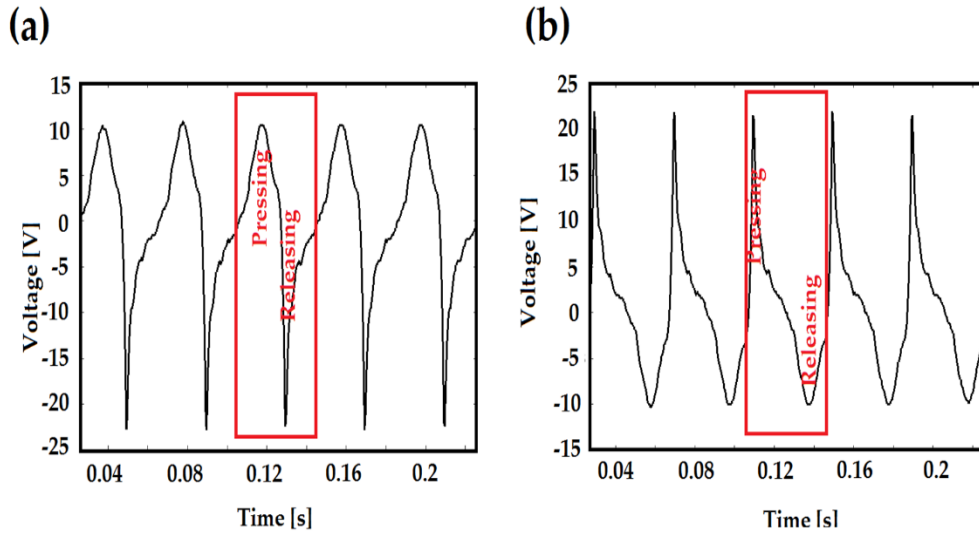


Figure 4.6 Mutual output enhancement of PENG and TENG (a) Voc of PENG when acting alone, (b) Voc of PENG enhanced by the electrostatic induced charge on the shim substrate, (c) Voc of TENG when acting alone, (d) Voc of TENG enhanced by the piezoelectric induced charge on the common electrode.

caused by the strained ZnO nanostructure, the peak to peak output voltage of TENG also increases from 352V to 420V. Detailed time domain output voltages with the output enhancement is shown in Figure 4.6.

Moreover, to confirm that the measured output signals of the PENG device are generated by the piezoelectric properties of the ZnO nanostructured materials, we conducted switching polarity test [195] and the polarity of the output signal is inverted



when the connection of the measurement instrument is switched as shown in Figure 4.7.

Figure 4.7 The measured output voltage signals of the PENG device in (a) forward connection, and (b) reverse connection of the measurement instrument during testing.

The load matching of the hybrid energy cell has been performed by varying the load resistor from  $5\Omega$  to  $105\text{M}\Omega$  and measuring the corresponding voltages across different loads and currents through different loads as shown in Figure 4.8 (a) and the power delivered to the load has been calculated from the measure values of currents and voltages and plotted against different loads (Figure 4.8 (b)) and the device yields a maximum output power of  $0.774\text{mW}$  at a match load of  $21\text{M}\Omega$ . To further investigate the supremacy of the hybrid device over its individual components, a  $4.7\mu\text{F}$  capacitor has been charged using the piezo, tribo and hybrid configuration of the device and Figure 4.8 (c) shows that with the hybrid operation mode the capacitor is charged up to  $12\text{V}$  within  $120\text{s}$  when the piezo and tribo electric device parts can charge the same capacitor up to  $3.7\text{V}$  and  $9.4\text{V}$  respectively in  $120\text{s}$ . Several other commercial capacitors have been charged with the hybrid device operation mode and the device is able to charge up to  $470\mu\text{F}$  capacitor quite fast as shown in Figure 4.8 (d).

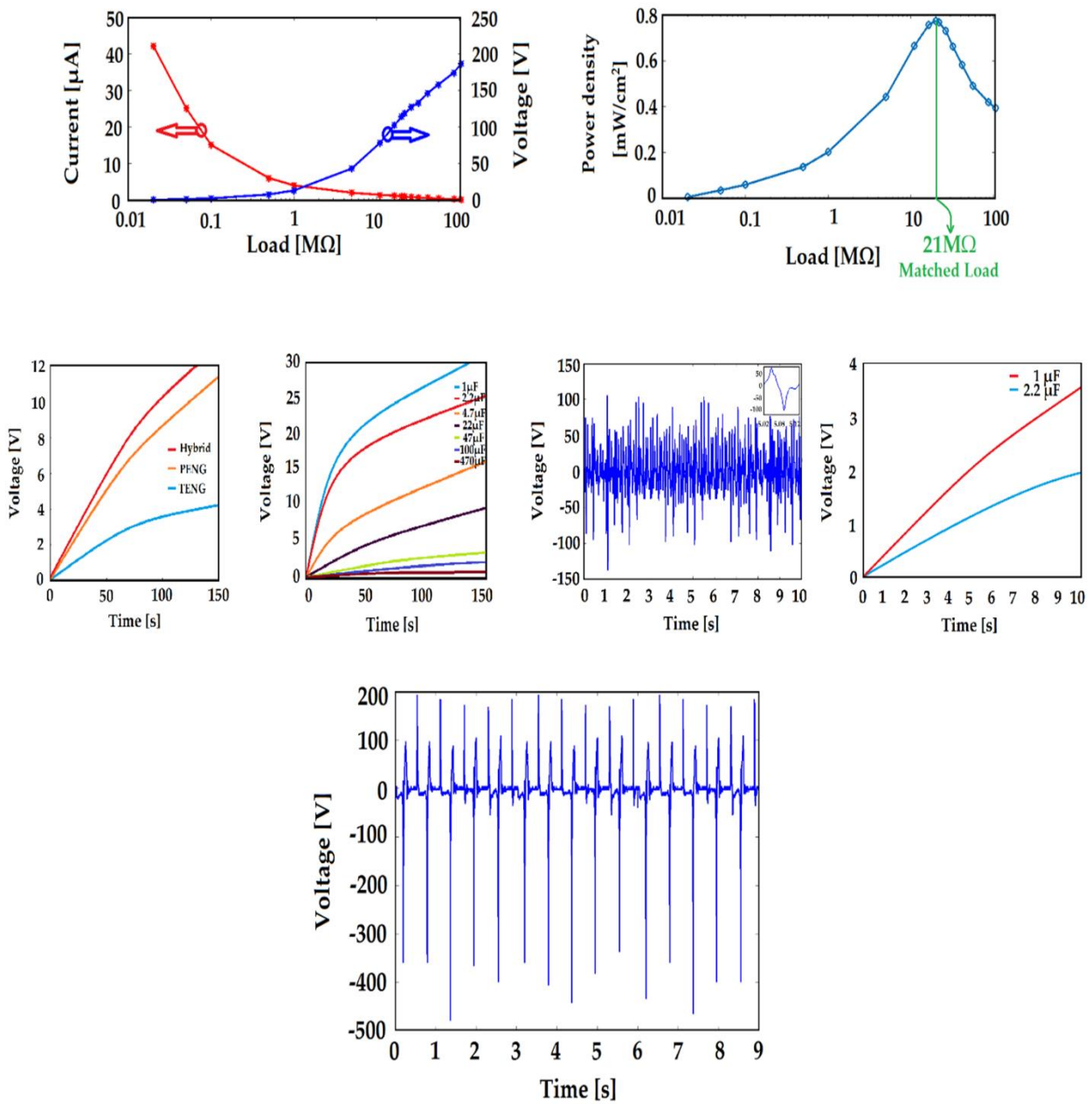


Figure 4.8 Electrical characterization of the hybrid device (a) output voltages and currents for different loads varying from 20k $\Omega$  to 105M $\Omega$ , (b) output power as a function of load resistance (c) Charging characteristic of the device with a 4.7 $\mu\text{F}$  capacitor. (d) Fast charging behavior of the device with different capacitors (e) –(f) Output voltage signal and charging behavior of the device with normal human movements (g) Collected output signal by the harvester from human walking.

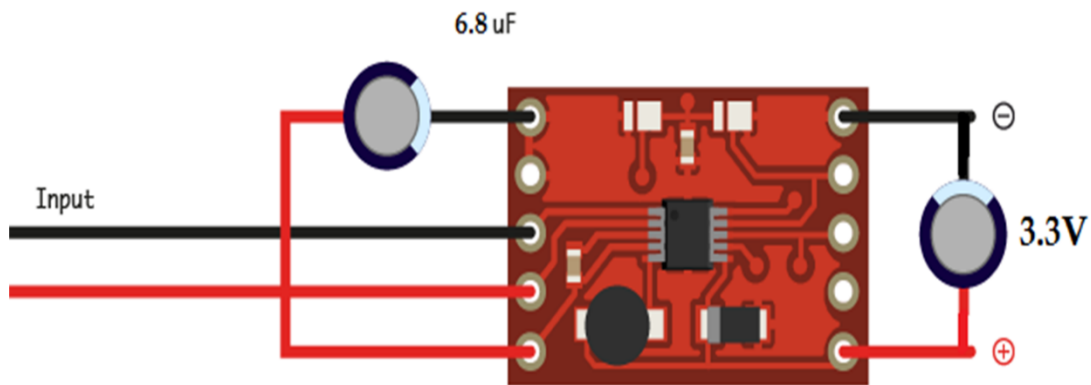
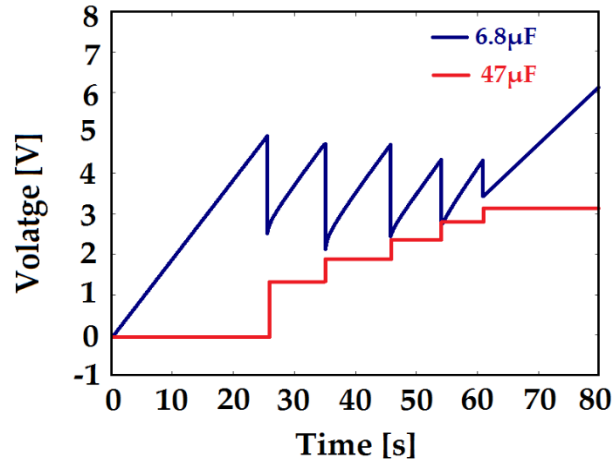


Figure 4.9 (a) Energy collection using commercial piezoelectric energy harvesting unit with  $6.8\mu\text{F}$  and  $47\mu\text{F}$  capacitors in the input and output side respectively. (b) Circuit diagram for energy collection from the hybrid device using Linear Technology's LTC3588-1LTC. (Input side capacitor =  $6.8\mu\text{F}$  and output side capacitor  $47\mu\text{F}$ ).

Later on, to validate the future possibility of the hybrid device for wearable devices, the device was placed under a wristband fitness tracker and the device produces an average peak to peak voltage of 160V from normal hand movement as shown in Figure 4.8 (e) and from this normal hand movement the device is able to charge commercial capacitors up to few volts within seconds (Figure 4.8 (f)) that clearly exhibits their ability to be used to develop self-powered wearable devices. Moreover, the device was assembled under the shoe to harvest energy from human walking to

corroborate its potential further for self-powered wearable electronics. Figure 4.8 (g) shows the output signal collected from walking using the hybrid configuration and the output voltage can go as high as 672V peak to peak that can be collected efficiently for subsequent use.

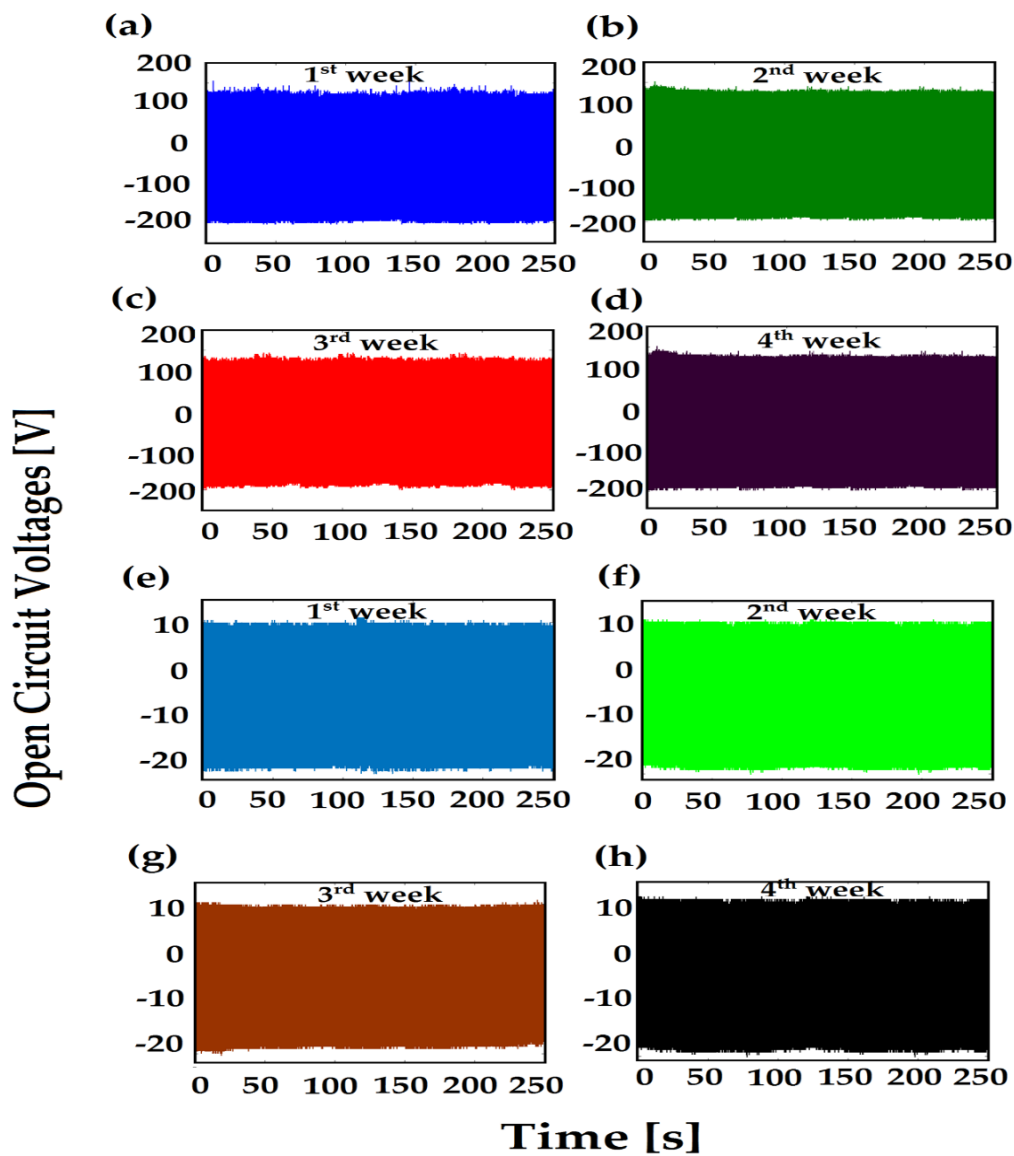


Figure 4.10 Measured open-circuit voltage of the (a) – (d) TENG, and (e) - (h) PENG device tested over three consecutive weeks. The response remains unchanged, which demonstrates the stability and reliability of the device. The excitation frequency and the acceleration amplitude were 25Hz and 1G respectively in all tests.

We also used the hybrid device as to collect energy efficiently using commercial piezoelectric energy harvesting power supplies unit (Linear Technology's LTC3588-1LTC) and the output voltage of the output capacitor reaches to 3.3V in 65s, as shown in Figure 4.9 (a), which clearly exhibits the potential of the hybrid device to run a wireless MCU unit that is used to acquire, process, and transmit data [196]. The circuit connection used for the energy collection is shown in Figure 4.9 (b).

Finally, to demonstrate the long-term mechanical stability and reliability of the device, it was tested over 200000 cycles over four consecutive weeks. The consistent output voltage waveforms from both the TENG and PENG parts of the hybrid device with no perceivable performance degradation over time as shown in Figure 4.10 clearly exhibits long-term stability and robustness of the device.

#### **4.4 Conclusion**

In summary, a novel hybrid energy harvester unit as a promising and reliable power source combining piezoelectric and triboelectric effects has been designed, fabricated and characterized, which is composed of p-n junction type ZnO nanostructures grown by low-temperature hydrothermal method for the piezoelectric part and nanostructured Al and PTFE films for the triboelectric part. In the open-circuit configuration, the piezoelectric and triboelectric output average peak-to-peak voltages are 34.8 V and 352 V with 25Hz frequency and 1G acceleration, respectively. Interestingly, due to mutual enhancement, peak-to-peak output open-circuit voltage of the PENG increases from 34.8V to 120V when TENG is shorted and peak-to-peak output open-circuit voltage of the TENG increases from 352V to 420V when PENG is shorted. To avoid the internal impedance mismatch as well as the voltage cancelation due to the phase difference of piezoelectric and triboelectric nanogenerator, two full-wave bridge rectifiers have been employed that leads to an average peak output voltage of 186 V, current density of 100.8 mA/m<sup>2</sup>, and average peak power density of 18.35 W/m<sup>2</sup> from the hybrid device. While connecting with varied external resistances,

the hybrid device produces an output power of 0.764mW under the matched load of 21M $\Omega$  and the device also demonstrates the energy harvesting capability by charging several commercial capacitors within seconds. Besides, the hybrid device can charge a particular capacitor faster compared to its individual components. The high output as well as the fast charging characteristics enable the hybrid energy harvester to be used as a power source to store electrical energy from mechanical vibrations in the surroundings, which shows great potential in the field of self-powered systems or sensor networks.



## Chapter 5

### Conclusions, Contributions and Recommendations

#### 5.1 Summary and Contributions

This thesis has been carried out with a systematic investigation of organic-/inorganic nanostructured materials based piezoelectric, triboelectric and hybrid energy harvesters, focusing on their materials synthesis and characterization using different hands-on processes, novel device structure design, device fabrication and characterization using state-of-the-art micro-/nano fabrication tools. Different aspects related to materials selection for piezoelectric and triboelectric energy harvesting as well as their structural and morphological impacts on device performance has been explored profoundly in the first part of this research, which not only gives a proper direction to improve the performance of the existing device designs but also provides insight on how to design novel device design with new nanomaterials. The literature review and theoretical background of different energy harvesting devices advance us to closely take into account different parameters related to materials synthesis as well as device design so that substantial contributions can be made towards the goal of this research, such as implementation of a self-powered systems, i.e., a fully wireless data transmission system for aircraft SHM.

In the next part of this research, a high performance and robust PENG device has been demonstrated that is based on 1D/2D ZnO nanostructures. A simple, low temperature solution based method has been employed to grow the piezoelectric ZnO nanomaterials and as this hydrothermal method can be easily tweaked by many process parameters, for example volume and concentration of solutions, solution temperature, thickness and type of seed layers, types of substrate used etc., a systematic analysis has been done to optimize the synthesis process to get the desired

ZnO nanostructure. ZnO nanowires and nanoplates are grown together on the same substrate directly using the optimized synthesis process to fabricate a PENG device and subsequently the device has been tested using a special characterization system designed particularly for the mechanical energy harvesting devices. A routine analysis of the device has been performed, for example the measurements of open circuit voltage and short circuit current signals from the device at different frequencies and accelerations of the applied mechanical vibration. Besides, a comparison of the device with another PENG device on PET substrate that is based on ZnO nanowires has been presented and then load matching of the nanogenerator has been carried out to find out the output load that can draw the maximum electrical power from the device.

Subsequently, since hybrid energy harvesting devices have strong potential to support a wide range of self-powered electronics due to their higher output performance and better charging characteristics than its individual energy harvester components, a hybrid nanogenerator has been designed by integrating a PENG and a TENG together, where these two parts can work independently and/or simultaneously. To increase the effective friction between the two tribo material layers to consequently enhance the performance of the TENG, nanostructures have been grown on both PTFE and Al surface using different simple yet powerful techniques, i.e., e-beam evaporation, RIE etching, DI water treatment etc. This hybrid harvester unit shows not only the mutual enhancement of the PENG and TENG parts from each other by sharing an electrode between them but also an innovative way of harvesting mechanical energy using two components in a single press-and-release cycle that leads to higher energy conversion efficiency. The hybrid device exhibits its potential for versatile applications, for example in portable/wearable biomedical devices and personal electronics as it can successfully harvest energy from normal hand movement and human walking. In short, this device shows a systematic way of integrating different kind of energy harvesting mechanisms together in a compact

structure that can either work independently as a single unit and/or simultaneously in the hybrid configuration and thus improving the output performance of energy harvesting devices, which is critical for their practical applications for various self-powered MNSs.

## **5.2 Recommendations for Future Work**

Since their first demonstration of PENGs and TENGs, they have evolved quite dramatically over the last decade and integrating them together in a single device structure to design a hybrid energy harvester unit has also drawn broad interest with particular focus on their performance improvement as well as addressing key challenges in their development. The progress of PENGs, TENGs and hybrid NGs would certainly open new routes to realize a highly efficient, miniaturized, reliable, intelligent, extremely sensitive and multifunctional nano system and even micro-systems. Finally, to follow this research on nanotechnology-enabled energy harvesting for self-powered electronics particularly for a fully wireless aircraft SHM system, there are two distinguished directions to work on in the future – (i) Device improvement, (ii) Implementation and integration of the devices in MNSs.

## Letters of Copyright Permission

Permission for Figure 1.1

9/26/2018

RightsLink Printable License

### JOHN WILEY AND SONS LICENSE TERMS AND CONDITIONS

Sep 26, 2018

---

This Agreement between University of Waterloo ("You") and John Wiley and Sons ("John Wiley and Sons") consists of your license details and the terms and conditions provided by John Wiley and Sons and Copyright Clearance Center.

License Number	4435401204376
License date	Sep 24, 2018
Licensed Content Publisher	John Wiley and Sons
Licensed Content Publication	Angewandte Chemie International Edition
Licensed Content Title	Nanotechnology-Enabled Energy Harvesting for Self-Powered Micro-/Nanosystems
Licensed Content Author	Zhong Lin Wang, Wenzhuo Wu
Licensed Content Date	Nov 4, 2012
Licensed Content Volume	51
Licensed Content Issue	47
Licensed Content Pages	22
Type of use	Dissertation/Thesis
Requestor type	University/Academic
Format	Electronic
Portion	Figure/table
Number of figures/tables	1
Original Wiley figure/table number(s)	Figure 2
Will you be translating?	No
Title of your thesis / dissertation	Advanced NEMS for energy harvesting
Expected completion date	Dec 2018
Expected size (number of pages)	1
Requestor Location	University of Waterloo 200 University Ave West  waterloo, ON n2l 3g1 Canada Attn: University of Waterloo
Publisher Tax ID	EU826007151
Total	0.00 USD

## Permission for Figure 1.4

9/26/2018

RightsLink Printable License

### JOHN WILEY AND SONS LICENSE TERMS AND CONDITIONS

Sep 26, 2018


---

This Agreement between University of Waterloo ("You") and John Wiley and Sons ("John Wiley and Sons") consists of your license details and the terms and conditions provided by John Wiley and Sons and Copyright Clearance Center.

License Number	4435400051730
License date	Sep 24, 2018
Licensed Content Publisher	John Wiley and Sons
Licensed Content Publication	Advanced Materials
Licensed Content Title	Sound-Driven Piezoelectric Nanowire-Based Nanogenerators
Licensed Content Author	Seung Nam Cha, Ju-Seok Seo, Seong Min Kim, et al
Licensed Content Date	Aug 30, 2010
Licensed Content Volume	22
Licensed Content Issue	42
Licensed Content Pages	5
Type of use	Dissertation/Thesis
Requestor type	University/Academic
Format	Electronic
Portion	Figure/table
Number of figures/tables	1
Original Wiley figure/table number(s)	Figure 2
Will you be translating?	No
Title of your thesis / dissertation	Advanced NEMS for energy harvesting
Expected completion date	Dec 2018
Expected size (number of pages)	1
Requestor Location	University of Waterloo 200 University Ave West  waterloo, ON n2l 3g1 Canada Attn: University of Waterloo
Publisher Tax ID	EU826007151
Total	0.00 CAD

# Permission for Figure 1.5

9/29/2018 Copyright Clearance Center



Back to view orders

Copy order

Confirmation Number: 11750996  
Order Date: 09/24/2018

Print this page  
Print terms & conditions  
Print citation information  
(What's this?)

**Customer Information**

Customer: Alam Mahmud  
Account Number: 3001332071  
Organization: Alam Mahmud  
Email: a3mahmud@uwaterloo.ca  
Phone: +1 (226) 978-9640

Search order details by:

**This is not an invoice**

**Order Details**

**Faraday discussions** Billing Status: N/A

Order detail ID: 71570796	Permission Status: <span style="color: green;">✔</span> <b>Granted</b>
ISSN: 1364-5498	Permission type: Republish or display content
Publication Type: e-Journal	Type of use: Thesis/Dissertation
Volume:	Order License Id: 4435400806562
Issue:	<a href="#">Hide details</a>
Start pages:	Requestor type: Academic institution
Publisher: FARADAY DIVISION, ROYAL CHEMICAL SOCIETY,	Format: Electronic
Author/Editor: Royal Society of Chemistry (Great Britain).Faraday Division ; Royal Society of Chemistry (Great Britain)	Portion: image/photo
	Number of images/photos requested: 1
	The requesting person/organization: Alam Mahmud
	Title or numeric reference of the portion(s): Figure 1
	Title of the article or chapter the portion is from: Triboelectric nanogenerators as new energy technology and self-powered sensors - Principles, problems and perspectives
	Editor of portion(s): N/A
	Author of portion(s): N/A
	Volume of serial or monograph: N/A
	Page range of portion: 447
	8th September 2014

<https://www.copyright.com/order/view.do?id=11750996&rp=main&sf=false&cp=1&viewOrder=1> 1/2

9/29/2018 Copyright Clearance Center

Publication date of portion	
Rights for	Main product
Duration of use	Life of current edition
Creation of copies for the disabled	no
With minor editing privileges	no
For distribution to	Worldwide
In the following language(s)	Original language of publication
With incidental promotional use	no
Lifetime unit quantity of new product	Up to 499
Title	Advanced NEMS for energy harvesting
Instructor name	Dr Dayan Ban
Institution name	University of Waterloo
Expected presentation date	Dec 2018


Note: This item was invoiced separately through our RightsLink service. More info \$ 0.00

<b>Total order items: 1</b>	<b>Order Total: \$0.00</b>
-----------------------------	----------------------------

<https://www.copyright.com/order/view.do?id=11750996&rp=main&sf=false&cp=1&viewOrder=1> 2/2

## Permission for Figure 2.1

9/28/2018 Copyright Clearance Center



[Back to view orders](#)

[Print this page](#)  
[Print terms & conditions](#)  
[Print citation information \(What's this?\)](#)

**Confirmation Number: 11749000**  
**Order Date: 09/17/2018**

---

**Customer Information**

Customer: Alam Mahmud  
 Account Number: 3001332071  
 Organization: Alam Mahmud  
 Email: a8mahmud@uwaterloo.ca  
 Phone: +1 (226) 978-9640


---

Search order details by:

**This is not an invoice**

**Order Details**

Journal of materials chemistry Billing Status: N/A

Order detail ID: 71559816	Permission Status:  <b>Granted</b>
ISSN: 1364-5501	Permission type: Republish or display content
Publication Type: e-Journal	Type of use: Thesis/Dissertation
Volume:	Order License Id: 4431390942650
Issue:	<a href="#">Hide details</a>
Start page:	Requestor type: Academic institution
Publisher: ROYAL SOCIETY OF CHEMISTRY,	Format: Electronic
Author/Editor: Royal Society of Chemistry (Great Britain)	Portion: image/photo
	Number of images/photos requested: 1
	The requesting person/organization: Alam Mahmud
	Title or numeric reference of the portion(s): Figure 1
	Title of the article or chapter the portion is from: Nanowire and nanobelt arrays of zinc oxide from synthesis to properties and to novel devices
	Editor of portion(s): N/A
	Author of portion(s): N/A
	Volume of serial or monograph: N/A
	Page range of portion: 712
	Publication date of portion: 19th January 2007
	Rights for: Main product

<https://www.copyright.com/order/view.do?ci=11749000&rp=main&sf=false&cp=1> 1/2

9/28/2018 Copyright Clearance Center

Duration of use	Life of current edition
Creation of copies for the disabled	no
With minor editing privileges	no
For distribution to	Canada
In the following language(s)	Original language of publication
With incidental promotional use	no
Lifetime unit quantity of new product	Up to 499
Title	Advanced NEMS for energy harvesting
Instructor name	Dr Dayan Ban
Institution name	University of Waterloo
Expected presentation date	Dec 2018

**Note:** This item was invoiced separately through our RightsLink service. [More info](#) \$ 0.00


---

<b>Total order items: 1</b>	<b>Order Total: \$0.00</b>
-----------------------------	----------------------------

<https://www.copyright.com/order/view.do?ci=11749000&rp=main&sf=false&cp=1> 2/2

## Permission for Figure 2.2

9/28/2018 Copyright Clearance Center



Back to view orders

[Copy order](#)

Confirmation Number: 11749021  
Order Date: 09/17/2018

Print this page  
Print terms & conditions  
Print citation information  
[\(What's this?\)](#)

**Customer Information**

Customer: Alam Mahmud  
Account Number: 3001332071  
Organizations: Alam Mahmud  
Email: a3mahmud@uwaterloo.ca  
Phone: +1 (226) 978-9640

Search order details by:

**This is not an invoice**

**Order Details**

Nanotechnology Billing Status: N/A

<b>Order detail ID:</b> 71550688	<b>Permission Status:</b> <span style="color: green;">✔</span> <b>Granted</b>
<b>ISSN:</b> 0957-4484	<b>Permission type:</b> Republish or display content
<b>Publication Type:</b> Journal	<b>Type of use:</b> Thesis/Dissertation
<b>Volumes:</b>	<b>Order License Id:</b> 4431420332207
<b>Issue:</b>	<a href="#">Hide details</a>
<b>Start page:</b>	<b>Requestor type:</b> Academic institution
<b>Publisher:</b> IOP Publishing	<b>Format:</b> Electronic
<b>Author/Editor:</b> Institute of Physics (Great Britain) ; American Institute of Physics	<b>Portion:</b> image/photo
	<b>Number of images/photos requested:</b> 1
	<b>The requesting person/organization:</b> Alam Mahmud
	<b>Title or numeric reference of the portion(s):</b> Figure 1
	<b>Title of the article or chapter the portion is from:</b> Synthesis and optical properties of single crystal ZnO nanorods
	<b>Editor of portion(s):</b> N/A
	<b>Author of portion(s):</b> 34, B P Zhang, N T Binh, K Wakatsuki, Y Segawa, Y Kashivaba and K Haga
	<b>Volume of serial or monograph:</b> N/A
	<b>Issue, if republishing an article from a serial:</b> 15
	<b>Page range of portion:</b> S383

<https://www.copyright.com/order/view.do?id=11749021&rp=main&sf=false&cp=1&viewOrder=1> 1/2

9/28/2018 Copyright Clearance Center

<b>Publication date of portion:</b>	27 April 2004
<b>Rights for:</b>	Main product
<b>Duration of use:</b>	Life of current edition
<b>Creation of copies for the disabled:</b>	no
<b>With minor editing privileges:</b>	no
<b>For distribution to:</b>	Worldwide
<b>In the following language(s):</b>	Original language of publication
<b>With incidental promotional use:</b>	no
<b>Lifetime unit quantity of new product:</b>	Up to 499
<b>Title:</b>	Advanced NEMS for energy harvesting
<b>Instructor name:</b>	Dr Dayan Ban
<b>Institution name:</b>	University of Waterloo
<b>Expected presentation date:</b>	Dec 2018

**Note:** This item was invoiced separately through our [RightsLink service](#). [More info](#) \$ 0.00


<b>Total order items:</b> 1	<b>Order Total:</b> \$0.00
-----------------------------	----------------------------

<https://www.copyright.com/order/view.do?id=11749021&rp=main&sf=false&cp=1&viewOrder=1> 2/2



## Permission for Figure 2.7

9/28/2018 Copyright Clearance Center



Back to view orders

Copy order

Confirmation Number: 11749105  
Order Date: 09/17/2018

Print this page  
Print terms & conditions  
Print citation information  
[/What's this?](#)

**Customer Information**

Customer: Alam Mahmud  
Account Number: 3001332071  
Organization: Alam Mahmud  
Email: a0mahmud@uwaterloo.ca  
Phone: +1 (226) 979-9640

Search order details by:

**This is not an invoice**

**Order Details**

Journal of Physics D : Applied Physics Billing Status: N/A

Order detail ID: 71558895	<b>Permission Status:</b> <span style="color: green;">✔</span> <b>Granted</b>
ISSN: 0022-3727	<b>Permission type:</b> Republish or display content
<b>Publication Type:</b> Journal	<b>Type of use:</b> Thesis/Dissertation
<b>Volume:</b>	<b>Order License Id:</b> 4431480750585
<b>Issue:</b>	<a href="#">Hide details</a>
<b>Start page:</b>	<b>Requestor type:</b> Academic institution
<b>Publisher:</b> IOP Publishing	<b>Format:</b> Print, Electronic
<b>Author/Editor:</b> Institute of Physics and the Physical Society ; Institute of Physics (Great Britain)	<b>Portion:</b> image/photo
	<b>Number of images/photos requested:</b> 1
	<b>The requesting person/organization:</b> Alam Mahmud
	<b>Title or numeric reference of the portion(s):</b> Figure 2
	<b>Title of the article or chapter the portion is from:</b> Contact electrification of insulating materials
	<b>Editor of portion(s):</b> N/A
	<b>Author of portion(s):</b> Daniel J Lacks and R. Mohan Sankaran
	<b>Volume of serial or monograph:</b> N/A
	<b>Issue, if republishing an article from a serial:</b> 44
	<b>Page range of portion:</b> n/a
	28 October 2011

<https://www.copyright.com/order/view.do?id=11749105&rp=main&sf=false&cp=1&viewOrder=1> 1/2

9/28/2018 Copyright Clearance Center

<b>Publication date of portion</b>	Main product
<b>Rights for</b>	Life of current edition
<b>Duration of use</b>	no
<b>Creation of copies for the disabled</b>	no
<b>With minor editing privileges</b>	no
<b>For distribution to</b>	Worldwide
<b>In the following language(s)</b>	Original language of publication
<b>With incidental promotional use</b>	no
<b>Lifetime unit quantity of new product</b>	Up to 499
<b>Title</b>	Advanced NEMS for energy harvesting
<b>Instructor name</b>	Dr Dayan Ban
<b>Institution name</b>	University of Waterloo
<b>Expected presentation date</b>	Dec 2018

Note: This item was invoiced separately through our RightsLink service. [More info](#) \$ 0.00

<b>Total order items: 1</b>	<b>Order Total: \$0.00</b>
-----------------------------	----------------------------

<https://www.copyright.com/order/view.do?id=11749105&rp=main&sf=false&cp=1&viewOrder=1> 2/2

## Permission for Figure 2.8

9/26/2018 Rightslink® by Copyright Clearance Center

 **Copyright Clearance Center**  
Most Trusted. Most Cited. Most Read.

**RightsLink®**

[Home](#) [Account Info](#) [Help](#) 

 **ACS Publications**  
Most Trusted. Most Cited. Most Read.

**Title:** Integrated Multilayered Triboelectric Nanogenerator for Harvesting Biomechanical Energy from Human Motions

**Author:** Peng Bai, Guang Zhu, Zong-Hong Lin, et al

**Publication:** ACS Nano

**Publisher:** American Chemical Society

**Date:** Apr 1, 2013

Copyright © 2013, American Chemical Society

Logged in as:  
Alam Mahmud  
Account #: 3001332071

[LOGOUT](#)

### PERMISSION/LICENSE IS GRANTED FOR YOUR ORDER AT NO CHARGE

This type of permission/license, instead of the standard Terms & Conditions, is sent to you because no fee is being charged for your order. Please note the following:

- Permission is granted for your request in both print and electronic formats, and translations.
- If figures and/or tables were requested, they may be adapted or used in part.
- Please print this page for your records and send a copy of it to your publisher/graduate school.
- Appropriate credit for the requested material should be given as follows: "Reprinted (adapted) with permission from (COMPLETE REFERENCE CITATION). Copyright (YEAR) American Chemical Society." Insert appropriate information in place of the capitalized words.
- One-time permission is granted only for the use specified in your request. No additional uses are granted (such as derivative works or other editions). For any other uses, please submit a new request.

If credit is given to another source for the material you requested, permission must be obtained from that source.

[BACK](#)

[CLOSE WINDOW](#)

Copyright © 2018 Copyright Clearance Center, Inc. All Rights Reserved. [Privacy statement](#). [Terms and Conditions](#).  
Comments? We would like to hear from you. E-mail us at [customercare@copyright.com](mailto:customercare@copyright.com)

## Permission for Figure 2.8

9/26/2018

RightsLink Printable License

### ELSEVIER LICENSE TERMS AND CONDITIONS

Sep 26, 2018

This Agreement between University of Waterloo ("You") and Elsevier ("Elsevier") consists of your license details and the terms and conditions provided by Elsevier and Copyright Clearance Center.

License Number	4436530629873
License date	Sep 26, 2018
Licensed Content Publisher	Elsevier
Licensed Content Publication	Nano Energy
Licensed Content Title	Power-generating shoe insole based on triboelectric nanogenerators for self-powered consumer electronics
Licensed Content Author	Guang Zhu,Peng Bai,Jun Chen,Zhong Lin Wang
Licensed Content Date	Sep 1, 2013
Licensed Content Volume	2
Licensed Content Issue	5
Licensed Content Pages	5
Start Page	688
End Page	692
Type of Use	reuse in a thesis/dissertation
Portion	figures/tables/illustrations
Number of figures/tables/illustrations	1
Format	both print and electronic
Are you the author of this Elsevier article?	No
Will you be translating?	No
Original figure numbers	Figure 1
Title of your thesis/dissertation	Advanced Nanoelectromechanical Systems for Next generation Energy Harvesting
Expected completion date	Nov 2018
Estimated size (number of pages)	100
Requestor Location	University of Waterloo 200 University Ave West  waterloo, ON n2l 3g1 Canada Attn: University of Waterloo
Publisher Tax ID	GB 494 6272 12
Total	0.00 USD

## Permission for Figure 2.9



RightsLink®

Home

Create Account

Help



ACS Publications  
Most Trusted. Most Cited. Most Read.

**Title:** r-Shaped Hybrid Nanogenerator with Enhanced Piezoelectricity  
**Author:** Mengdi Han, Xiao-Sheng Zhang, Bo Meng, et al  
**Publication:** ACS Nano  
**Publisher:** American Chemical Society  
**Date:** Oct 1, 2013  
Copyright © 2013, American Chemical Society

LOGIN

If you're a [copyright.com](#) user, you can login to RightsLink using your [copyright.com](#) credentials. Already a [RightsLink](#) user or want to [learn more?](#)

### PERMISSION/LICENSE IS GRANTED FOR YOUR ORDER AT NO CHARGE

This type of permission/license, instead of the standard Terms & Conditions, is sent to you because no fee is being charged for your order. Please note the following:

- Permission is granted for your request in both print and electronic formats, and translations.
- If figures and/or tables were requested, they may be adapted or used in part.
- Please print this page for your records and send a copy of it to your publisher/graduate school.
- Appropriate credit for the requested material should be given as follows: "Reprinted (adapted) with permission from (COMPLETE REFERENCE CITATION). Copyright (YEAR) American Chemical Society." Insert appropriate information in place of the capitalized words.
- One-time permission is granted only for the use specified in your request. No additional uses are granted (such as derivative works or other editions). For any other uses, please submit a new request.

If credit is given to another source for the material you requested, permission must be obtained from that source.

BACK

CLOSE WINDOW

Copyright © 2018 [Copyright Clearance Center, Inc.](#) All Rights Reserved. [Privacy statement](#). [Terms and Conditions](#). Comments? We would like to hear from you. E-mail us at [customer care@copyright.com](mailto:customer care@copyright.com)

## Permission for Figure 3.5

9/26/2018

Rightslink® by Copyright Clearance Center



RightsLink®

Home

Account Info

Help



**Title:** Two-Dimensional Vanadium-Doped ZnO Nanosheet-Based Flexible Direct Current Nanogenerator

Logged in as:  
Alam Mahmud  
Account #:  
3001332071

**Author:** Manoj Kumar Gupta, Ju-Hyuck Lee, Keun Young Lee, et al

LOGOUT

**Publication:** ACS Nano

**Publisher:** American Chemical Society

**Date:** Oct 1, 2013

Copyright © 2013, American Chemical Society

### PERMISSION/LICENSE IS GRANTED FOR YOUR ORDER AT NO CHARGE

This type of permission/license, instead of the standard Terms & Conditions, is sent to you because no fee is being charged for your order. Please note the following:

- Permission is granted for your request in both print and electronic formats, and translations.
- If figures and/or tables were requested, they may be adapted or used in part.
- Please print this page for your records and send a copy of it to your publisher/graduate school.
- Appropriate credit for the requested material should be given as follows: "Reprinted (adapted) with permission from (COMPLETE REFERENCE CITATION). Copyright (YEAR) American Chemical Society." Insert appropriate information in place of the capitalized words.
- One-time permission is granted only for the use specified in your request. No additional uses are granted (such as derivative works or other editions). For any other uses, please submit a new request.

If credit is given to another source for the material you requested, permission must be obtained from that source.

BACK

CLOSE WINDOW

Copyright © 2018 [Copyright Clearance Center, Inc.](#) All Rights Reserved. [Privacy statement.](#) [Terms and Conditions.](#) Comments? We would like to hear from you. E-mail us at [customercare@copyright.com](mailto:customercare@copyright.com)

## References

- [1] Z. L. Wang, and W. Wu, "Nanotechnology-Enabled Energy Harvesting for Self-Powered Micro-/Nanosystems," *Angew. Chem. Int. Ed.* **2012**, 51, 2 – 24.
- [2] G. E. Moore, "Cramming More Components onto Integrated Circuits," *Proceedings of the IEEE* **1998**, 86, 1.
- [3] Z. L. Wang, "Self-Powered Nanosensors and Nanosystems," *Adv. Mater.* **2012**, 24, 280–285.
- [4] P. Glynne-Jones, and N. M. White, "Self-powered systems: a review of energy sources," *Sensor Review* **2001**, 21 (2), 91-98.
- [5] M. Grätzel, "Dye-sensitized solar cells," *Journal of Photochemistry and Photobiology C: Photochemistry Reviews* **2003**, 4, 145–153.
- [6] S. Aricò, P. Bruce, B. Scrosati, J. -M. Tarascon, and W. V. Schalkwijk, "Nanostructured materials for advanced energy conversion and storage devices," *Nature materials* **2005**, 4, 366–377.
- [7] Z. L. Wang, and J. Song, "Piezoelectric Nanogenerators Based on Zinc Oxide Nanowire Arrays" *Science* **2006**, 312 (5771): 242–246.
- [8] F. R. Fan, Z. Q. Tian, and Z. L. Wang, "Flexible triboelectric generator," *Nano Energy* **2012**, 1 (2): 328–334.
- [9] Y. Yang, W. Guo, K. C. Pradel, G. Zhu, Y. Zhou, Y. Zhang, Y. Hu, L. Lin, and Z. L. Wang, "Pyroelectric Nanogenerators for Harvesting Thermoelectric Energy," *Nano Lett.* **2012**, 12 (6), 2833–2838 P. Li, Y. Wen, P. Liu, X. Li, and C. Jia, "A magnetoelectric energy harvester and management circuit for wireless sensor network," *Sensors and Actuators A* **2010**, 157, 100–106.
- [10] X. Wang, "Piezoelectric nanogenerators—Harvesting ambient mechanical energy at the nanometer scale," *Nano Energy* **2012**, 1, 13–24.

- [11] Y. Wang, Y. Yang, and Z. L. Wang, "Triboelectric nanogenerators as flexible power sources," *npj Flexible Electronics* **2017**, 1, 10.
- [12] D. Montalvao, N. M. M. Maia, and A. M. R. Ribeiro, "A Review of Vibration-based Structural Health Monitoring with Special Emphasis on Composite Materials," *Shock and Vibration Digest* **2006**, 38, 4, 295-326.
- [13] W. Fan, and P. Z. Qiao, "Vibration-based Damage Identification Methods: A Review and Comparative Study," *Structural Health Monitoring* **2010**, 10, 1, 83-111.
- [14] D.-H. Wang, and W.-H. Liao, "Wireless transmission for health monitoring of large structures," *IEEE Trans. Instrum. Meas.* **2006**, 55, 972-981.
- [15] Z. L. Wang, and J. H. Song, "Piezoelectric Nanogenerators Based on Zinc Oxide Nanowire Arrays," *Science* **2006**, 312, 242-246.
- [16] X. D. Wang, J. H. Song, J. Liu, and Z. L. Wang, "Direct-Current Nanogenerator Driven by Ultrasonic Waves," *Science* **2007**, 316, 102-105.
- [17] H. S. Kim, J. -H. Kim, and J. Kim, "A review of piezoelectric energy harvesting based on vibration," *J. Int. J. Precis. Eng. Manuf.* **2011**, 12, 6, 1129-1141.
- [18] L. E. Greene, M. Law, J. Goldberger, F. Kim, J. C. Johnson, Y. Zhang, R. J. Saykally, and P. Yang, "Low-temperature wafer-scale production of ZnO nanowire arrays," *J. Angew. Chem. Int. Ed.* **2003**, 42, 3031-3034.
- [19] Z. L. Wang, "Zinc oxide nanostructures: growth, properties and applications," *J. Phys.: Condens. Matter* **2004**, 16, 829-858.
- [20] M. Riaz, J. Song, O. Nur, Z. L. Wang, and M. Willander, "Study of the Piezoelectric Power Generation of ZnO Nanowire Arrays Grown by Different Methods," *Adv. Funct. Mater.* **2011**, 21, 628-633.
- [21] S. N. Cha, J. -S. Seo, S. M. Kim, H. J. Kim, Y. J. Park, S. -W. Kim, and J. M. Kim, "Sound-Driven Piezoelectric Nanowire-Based Nanogenerators," *Adv. Mater.* **2010**, 22, 4726-4730.

- [22] M. -P. Lu, J. Song, M. -Y. Lu, M. -T. Chen, Y. Gao, L. -J. Chen, and Z. L. Wang, "Piezoelectric Nanogenerator Using p-Type ZnO Nanowire Arrays," *Nano Lett.* **2009**, 9 (3), 1223–1227.
- [23] M. -Y. Lu, J. Song, M. -P. Lu, C. -Y. Lee, L. -J. Chen, and Z. L. Wang, "ZnO–ZnS Heterojunction and ZnS Nanowire Arrays for Electricity Generation," *ACS Nano* **2009**, 3, 2, 357-362.
- [24] C. -T. Huang, J. Song, W. -F. Lee, Y. Ding, Z. Gao, Y. Hao, L. -J. Chen, and Z. L. Wang, "GaN Nanowire Arrays for High-Output Nanogenerators," *J. Am. Chem. Soc.* **2010**, 132, 13, 4766–4771.
- [25] Y. -F. Lin, J. Song, Y. Ding, S. -Y. Lu, and Z. L. Wang, "Piezoelectric nanogenerator using CdS nanowires," *Appl. Phys. Lett.* **2008**, 92, 022105.
- [26] Z. Wang, J. Hu, A. P. Suryavanshi, K. Yum, and M. F. Yu, "Voltage Generation from Individual BaTiO<sub>3</sub> Nanowires under Periodic Tensile Mechanical Load," *Nano Lett.* **2007**, 7 (10), 2966–2969
- [27] C. Chang, V. H. Tran, J. Wang, Y. -K. Fuh, and L. Lin, "Direct-Write Piezoelectric Polymeric Nanogenerator with High Energy Conversion Efficiency," *Nano Lett.* 2010, 10 (2): 726–731.
- [28] X. Chen, S. Xu, N. Yao, and Y. Shi, "1.6 V Nanogenerator for Mechanical Energy Harvesting Using PZT Nanofibers," *Nano Lett.* **2010**, 10, 2133–2137.
- [29] K. H. Kim, B. Kumar, K. Y. Lee, H. K. Park, J. H. Lee, H. H. Lee, H. Jun, D. Lee, S. W. Kim, "Piezoelectric two-dimensional nanosheets/anionic layer heterojunction for efficient direct current power generation," *Sci. Rep.* **2013**, 3(6), 2017.
- [30] Z. L. Wang, J. Chen, and L. Lin, "Progress in triboelectric nanogenerators as a new energy technology and self-powered sensors," *Energy Environ. Sci.* **2015**, 8, 2250-2282.



- [31] Q. Zheng, B. Shi, Z. Li, and Z. L. Wang, "Recent Progress on Piezoelectric and Triboelectric Energy Harvesters in Biomedical Systems," *Adv. Sci.* **2017**, 4, 1700029.
- [32] N. Kaur, and K. Pal, "Triboelectric Nanogenerators for Mechanical Energy Harvesting," *Energy Technol.* **2018**, 6, 958 – 997.
- [33] Z. L. Wang, "Triboelectric nanogenerators as new energy technology and self-powered sensors – Principles, problems and perspectives," *Faraday Discuss.* **2014**, 176, 447.
- [34] C. Xu, X. Wang, and Z. L. Wang, "Nanowire Structured Hybrid Cell for Concurrently Scavenging Solar and Mechanical Energies," *J. Am. Chem. Soc.* **2009**, 131 (16), 5866–5872.
- [35] C. Xu, Z. L. Wang, "Compact Hybrid Cell Based on a Convuluted Nanowire Structure for Harvesting Solar and Mechanical Energy", *Adv. Mater.* **2011**, 23, 7, 873-877.
- [36] G. Liu, N. Mrad, E. Abdel-Rahman, and Dayan Ban, "Cascade-type hybrid energy cells for driving wireless sensors," *Nano Energy* **2016**, 26, 641-647.
- [37] C. Pan, Z. Li, W. Guo, J. Zhu, Z. L. Wang, "Fiber Based Hybrid Nanogenerators for/as Self Powered Systems in Biological Liquid", *Angew. Chem. Int. Ed.* **2011**, 50, 11192 –11196.
- [38] W. -S. Jung, M. -G. Kang, H. G. Moon, S. -H. Baek, S. -J. Yoon, Z. L. Wang, S. -W. Kim, and C. -Y. Kang, "High Output Piezo/Triboelectric Hybrid Generator," *Sci. Rep.* **2015**, 5, 9309-9314.
- [39] X. Li, Z. -H. Lin, G. Cheng, X. Wen, Y. Liu, S. Niu, and Z. L. Wang, "3D Fiber-Based Hybrid Nanogenerator for Energy Harvesting and as a Self-Powered Pressure Sensor," *ACS Nano* **2014**, 8, 10, 10674-10681.

- [40] Y. Wu, X. Zhong, X. Wang, Y. Yang, Z. L. Wang, "Hybrid energy cell for simultaneously harvesting wind, solar, and chemical energies," *Nano Res.* **2014**, 7, 11, 1631-1639.
- [41] Y. Yang, H. Zhang, Y. Liu, Z. -H. Lin, S. Lee, Z. Lin, C. P. Wong, and Z. L. Wang, "Silicon-Based Hybrid Energy Cell for Self-Powered Electrodegradation and Personal Electronics," *ACS Nano* **2013**, 7, 3, 2808-2813.
- [42] S. Wang, X. Wang, Z. L. Wang, and Y. Yang, "Efficient Scavenging of Solar and Wind Energies in a Smart City," *ACS Nano* **2016**, 10, 6, 5696-5700.
- [43] M. K. Kim, M. -S. Kim, S. -E. Jo and Y. -J. Kim, "Trieboelectric-thermoelectric hybrid nanogenerator for harvesting frictional energy," *Smart Materials and Structures* **2016**, 25, 12, 125007.
- [44] T. Quan, X. Wang, Z. L. Wang, and Y. Yang, "Hybridized Electromagnetic-Trieboelectric Nanogenerator for a Self-Powered Electronic Watch," *ACS Nano* **2015**, 9, 12, 12301-12310.
- [45] B. Zhang, J. Chen, L. Jin, W. Deng, L. Zhang, H. Zhang, M. Zhu, W. Yang, and Z. L. Wang, "Rotating-Disk-Based Hybridized Electromagnetic-Trieboelectric Nanogenerator for Sustainably Powering Wireless Traffic Volume Sensors," *ACS Nano* **2016**, 10, 6, 6241-6247.
- [46] Z. L. Wang, "On Maxwell's displacement current for energy and sensors: the origin of nanogenerators", *Materials Today* **2017**, 20, 2, 74-82.
- [47] S. Chen, X. Tao, W. Zeng, B. Yang, and S. Shang, "Quantifying Energy Harvested from Contact-Mode Hybrid Nanogenerators with Cascaded Piezoelectric and Trieboelectric Units", *Adv. Energy Mater.* **2016**, 7, 5, 1614-6832.
- [48] J. Song, B. Yang, W. Zeng, Z. Peng, S. Lin, S. J. Li, and X. Tao, "Highly Flexible, Large-Area, and Facile Textile-Based Hybrid Nanogenerator with Cascaded Piezoelectric and Trieboelectric Units for Mechanical Energy Harvesting," *Adv. Mater. Technol.* **2018**, 3, 1800016.

- [49] Q. Zheng, Y. Zou, Y. Zhang, Z. Liu, B. Shi, X. Wang, Y. Jin, H. Ouyang, Z. Li, and Z. L. Wang, "Biodegradable triboelectric nanogenerator as a lifetime designed implantable power source", *Science Advances* **2016**, 2, 3, 1501478.
- [50] Trilaksono<sup>1</sup>, N. Watanabe, H. Hoshi, A. Kondo, Y. Iwahori, S. -I. Takeda, "Continuous Damage Monitoring of a Thin Composite Structural with Mismatched Stiffener in a Combined Joint Using Fiber Bragg Grating under Tension and Three-Point Loading," *Open Journal of Composite Materials* **2013**, 3, 63-87.
- [51] E. J. Lee, T. Y. Kim, S. -W. Kim, S. Jeong, Y. Choi, and S. Y. Lee, "High-performance piezoelectric nanogenerators based on chemically-reinforced composites," *Energy Environ. Sci.* **2018**, 11, 1425-1430.
- [52] C. R. Bowen, H. A. Kim, P. M. Weaver and S. Dunn, "Piezoelectric and ferroelectric materials and structures for energy harvesting applications," *Energy Environ. Sci.* **2014**, 7, 25-44.
- [53] Z. L. Wang, and J. Song, "Piezoelectric Nanogenerators Based on Zinc Oxide Nanowire Arrays," *Science* **2006**, 312, 5771, 242-246.
- [54] G. Zhu, R. Yang, S. Wang, and Z. L. Wang, "Flexible High-Output Nanogenerator Based on Lateral ZnO Nanowire Array," *Nano Lett.* **2010**, 10 (8), 3151-3155.
- [55] K. -H. Kim, B. Kumar, K. Y. Lee, H. -K. Park, J. -H. Lee, H. H. Lee, H. Jun, D. Lee, and S. -W. Kim, "Piezoelectric two-dimensional nanosheets/anionic layer heterojunction for efficient direct current power generation," *Sci. Rep.* **2013**, 3, 2017.
- [56] C. T. Huang, J. H. Song, Y. Li, Y. Ding, Y. Gao, Y. Hao, L. J. Chen, and Z. L. Wang, "GaN Nanowire Arrays for High-Output Nanogenerators," *J. Am. Chem. Soc.* **2010**, 132, 4766-4771.

- [57] W. W. Wu, S. Bai, M. M. Yuan, Y. Qin, Z. L. Wang, and T. Jing, "Lead zirconate titanate nanowire textile nanogenerator for wearable energy-harvesting and self-powered devices," *ACS Nano* **2012**, 6, 6231–6235.
- [58] M. -G. Kan, W. -S. Jung, C. -Y. Kang, and S. -J. Yoon, "Recent Progress on PZT Based Piezoelectric Energy Harvesting Technologies," *Actuators* **2016**, 5, 5.
- [59] S. H. Shin, Y. H. Kim, M. H. Lee, J. Y. Jung, and J. Nah, "Hemispherically Aggregated BaTiO<sub>3</sub> Nanoparticle Composite Thin Film for High-Performance Flexible Piezoelectric Nanogenerator," *ACS Nano* **2014**, 8, 2766–2773.
- [60] Z. Pi, J. Zhang, C. Wen, Z. Zhang, D. Wu, "Flexible piezoelectric nanogenerator made of poly(vinylidene fluoride-co-trifluoroethylene) (PVDF-TrFE) thin film," *Nano Energy* **2014**, 7, 33–41.
- [61] K. I. Park, M. Lee, Y. Liu, S. Moon, G. T. Hwang, G. Zhu, J. E. Kim, S. O. Kim, D. K. Kim, Z. L. Wang, and K. J. Lee, "Flexible Nanocomposite Generator Made of BaTiO<sub>3</sub> Nanoparticles and Graphitic Carbons," *Adv. Mater.* **2012**, 24, 2999–3004.
- [62] Y. F. Hu, Y. Zhang, C. Xu, L. Lin, R. L. Snyder, and Z. L. Wang, "A Nanogenerator for Energy Harvesting from a Rotating Tire and its Application as a Self-Powered Pressure/Speed Sensor," *Adv. Mater.* **2011**, 23, 4068–4071.
- [63] S. Lu, Q. Liao, J. Qi, S. Liu, Y. Liu, Q. Liang, G. Zhang, and Y. Zhang, "The enhanced performance of piezoelectric nanogenerator via suppressing screening effect with Au particles/ZnO nanoarrays Schottky junction," *Nano Res.* **2016**, 9(2), 372–379.
- [64] L. E. Greene, M. Law, J. Goldberger, F. Kim, J. C. Johnson, Y. Zhang, R. J. Saykally, and P. Yang, "Low-Temperature Wafer-Scale Production of ZnO Nanowire Arrays," *J. Angew. Chem. Int. Ed.* **2003**, 42, 3031-3034.

- [65] B. Liu, and H. C. Zeng, "Hydrothermal Synthesis of ZnO Nanorods in the Diameter Regime of 50 nm," *J. Am. Chem. Soc.* **2003**, 125, 4430-4431.
- [66] L. Vayssieres, "Growth of Arrayed Nanorods and Nanowires of ZnO from Aqueous Solutions," *Adv. Mater.* **2003**, 15, No. 5.
- [67] H. Yu, Z. Zhang, M. Han, X. Hao, and F. Zhu, "A General Low-Temperature Route for Large-Scale Fabrication of Highly Oriented ZnO Nanorod/Nanotube Arrays," *J. Am. Chem. Soc.* **2005**, 127, 8, 2378-2379.
- [68] M. Guo, P. Diao, and S. Cai, "Hydrothermal growth of well-aligned ZnO nanorod arrays: Dependence of morphology and alignment ordering upon preparing conditions," *Journal of Solid State Chemistry* **2005**, 178, 1864-1873.
- [69] Z. L. Wang, "Nanostructures of zinc oxide," *Materials Today* **2004**, 7, 6, 26-33.
- [70] Z. L. Wang, "Towards Self-Powered Nanosystems: From Nanogenerators to Nanopiezotronics," *Adv. Funct. Mater.* **2008**, 18, 3553-3567.
- [71] K. C. Pradel, W. Wu, Y. Zhou, X. Wen, Y. Ding, and Z. L. Wang, "Piezotronic effect in solution-grown p-type ZnO nanowires and films," *Nano Lett.* **2013**, 13, 2647-2653.
- [72] Y. Hu, L. Lin, Y. Zhang, and Z. L. Wang, "Replacing a Battery by a Nanogenerator with 20 V Output," *Adv. Mater.* **2012**, 24, 110-114.
- [73] H. Kim, S. M. Kim, H. Son, H. Kim, B. Park, J. Ku, J. I. Sohn, K. Im, J. E. Jang, and J.-J. Park, "Enhancement of piezoelectricity via electrostatic effects on a textile platform," *Energy Environ. Sci.* **2012**, 5, 8932-8936.
- [74] S.-H. Shin, M. H. Lee, J.-Y. Jung, J. H. Seol, and J. Nah, "Piezoelectric performance enhancement of ZnO flexible nanogenerator by a CuO-ZnO p-n junction formation," *J. Mater. Chem. C* **2013**, 1, 8103-8107.
- [75] J. Briscoe, M. Stewart, M. Vopson, M. Cain, P. M. Weaver, and S. Dunn, "Nanostructured p-n Junctions for Kinetic-to-Electrical Energy Conversion," *Adv. Energy Mater.* **2012**, 2, 1261-1268.

- [76] G. Liu, E. Abdel-Rahman, and D. Ban, "Performance optimization of p-n homojunction nanowire based piezoelectric nanogenerators through control of doping concentration," *Journal of Applied Physics* **2015**, 118, 094307.
- [77] X. Wang, J. Song, and Z. L. Wang, "Nanowire and nanobelt arrays of zinc oxide from synthesis to properties and to novel devices," *J. Mater. Chem.* **2007**, 17, 711–720.
- [78] Z. L. Wang, X. Y. Kong, Y. Ding, P. Gao, W. L. Hughes, R. Yang, and Y. Zhang, "Semiconducting and Piezoelectric Oxide Nanostructures Induced by Polar Surfaces," *Adv. Funct. Mater.* **2004**, 14, No. 10, October.
- [79] S. Y. Li, C. Y. Lee, and T. Y. Tseng, "Copper-catalyzed ZnO nanowires on silicon (1 0 0) grown by vapor-liquid-solid process." *Journal of Crystal Growth* **2003**, 247(3-4), 357-362.
- [80] Z. Yin, S. Wu, X. Zhou, X. Huang, Q. Zhang, F. Boey, H. Zhang, "Electrochemical Deposition of ZnO Nanorods on Transparent Reduced Graphene Oxide Electrodes for Hybrid Solar Cells," *small* **2010**, 6, 2, 307–312.
- [81] S. E. Ahn, J. S. Lee, H. Kim, S. Kim, B. H. Kang, K. H. Kim, and G. T., "Photoresponse of sol-gel-synthesized ZnO nanorods," *Applied Physics Letters* **2004** 84(24), 5022-5024.
- [82] R.-Q. Zhang, Y. Lifshitz, and S.-T. Lee, "Oxide-Assisted Growth of Semiconducting Nanowires," *Adv. Mater.* **2003**, 15, 7, April 17.
- [83] Z. L. Wang, "ZnO nanowire and nanobelt platform for nanotechnology," *Materials Science & Engineering R-Reports* **2009**, 64(3-4), 33-71.
- [84] B. P. Zhang, N. T. Binh, K. Wakatsuki, Y. Segawa, Y. Kashiwaba, and K. Haga, "Synthesis and optical properties of single crystal ZnO nanorods," *Nanotechnology* **2004**, 15, 382–388.

- [85] Ü. Özgür, Ya. I. Alivov, C. Liu, A. Teke, M. A. Reshchikov, S. Doğan, Vitaliy Avrutin, S.-J. Cho, and H. Morkoç, "A comprehensive review of ZnO materials and devices," *Journal of Applied Physics* **2005**, 98, 041301.
- [86] B. -P. Zhang, L. -H. Manh, K. Wakatsuki, T.i Ohnishi, M. Lippmaa, N. Usami, M. Kawasaki, and Y. Segawa, "Epitaxial growth and polarity of ZnO films on sapphire (0001) substrates by low-pressure metal organic chemical vapor deposition," *Jpn. J. Appl. Phys.* **2003**, 42, 2291–2295.
- [87] M. Ladanov, M. K. Ram, G. Matthews, and A. Kumar, "Structure and Opto-electrochemical Properties of ZnO Nanowires Grown on n-Si Substrate," *Langmuir* **2011**, 27, 9012–9017.
- [88] M. Pathirane, Ph.D. Thesis, "Flexible 3-Dimensional Hybrid ZnO Nanowire/a-Si:H Thin-Film Solar Cells" University of Waterloo, Canada 2016.
- [89] S. Yamabi, and H. Imai, "Growth conditions for wurtzite zinc oxide films in aqueous solutions," *J. Mater. Chem.* **2002**, 12, 3773–3778.
- [90] Z. L. Wang, J. Chen, and L. Lin, "Progress in triboelectric nanogenerators as a new energy technology and self-powered sensors," *Energy Environ. Sci.* **2015**, 8, 2250-2282.
- [91] F. -R. Fan, Z. -Q. Tian, and Z. L. Wang, "Flexible triboelectric generator!," *Nano Energy* **2012**, 1, 328–334.
- [92] N. Kaur, and K. Pal, "Triboelectric Nanogenerators for Mechanical Energy Harvesting," *Energy Technol.* **2018**, 6, 958 –997.
- [93] Z. L. Wang, L. Lin, J. Chen, S. Niu, and Y. Zi, "Triboelectric Nanogenerators," August 17, **2016**, Springer.
- [94] T. Huang, M. Lu, H. Yu, Q. Zhang, H. Wang, and M. Zhu, "Enhanced Power Output of a Triboelectric Nanogenerator Composed of Electrospun Nanofiber Mats Doped with Graphene Oxide," *Sci Rep.* **2015**, 5: 13942.

- [95] D. J. Lacks, and R. M. Sankaran, "Contact electrification of insulating materials," *J. Phys. D: Appl. Phys.* **2011**, 44, 453001.
- [96] C. A. Sperati, and H. W. Starkweather, "Fluorine-Containing Polymers. II. Polytetrafluoroethylene\*," *Fortschr. Hochpolym.-Forsch.* **1961**, 2, 465–495.
- [97] P. Bai, G. Zhu, Z. -H. Lin, Q. Jing, J. Chen, G. Zhang, J. Ma, and Z. L. Wang, "Integrated Multilayered Triboelectric Nanogenerator for Harvesting Biomechanical Energy from Human Motions," *ACS Nano* **2013**, 7 (4), 3713–3719.
- [98] G. Zhu, P. Baia, J. Chena, and Z. L. Wang, "Power-generating shoe insole based on triboelectric nanogenerators for self-powered consumer electronics," *Nano Energy* **2013**, 2, 688–692.
- [99] J. Chen , G. Zhu , W. Yang , Q. Jing , P. Bai , Y. Yang , T. -C. Hou , and Z. L. Wang, "Harmonic-Resonator-Based Triboelectric Nanogenerator as a Sustainable Power Source and a Self-Powered Active Vibration Sensor," *Adv. Mater.* **2013**, 25, 6094–6099.
- [100] M. Han, X. -S. Zhang, B. Meng, W. Liu, W. Tang, X. Sun, W. Wang, and H. Zhang, "r-Shaped Hybrid Nanogenerator with Enhanced Piezoelectricity," *ACS Nano* **2013**, 7, 10, 8554-8560.
- [101] X. Chen, M. Han, H. Chen, X. Cheng, Y. Song, Z. Su, Y. Jiangc, and H. Zhang, "A wave-shaped hybrid piezoelectric and triboelectric nanogenerator based on P(VDF-TrFE) nanofibers," *Nanoscale* **2017**, 9, 1263–1270.
- [102] X. Li, Z. H. Lin, G. Cheng, X. Wen, Y. Liu, S. Niu, and Z. L. Wang, "3D Fiber-Based Hybrid Nanogenerator for Energy Harvesting and as a Self-Powered Pressure Sensor," *ACS Nano* **2014**, 8, 10674–10681.
- [103] W. S. Jung, M. G. Kang, H. G. Moon, S. H. Baek, S. J. Yoon, Z. L. Wang, S. W. Kim, and C. Y. Kang, "High Output Piezo/Triboelectric Hybrid Generator," *Sci. Rep.* **2015**, 5, 9309.



- [104] D. Montalvao, N. M. M. Maia, and A. M. R. Ribeiro, "A Review of Vibration-based Structural Health Monitoring with Special Emphasis on Composite Materials," *Shock and Vibration Digest* **2006**, 38, 4, 295-326.
- [105] D. Brian, "Vibration Condition Monitoring Techniques for Rotating Machinery," *The Shock and Vibration Digest*, **1976**, 8 (12): 3.
- [106] W. Fan, P. Z. Qiao, "Vibration-based Damage Identification Methods: A Review and Comparative Study," *Structural Health Monitoring* **2010**, 10, 1, 83-111.
- [107] Z. L. Wang, and J. H. Song, "Piezoelectric Nanogenerators Based on Zinc Oxide Nanowire Arrays," *Science* **2006**, 312, 242–246.
- [108] H. A. Sodano, D. J. Inman, and G. Park, "Vibration Energy Harvesting Using Piezoelectric Transducer and NonControlled Rectifiers Circuits," *The Shock and Vibration Digest* **2004**, 36, 197–205.
- [109] X. D. Wang, J. H. Song, J. Liu, and Z. L. Wang, "Direct-Current Nanogenerator Driven by Ultrasonic Waves," *Science* **2007**, 316, 102–105.
- [110] Z. L. Wang, "Towards Self-Powered Nanosystems: From Nanogenerators to Nanopiezotronics," *Adv. Funct. Mater.* **2008**, 18, 3553–3567.
- [111] R. Yang, Y. Qin, C. Li, G. Zhu, and Z. L. Wang, "Converting Biomechanical Energy into Electricity by a Muscle-Movement-Driven Nanogenerator," *Nano Letters* **2009**, 9, 1201–1205.
- [112] K. Miyazaki, and N. Islam, "Nanotechnology Systems of Innovation—An Analysis of Industry and Academia Research Activities," *Technovation* **2007**, 27, 661–675.
- [113] C. M. Niemeyer, "Tools for the Biomolecular Engineer," *Science* **2002**, 297, 62-63.
- [114] C.M. Shea, "Future Management Research Directions in Nanotechnology: A Case Study," *J. Eng. Technol. Manage* **2005**, 22, 185–200

- [115] N. R. Kumar, "A Review of Low-Power VLSI Technology Developments," *Lecture Notes in Networks and Systems*, 7, Springer, Singapore.
- [116] S. Xu, Y. Qin, C. Xu, Y. Wei, R. Yang, and Z. L. Wang, "Self-powered Nanowire Devices," *Nature Nanotechnology* **2010**, 5, 366–373.
- [117] C. Sun, J. Shi, D. Bayerl, and X. D. Wang, "PVDF microbelts for harvesting energy from respiration," *Energy Environ. Sci.* **2011**, 4, 4508-4512.
- [118] Y. Zhang, X. Yan, Y. Yang, Y. Huang, Q. Liao, and J. Qi, "Scanning Probe Study on the Piezotronic Effect in ZnO Nanomaterials and Nanodevices," *Adv. Mater.* **2012**, 24, 4647-4655.
- [119] Z. L. Wang, "Progress in Piezotronics and Piezo-Phototronics," *Adv. Mater.* **2012**, 24, 4632-4646.
- [120] Z. L. Wang, X. Y. Kong, Y. Ding, P. Gao, W. L. Hughes, R. Yang, and Y. Zhang, "Semiconducting and Piezoelectric Oxide Nanostructures Induced by Polar Surfaces," *Adv. Funct. Mater.* **2004**, 14, 943–956.
- [121] G. C. Yoon, K. S. Shin, M. K. Gupta, K. Y. Lee, J. H. Lee, Z. L. Wang, and S. W. Kim, "High-performance hybrid cell based on an organic photovoltaic device and a direct current piezoelectric nanogenerator," *Nano Energy* **2015**, 12, 547-555.
- [122] Q. Wang, D. Yang, Y. Qiu, X. Zhang, W. Song, and L. Hu, "Two-dimensional ZnO nanosheets grown on flexible ITO-PET substrate for self-powered energy-harvesting nanodevices," *Appl. Phys. Lett.* **2018**, 112, 063906.
- [123] L. E. Greene, M. Law, J. Goldberger, F. Kim, J. C. Johnson, Y. Zhang, R. J. Saykally, and P. Yang, "Low-temperature wafer-scale production of ZnO nanowire arrays," *J. Angew. Chem. Int. Ed.* **2003**, 42, 3031-3034.
- [124] B. C. Iheanacho, *Ph.D. Thesis*, "Optoelectronic Properties and Applications of 3-D Hybrid a-Si:H/ZnO Nanowire Structures," University of Waterloo, Canada **2017**.

- [125] M. Pathirane, *Ph.D. Thesis*, "Flexible 3-Dimensional Hybrid ZnO Nanowire/a-Si:H Thin-Film Solar Cells," University of Waterloo, Canada **2016**.
- [126] M. Ladanov, M. K. Ram, G. Matthews, and A. Kumar, "Structure and Opto-electrochemical Properties of ZnO Nanowires Grown on n-Si Substrate," *Langmuir* **2011**, *27*, 9012–9017.
- [127] S. F. Wang, T. Y. Tseng, Y. R. Wang, C. Y. Wang, H. C. Lu, and W. L. Shih, "Effects of Preparation Conditions on the Growth of ZnO Nanorod Arrays Using Aqueous Solution Method," *International Journal of Applied Ceramic Technology* **2008**, *5*, 419–429.
- [128] J. P. Cheng, X. B. Zhang, and Z. Q. Luo, "Oriented growth of ZnO nanostructures on Si and Al substrates," *Surface & Coatings Technology* **2008**, *202*, 4681–4686.
- [129] T. Ishikawa, K. Matsumoto, A. Ysukawa, K. Kandori, T. Nakayama, and T. Tsubota, "Oriented growth of ZnO nanostructures on Si and Al substrates," *Corros. Sci.* **2004**, *46*, 329.
- [130] F. Xu, Z. Y. Yuan, G. H. Du, M. Halasa, and B. L. Su, "High-yield synthesis of single-crystalline ZnO hexagonal nanoplates and accounts of their optical and photocatalytic properties," *Appl. Phys. A* **2007**, *86*: 181.
- [131] G. Liu, *Ph.D. Thesis*, "Semiconductor Nanowire Based Piezoelectric Energy Harvesters: Modeling, Fabrication, and Characterization," University of Waterloo, Canada **2016**.
- [132] K. H. Kim, B. Kumar, K. Y. Lee, H. K. Park, J. H. Lee, H. H. Lee, H. Jun, D. Lee, and S. -W. Kim, "Piezoelectric two-dimensional nanosheets/anionic layer heterojunction for efficient direct current power generation," *Sci. Rep.* **2013**, *3*(6), 2017.

- [133] M. K. Gupta, J. Lee, K. Y. Lee, and S. -W. Kim, "Two-Dimensional Vanadium-Doped ZnO Nanosheet-Based Flexible Direct Current Nanogenerator," *ACS Nano* **2013**, 7 (10), 8932–8939.
- [134] K. Pradel, W. Wu, Y. Ding, and Z. L. Wang, "Solution-Derived ZnO Homojunction Nanowire Films on Wearable Substrates for Energy Conversion and Self-Powered Gesture Recognition," *Nano Lett.* **2014**, 14, 12, 6897-6905.
- [135] G. Liu, E. Abdel-Rahman, and D. Ban, "Performance optimization of p-n homojunction nanowire-based piezoelectric nanogenerators through control of doping concentration," *Journal of Applied Physics* **2015**, 118, 094307.
- [136] S. Lee, S. H. Bae, L. Lin, Y. Yang, C. Park, S. W. Kim, S. N. Cha, H. Y. Kim, J. Park, and Z. L. Wang, "Super-Flexible Nanogenerator for Energy Harvesting from Gentle Wind and as an Active Deformation Sensor," *Adv. Funct. Mater.* **2013**, 23, 2445-2449.
- [137] G. Zhu, A. C. Wang, Y. Liu, Y. Zhou, and Z. L. Wang, "Functional Electrical Stimulation by Nanogenerator with 58 V Output Voltage," *Nano Lett.* **2012**, 12, 3086-3090.
- [138] C. Liu, S. Hu, and S. Shen, "Effect of flexoelectricity on electrostatic potential in a bent piezoelectric nanowire," *Smart Mater. Struct.* **2012**, 21, 115024.
- [139] S. L. Hu, and S. Shen, "Variational principles and governing equations in nano-dielectrics with the flexoelectric effect," *Sci. China G* **2010**, 53, 1497–1504.
- [140] R. D. Mindlin, "Polarization gradient in elastic dielectrics," *Int. J. Solids Structures* **1968**, 4, 637-642.
- [141] P. Zubko, G. Catalan, and A. K. Tagantsev, "Flexoelectric Effect in Solids," *Annu. Rev. Mater. Res.* **2013**, 43, 387–421.

- [142] H. Yu, J. Zhou, L. Deng, and Z. Wen, "A Vibration-Based MEMS Piezoelectric Energy Harvester and Power Conditioning Circuit," *Sensors* **2014**, *14*, 3323-3341.
- [143] G. Tang, B. Yang, C. Hou, G. Li, J. Liu, X. Chen, and C. Yang, "A piezoelectric micro generator worked at low frequency and high acceleration based on PZT and phosphor bronze bonding," *Sci. Reports* **2016**, *6*, 38798.
- [144] D. Shen, J. H. Park, J. H. Noh, S. Y. Choe, S. H. Kim, H. C. Wickle III, and D. J. Kim, "Micromachined PZT cantilever based on SOI structure for low frequency vibration energy harvesting," *Sens. Actuators A* **2009**, *154*, 103–108.
- [145] S. Roundy, P. K. Wright, and J. Rabaey, "A study of low level vibrations as a power source for wireless sensor nodes," *J. Comput. Commun.* **2003**, *26*, 1131–1144.
- [146] T. C. Houa, Y. Yanga, H. Zhanga, J. Chena, L. J. Chen, and Z. L. Wang, "Triboelectric nanogenerator built inside shoe insole for harvesting walking energy," *Nano Energy* **2013**, *2*, 856–862.
- [147] J. Liu, P. Fei, J. Song, X. Wang, C. Lao, R. Tummala, and Z. L. Wang, "Carrier Density and Schottky Barrier on the Performance of DC Nanogenerator," *Nano Letters* **2008**, *8* (1), 328–332.
- [148] S. Liu, Q. Liao, S. Lu, Z. Zhang, G. Zhang, and Y. Zhang, "Strain Modulation in Graphene/ZnO Nanorod Film Schottky Junction for Enhanced Photosensing Performance," *Adv. Func. Mater.* **2016**, *26*(9), 1347-1353.
- [149] S. Lu, Q. Liao, J. Qi, S. Liu, Y. Liu, Q. Liang, G. Zhang, and Y. Zhang, "The enhanced performance of piezoelectric nanogenerator via suppressing screening effect with Au particles/ZnO nanoarrays Schottky junction," *Nano Res.* **2016**, *9*, 372-379.
- [150] J. Briscoe, M. Stewart, M. Vopson, M. Cain, P. M. Weaver, and S. Dunn, "Nanostructured p-n Junctions for Kinetic-to-Electrical Energy Conversion," *Adv. Energy Mater.* **2012**, *2*, 1261–1268.

- [151] K. Y. Lee, B. Kumar, J. S. Seo, K. H. Kim, J. I. Sohn, S. N. Cha, D. Choi, Z. L. Wang, and S. -W. Kim, "p-Type polymer-hybridized high-performance piezoelectric nanogenerators," *Nano Letters* **2012**, *12*, 1959–1964.
- [152] Z. Zhang, Q. Liao, Y. Yu, X. Wang, and Y. Zhang, "Enhanced photoresponse of ZnO nanorods-based self-powered photodetector by piezotronic interface engineering," *Nano Energy* **2014**, *9*, 237-244.
- [153] G. Liu, N. Mrad, E. Abdel-Rahman, and D. Ban, "Cascade-type hybrid energy cells for driving wireless sensors," *Nano Energy* **2016**, *26*, 641-647.
- [154] R. Zhang, M. Hummelgård, M. Olsen, J. Örtengren, and H. Olin, "Nanogenerator made of ZnO nanosheet networks," *Semicond. Sci. Technol* **2017**, *32* 054002.
- [155] B. Kumara , and S. -W. Kim, "Energy harvesting based on semiconducting piezoelectric ZnO nanostructures," *Nano Energy* **2012**, *1*, 342–355.
- [156] H. K. Park, K. Y. Lee, J. S. Seo, J. A. Jeong, H. K. Kim, D. Choi, and S. -W. Kim, "Charge-Generating Mode Control in High-Performance Transparent Flexible Piezoelectric Nanogenerators," *Advanced Functional Materials* **2011**, *21*, 1187–1193.
- [157] B. Saravanakumar, and S. J. Kim, "Growth of 2D ZnO Nanowall for Energy Harvesting Application," *J. Phys. Chem. C* **2014**, *118*, 8831–8836.
- [158] M. H. Jung, and M. J. Chu, "Synthesis of hexagonal ZnO nanodrums, nanosheets and nanowires by the ionic effect during the growth of hexagonal ZnO crystals," *J. Mater. Chem. C* **2014**, *2*, 6675-6682.
- [159] Z. L. Wang, and W. Wu, "Nanotechnology-Enabled Energy Harvesting for Self Powered Micro-/Nanosystems," *Angew. Chem. Int. Ed.* **2012**, *51*, 11700-11721.
- [160] F. R. Fan, W. Tang, and Z. L. Wang, "Flexible Nanogenerators for Energy Harvesting and Self-Powered Electronics," *Adv. Mater.* **2016**, *28*, 4283–4305.

- [161] J. A. Paradiso, and T. Starner, "Energy Scavenging for Mobile and Wireless Electronics," *IEEE Pervasive Computing* **2005**, 4, 18-27.
- [162] C. Thomas, M. Greenstone, and C. R. Knittel, "Will We Ever Stop Using Fossil Fuels?," *Journal of Economic Perspectives* **2016**, 30 (1): 117-38.
- [163] S. R. Anton, and H. A. Sodano, "A review of power harvesting using piezoelectric materials (2003–2006)," *Smart Mater. Struct.* **2007**, 16 , R1–R21.
- [164] X. Wang, "Piezoelectric nanogenerators—Harvesting ambient mechanical energy at the nanometer scale," *Nano Energy* **2012**, 1, 13–24.
- [165] J. Briscoe, and S. Dunn, "Piezoelectric nanogenerators – a review of nanostructured piezoelectric energy harvesters," *Nano Energy* **2015**, 14, 15–29.
- [166] Z. L. Wang, G. Zhu, Y. Yang, S. Wang, and C. Pan, "Progress in nanogenerators for portable electronics," *Materials Today* **2012**, 15, 12, 2012, 532-543.
- [167] Z. L. Wang, J. Chen, and L. Lin, "Progress in triboelectric nanogenerators as a new energy technology and self-powered sensors," *Energy Environ. Sci.* **2015**, 8, 2250-2282.
- [168] R. Hinchet, W. Seung, and S. -W. Kim, "Recent Progress on Flexible Triboelectric Nanogenerators for Self-Powered Electronics," *Chem Sus Chem* **2015**, 8, 2327 –2344.
- [169] Z. L. Wang, "Triboelectric nanogenerators as new energy technology and self-powered sensors – Principles, problems and perspectives," *Faraday Discuss.* **2014**, 176, 447-458
- [170] M. Ma, Z. Kang, Q. Liao, Q. Zhang, F. Gao, X. Zhao, Z. Zhang, and Y. Zhang, "Development, applications, and future directions of triboelectric nanogenerators," *Nano Res.* **2018**, 11(6): 2951–2969.
- [171] Z. L. Wang, T. Jiang, L. Xu, "Toward the blue energy dream by triboelectric nanogenerator networks," *Nano Energy* **2017**, 39, 9–23.

- [172] Y. Wang, Y. Yang, and Z. L. Wang, "Triboelectric nanogenerators as flexible power sources," *npj Flexible Electronics* **2017**, 1, 10.
- [173] Z. L. Wang, L. Lin, J. Chen, S. Niu, and Y. Zi (2016), "Triboelectric Nanogenerators," Switzerland: Springer, Cham.
- [174] M. Han, X. -S. Zhang, B. Meng, W. Liu, W. Tang, X. Sun, W. Wang, and H. Zhang, "r-Shaped Hybrid Nanogenerator with Enhanced Piezoelectricity," *ACS Nano* **2013**, 7, 10, 8554-8560.
- [175] Z. L. Wang, "Progress in Piezotronics and Piezo-Phototronics," *Adv. Mater.* **2012**, 24, 4632-4646
- [176] S. Lu, Q. Liao, J. Qi, S. Liu, Y. Liu, Q. Liang, G. Zhang, and Y. Zhang, *Nano Res.* **2016**, 9(2): 372-379.
- [177] X. Wang, B. Yang, J. Liu, Y. Zhu, C. Yang, and Q. He, "A flexible triboelectric-piezoelectric hybrid nanogenerator based on P(VDF-TrFE) nanofibers and PDMS/MWCNT for wearable devices," *Sci. Rep.* **2016**, 6: 36409.
- [178] J. Wang, C. Wu, Y. Dai, Z. Zhao, A. Wang, T. Zhang, and Z. L. Wang, "Achieving ultrahigh triboelectric charge density for efficient energy harvesting," *Nature Communications* **2017**, 8: 88.
- [179] W. S. Jung, M. G. Kang, H. G. Moon, S. H. Baek, S. J. Yoon, Z. L. Wang, S. W. Kim, and C. Y. Kang, "High Output Piezo/Triboelectric Hybrid Generator," *Sci. Rep.* **2015**, 5: 9309.
- [180] X. Chen, M. Han, H. Chen, X. Cheng, Y. Song, Z. Su, Y. Jiangc, and H. Zhang, "A wave-shaped hybrid piezoelectric and triboelectric nanogenerator based on P(VDF-TrFE) nanofibers," *Nanoscale* **2017**, 9, 1263-1270.
- [181] X. Li, Z. H. Lin, G. Cheng, X. Wen, Y. Liu, S. Niu, and Z. L. Wang, "3D fiber-based hybrid nanogenerator for energy harvesting and as a self-powered pressure sensor," *ACS Nano* **2014**, 8, 10674-10681.



- [182] X. Yang, and W. A. Daoud, "Synergetic effects in composite-based flexible hybrid mechanical energy harvesting generator," *J. Mater. Chem. A* **2017**, 5, 9113–9121.
- [183] J. Chen , G. Zhu , W. Yang , Q. Jing , P. Bai , Y. Yang , T. -C. Hou , and Z. L. Wang, "Harmonic-Resonator-Based Triboelectric Nanogenerator as a Sustainable Power Source and a Self-Powered Active Vibration Sensor," *Adv. Mater.* **2013**, 25, 6094–6099.
- [184] Y. Wu, X. Zhong, X. Wang, Y. Yang, and Z. L. Wang, "Hybrid energy cell for simultaneously harvesting wind, solar, and chemical energies," *Nano Res.* **2014**, 7(11), 1631–1639.
- [185] G. Liu, E. Abdel-Rahman, and D. Ban, "Performance optimization of p-n homojunction nanowire-based piezoelectric nanogenerators through control of doping concentration," *Journal of Applied Physics* **2015**, 118, 094307.
- [186] K. C. Pradel, W. Wu, Y. Ding, and Z. L. Wang, "Solution-Derived ZnO Homojunction Nanowire Films on Wearable Substrates for Energy Conversion and Self-Powered Gesture Recognition," *Nano Lett.* **2014**, 14, 6897–6905.
- [187] G. Liu, N. Mrad, E. Abdel-Rahman, and D. Ban, "Cascade-type hybrid energy cells for driving wireless sensors," *Nano Energy* **2016**, 26, 641-647.
- [188] C. B. Walsh, and E. I. Franses, "Ultrathin PMMA films spin-coated from toluene solutions," *Thin Solid Films* **2003**, 429, 1–2, 71-76.
- [189] R. Hinchet, S. Lee , G. Ardila, L. Montès, M. Mouis, and Z. Lin Wang, "Performance Optimization of Vertical Nanowire-based Piezoelectric Nanogenerators", *Adv. Funct. Mater.* **2014**, 24, 971–977.
- [190] J. P. Cheng, X. .B. Zhang, and Z. Q. Luo, "Oriented growth of ZnO nanostructures on Si and Al substrates," *Surface & Coatings Technology* **2008**, 202, 4681–4686.

- [191] T. Ishikawa, K. Matsumoto, A. Ysukawa, K. Kandori, T. Nakayama, and T. Tsubota, "Influence of metal ions on the formation of artificial zinc rusts," *Corros. Sci.* **2004**, *46*, 329-342.
- [192] Y. Qi, and M. C. McAlpine, "Nanotechnology-enabled flexible and biocompatible energy harvesting," *Energy Environ. Sci.* **2010**, *3*, 1275–1285.
- [193] H. Kim, S. M. Kim, H. Son, H. Kim, B. Park, J. Y. Ku, J. I. Sohn, K. Im, J. E. Jang, and J. -J. Park, "Enhancement of Piezoelectricity via Electrostatic Effects on a Textile Platform," *Energy Environ. Sci.* **2012**, *5*, 8932 –8936.
- [194] E. J. Lee, T. Y. Kim, S. -W. Kim, S. Jeong, Y. Choi, and S. Y. Lee, "High-performance piezoelectric nanogenerators based on chemically-reinforced composites," *Energy Environ. Sci.* **2018**, *11*, 1425-1430.
- [195] J. Borgeson, S. Schauer, and H. Diewald, "Benchmarking MCU power consumption for ultra-low-power applications," *Texas Instruments* 2012.